Study of the Plasma Based Production of Tetrafluoroethylene

by

Annalien Nell

Thesis presented as partial fulfilment of the requirements for the degree of Master of Engineering (Chemical) at the University of Stellenbosch.

Promoters

Prof. C. Aldrich

Dr. P.L. Crouse

June 1999

I, the undersigned, hereby declare that the work in this thesis is my own original work and has not been previously in its entirety or in part been submitted at any university for a degree.

Signature: **Date:**

Summary

A method was developed at the Atomic Energy Corporation of South Africa (AEC) for the plasma based production of tetrafluoroethylene (TFE). The process involves the feeding of carbon particles into a direct-current CF_4 plasma. The resultant plasma gas is quenched rapidly to obtain TFE and other fluorocarbons. The mixing of the particles with the plasma gas is very important in order to achieve a high C:F-ratio in the gas phase, which promotes the desired reactions. The gas enthalpy in the reactor is a governing factor in the TFE yields that are obtained.

In this study research was done on particle mixing and the enthalpy distribution in the laboratory scale reactor. An enthalpy probe was used as the main diagnostic tool. Results indicated that particle mixing is quite uniform throughout the reactor. A basic one-dimensional mechanistic model of the reactor was also expanded to assist in the scale-up of the process. In its present form the model is adequate for predicting trends in the reactor. The model could still be expanded further to include reaction kinetics and internal heat transfer in the particles. Considering the restrictions of the model, satisfactory agreement was obtained between the model and experimental results.

Opsomming

'n Proses vir die plasmagebaseerde produksie van tetrafluoroetileen (TFE) is deur die Atoomenergiekorporasie van Suid-Afrika (AEK) ontwikkel. Koolstofpartikels word in 'n gelykstroom-CF_4-plasma gevoer en die resulterende plasmagas word vinnig geblus ten einde TFE en ander fluoor-koolstofverbindings as produkte te verkry. Goeie vermenging van die koolstofpartikels met die plasmagas is van uiterste belang ten einde 'n hoë C:F-verhouding, wat die gewenste reaksies bevorder, in die gasfase te verkry. Die entalpie van die plasmagas in die reaktor is 'n bepalende faktor in die opbrengs TFE wat verkry word.

Vir die doel van hierdie werkstuk is navorsing op laboratoriumskaal gedoen oor partikelvermenging en die entalpie-verspreiding in die reaktor. Die hoof diagnostiese apparaat wat vir dié doel aangewend is, is die entalpiesonde. Resultate toon dat partikelvermenging naastenby uniform deur die reaktor voorkom. Verder is 'n basiese een-dimensionele meganistiese model van die reaktor uitgebrei ten einde van nut te wees in die opskaling van die proses. In sy huidige vorm is die model voldoende om algemene neigings in die reaktor te voorspel. Die model kan nog verder uitgebrei word om reaksie-kinetika en interne hitte-oordrag in die partikels in te sluit. Die beperkings van die model in ag genome, is ooreenstemming tussen die model en eksperimentele resultate egter bevredigend.

ACKNOWLEDGEMENTS

I would like to give thanks to the following:

- My Heavenly Father for strength and wisdom.
- Dr. Philip Crouse for his guidance.
- My parents for their encouragement.
- My husband, Morné, for his patience and support.
- The AEC for the opportunity to do this research.

BEDANKINGS

Dankie aan:

- My Hemelse Vader vir krag en verstand.
- Dr. Philip Crouse vir sy leiding.
- My ouers vir hulle aanmoediging.
- My man, Morné, vir sy geduld en ondersteuning.
- Die AEK vir die geleentheid om die navorsing te kon doen.

Contents

List of Tables

List of Figures

1. INTRODUCTION

Tetrafluoroethylene (TFE) is a precursor to high value products like the polymer polytetrafluoroethylene and speciality gases like cyclic C_4F_8 and C_5F_8. Research on the plasma based production of TFE was started at the Atomic Energy Corporation of South Africa (AEC) in 1991 in reference to a number of patents and publications on the subject. In principle the process developed by the AEC involves feeding carbon particles into the tail flame of a direct current non-transferred CF_4 plasma. The resultant plasma gas is then quenched rapidly to obtain TFE and other fluorocarbons. This process is at present being developed on a pilot plant scale that will utilise a 450 kW plasma torch.

Experimental studies of the process thus far have revealed the following:

- The system operating pressure is an important parameter – TFE yields increase with decrease in pressure.
- The higher the enthalpy of the gas leaving the plasma torch, the higher the TFE yield.
- The inside diameter of the reactor also influences the yield – smaller inside diameter resulted in higher TFE yields.
- The rate at which the plasma gas is quenched has to exceed 10^5 K/s before significant TFE yields are obtained.

Questions that still need to be addressed are: (i) how well is the carbon mixing with the gas and (ii) what is the mechanism of the reaction between the injected carbon particles and the plasma constituents. Over the years a number of empirical and semi-empirical models have been developed for the process by scientists at the AEC and in Russia. These were largely global in nature and the factors mentioned above was not incorporated individually. Results obtained from these models indicate that the kinetics of the plasma-particle interaction is probably mass transfer controlled.

Purpose of this study

The research described in this work was done on the process at lab scale, using a 30 kW plasma torch. The purpose is to expand on a basic one-dimensional mechanistic model of the reactor system, which can in future be modified to model the bigger systems and to include reaction

kinetics. This will promote a better understanding of the system and assist in scale-up of the process. The experimental research comprises the study of particle mixing and the enthalpy distribution in the reactor. This includes the testing and further developing of the enthalpy probe as a reliable diagnostic tool for the plasma system. The model is to be compared with the experimental results to determine its accuracy and to decide which of the empirical correlations found in literature are applicable to the process and whether other empirical correlations should be derived for this specific system.

2. LITERATURE OVERVIEW

2.1 Background on Plasmas

2.1.1 What is a Plasma?

A plasma is an ionised gas consisting of molecules, atoms, ions in their ground or excited states, electrons and photons and is often referred to as the fourth state of matter.[14,22] By far the greater part (up to 99%) of the detectable matter in the universe is in the plasma state, as this is the state of matter found in the sun and other stars.[5] Other examples of plasmas in nature are the aurora borealis, which is due to excitation of gas molecules and atoms in the upper atmosphere, and lightning bolts. Examples of practical applications are neon and fluorescent lighting, electric arc welding and large-scale chemical processes.[5,22]

In contrast to an ordinary gas, plasma contains free electrons and ions, produced by a variety of ionisation processes that cause it to be electrically conducting. The electrical conductivities of plasmas can even exceed those of some metals. Overall, however, the plasma is electrically neutral. This property is referred to as quasi-neutrality.[2,14] The ionisation processes may be due to high energy radiation (UV, X-rays, etc.) or to collision processes. Most industrial plasmas are generated by passing an electrical current through a gas.[14] In this case ionisation is effected by the acceleration of electrons by an electric field and the collision of these energetic electrons with neutral species.

At room temperature, gases are usually excellent insulators, so that a moderate electrical field applied over a gas between two electrodes gives only an infinitesimal current. When the field reaches a certain value, however, the electrons present are accelerated to energies above the ionisation potential of the neutrals, ionisation occurs and the electrons thus released are again accelerated and in turn can induce ionisation. A steady state is reached when the electron production rate is balanced by an equal electron loss. Electrons are lost from the system by recombination and diffusion.

Only a small percentage of charge carriers can be sufficient to make the gas electrically conducting. This process is known as electrical breakdown and it establishes a conducting path between two electrodes to produce a gaseous discharge. Once breakdown is achieved, a smaller electric field is sufficient to maintain the current through the gas. Plasmas can also be produced by electrodeless RF discharges, or by microwaves, shock waves, laser beams or high-energy particle beams as means of external ionisation. Plasmas of metal vapours with low ionisation potentials can be produced by heating the vapours in high-temperature furnaces.[14,22]

2.1.2 Equilibrium in Plasmas

The heavy particles (neutral and ions) in a plasma are more than three orders of magnitude heavier than the electrons. The acceleration of the electrons is thus more than a thousand times greater than that of the heavy particles. The electrons, therefore, act as the chief agents for transferring energy from the electric field to the gas through electron-molecule and electron-atom collisions. The kinetic energy of the molecules is increased by elastic electron-molecule collisions, while inelastic collisions lead to excitation, fragmentation or ionisation of the molecules.[2,14]

Plasmas are usually separated into two different types: equilibrium or thermal plasmas and non-equilibrium or non-thermal plasmas. Two of the most important features of thermal plasmas are the equality between electron and heavy particle temperature ($T_e = T_h$) and the existence of local thermodynamic equilibrium. By contrast, non-thermal plasmas are characterised by strong deviations from thermodynamic equilibrium ($T_e >> T_h$). The two temperatures tend to equilibrate as the interaction rate between the electrons and the heavy particles increases.[2,14]

The experimental parameter, E/p, where E is the electric field and p the pressure, is often used as a general criterion for the existence of a thermal or non-thermal plasma. This parameter reflects the energy exchange processes between electrons and heavy particles in plasma. High particle densities or high pressures enhance collisions and the associated energy exchange between the electrons and the heavy particles. By contrast, high electric fields tend to increase the excess energy of the electron gas. Thermal plasmas are therefore characterised by small values of E/p, several orders of magnitude lower than that of non-thermal plasmas.[14]

Complete thermodynamic equilibrium (CTE) prevails in a uniform, homogenous plasma volume only if the following conditions are met:

- All plasma properties are unambiguous functions of the plasma temperature, which is the same for all plasma constituents and their possible reactions.
- The velocity functions of all the plasma constituents obey a Maxwell-Boltzmann distribution.
- The population density of the excited states of every species in the plasma obeys a Boltzmann distribution.
- Thermodynamic equilibrium prevails in the plasma so that all particle densities (ions, neutrals and electrons) are described by the Saha equation. This may be considered as a mass action law that gives the amount of ionisation to be expected in a gas in thermal equilibrium.
- The electromagnetic radiation field is that of a blackbody as described by the Planck function.[5,14]

To satisfy all these conditions, the plasma would have to be in a hypothetical container of which the walls are at the same temperature as the plasma temperature, or the plasma volume would have to be so large that the centre of the plasma, where CTE prevails, does not sense the plasma boundaries. In this way, the plasma would be penetrated by blackbody radiation of its own temperature. This is however not possible in an industrial plasma. The plasma radiation would be less than blackbody radiation, because most plasmas are optically thin. Conduction, convection and diffusion cause further energy losses, which also disturb the thermodynamic equilibrium.[14]

Actual, optically thin, thermal plasmas approximate local thermodynamic equilibrium (LTE). For LTE to prevail similar conditions as for CTE have to be met, except for blackbody radiation. Collision processes and not radiative processes govern transitions and reactions in the plasma and a detailed equilibrium between each collision process and its reverse process is a necessary requirement for LTE. LTE also requires that local gradients of the plasma properties are sufficiently small so that a given particle which diffuses from one location to another, has sufficient time to equilibrate.[14]

If the electron density is lower than 10^{16} electrons/cm^3, collisions between the electrons and the heavy particles are not numerous enough. Thus, the mean kinetic energy of the electrons, and therefore their temperature, are higher than those of the heavy particles. Non-equilibrium plasmas are also found when the temperature and concentration gradients are so high that diffusion of the

electrons becomes important in the boundaries of the plasma jet or near the walls or the electrodes of the plasma generator.[14]

2.1.3 Thermal Arcs

As mentioned, plasmas can be generated in different ways. Of these, the most common methods are direct-current discharges and high-frequency discharges. Direct-current discharges are generated between two electrodes over which an electric field is applied. The principal types of dc discharges, of which the current-voltage characteristics are shown in Figure 2.1, are the dark discharge, the glow discharge and the plasma arc. High-frequency discharges consist of radio frequency and microwave-sustained discharges in which the presence of electrodes within the discharge zone is eliminated.[2]

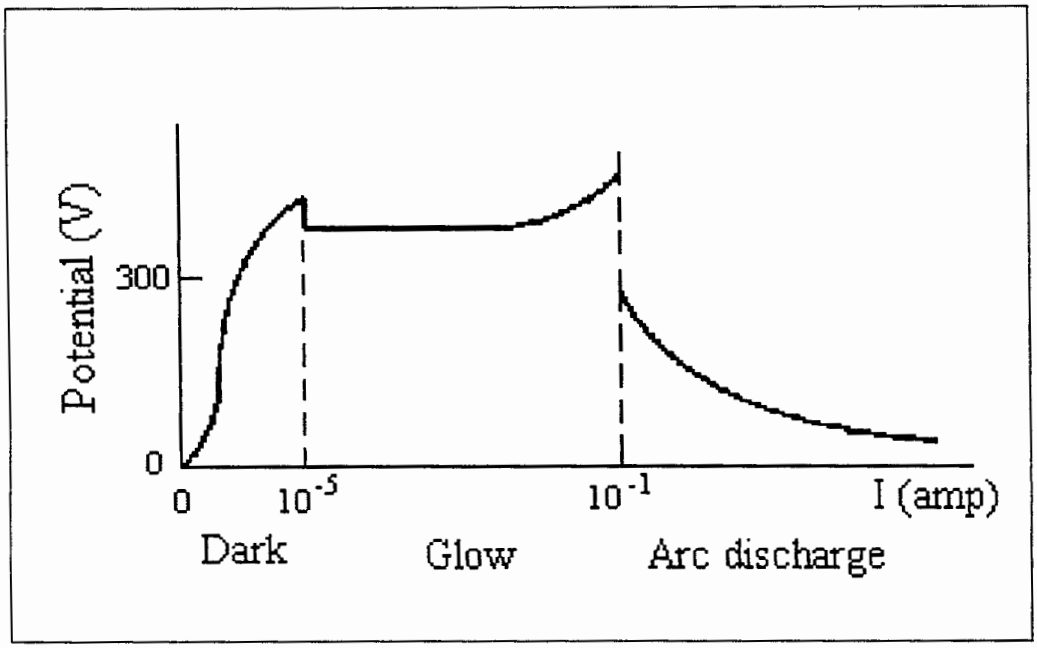

Figure 2.1: Current-Voltage characteristics of dc discharges

A commonly used plasma configuration is the plasma arc. Three typical features that distinguishes arcs from other forms of discharge, are: (i) a low cathode potential fall; (ii) a relatively high current density and (iii) high luminosity of the arc column.[14] Arc plasmas are largely thermal in nature[22] and are characterised by high temperatures and high specific enthalpies.[2]

Electric arcs may be initiated in three different ways:

a) An electric potential may be applied to two electrodes in contact with one another. The short circuit current flowing between the two electrodes heats the contact point sufficiently for evaporation and ionisation of the electrode material to form the required initial charge carriers for the development of an arc when the two electrodes are separated.

b) The voltage necessary to induce an arc between two electrodes may be reduced to convenient values by pre-ionisation of the electrode gap, for example by using a high frequency spark to generate the charge carriers needed.

c) A thin wire may be stretched across the electrode gap. The applied voltage leads to wire explosion that supplies the necessary charge carriers for establishing an arc.

d) The breakdown voltage necessary for ignition of the arc can also be lowered by first supplying the plasma generator with an easily ionised gas such as argon. This method is often used in conjunction with one of the above methods.[14]

The potential distribution across a plasma arc can be divided into three regions: the cathode region, the arc column and the anode region (see Figure 2.2). The cathode and anode regions are the thin boundary layers overlying the electrodes and are characterised by electric fields much higher than that of the arc column. The arc column, with its relatively small potential gradient, represents the main body of the arc. In contrasts to the electrode regions, the arc column is a true plasma in which quasi-neutrality prevails.[14]

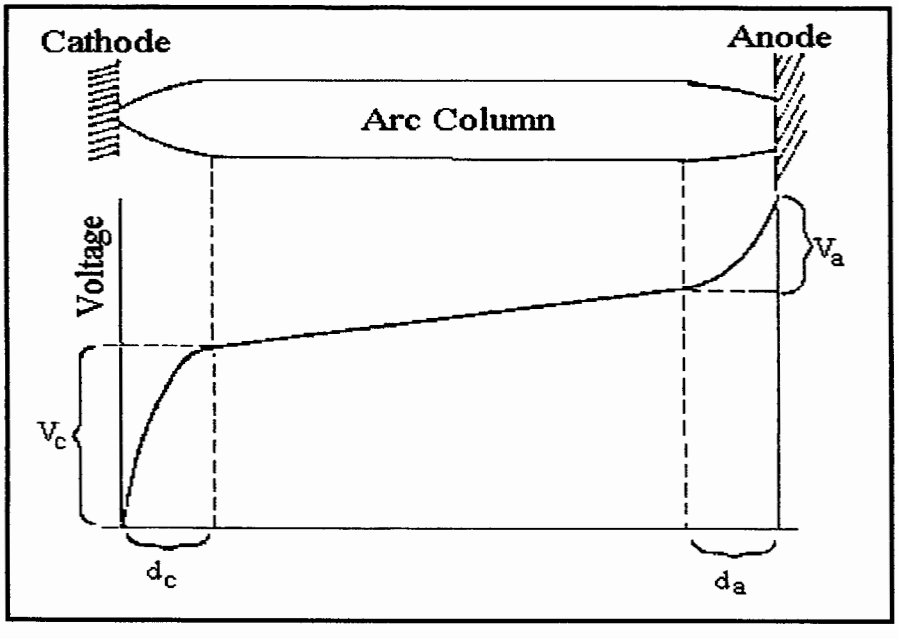

Figure 2.2: Typical potential distribution along an arc

Most electric arcs require some kind of stabilisation, which may be either provided externally or produced by the arc itself. Stabilisation refers to a mechanism that keeps the arc column in a given, stable position. This stable position need not necessarily be a stationary position. Arcs are often classified according to their stabilising mechanisms:

- **Free-burning arcs** - no external stabilising mechanism is applied to the arc, but the arc may generate its own stabilising mechanism through natural convection.
- **Wall-stabilised arcs** - a long arc enclosed in a narrow tube with circular cross section will assume a rotationally symmetric coaxial position within the tube.
- **Vortex-stabilised arcs** - the arc is confined to the centre of a tube in which an intense vortex of a gas or liquid is maintained.
- **Electrode-stabilised arcs** - in extremely short arcs (in the order of 1 mm) the behaviour of the arc is determined by the vicinity of the electrodes as the arc column as such, does not exist any more.
- **Self-stabilised arcs** - For high intensity arcs with arc currents in the range of 50 to 100 A, the column becomes stiff and motionless with a visually well defined boundary.
- **Forced-convection-stabilised arcs** - stability can also be achieved by superimposing an axial flow onto an otherwise unstable arc.
- **Magnetically-stabilised arcs** - since an arc is an electrically conducting medium, it will interact not only with its own magnetic field, but also with magnetic fields applied externally for stabilisation purposes.[14]

2.1.4 Plasma Generation Characteristics[14]

The ordinary plasma generator consists of two or more electrodes of which at least one is axial. Electrodes are commonly made from copper, which is relatively inexpensive and has a high thermal and electrical conductivity. Electron transfer takes place at the electrode surfaces. With direct current, electrons are emitted from the cathode and absorbed at the anode. The electrode surfaces thus form the boundary between the plasma phase and the rest of the electric circuit. Water-cooling is usually employed to help prevent rapid erosion and melting of the electrodes.

The gas to be heated must pass close to the arc and the arc must therefore be surrounded by an arc chamber. The gas flow is often introduced to stabilise the arc path. Most industrial plasma

arcs are vortex stabilised. This is accomplished by injecting the gas through tangential ports, often at high velocity. The high power plasma generator is characterised by a very high energy density surpassing ordinary flames by at least one order of magnitude. The gas throughput is high with residence times of much less than a second.

Arc devices designed to heat gas normally have at least one tubular electrode from which the hot gas heated by the arc emerges. A plasma torch of this type is said to be non-transferred. If only one of the electrodes is in the torch and the other electrode is the material to be heated and melted, the plasma torch is said to be transferred. The operating voltages of non-transferred torches are normally higher than those of transferred torches.

A typical voltage-current characteristic of an arc is shown in Figure 2.3. The actual shape of this arc characteristic depends upon the plasma generator geometry, type of gas, gas flow rate, pressure, etc. The breakdown voltage must be exceeded to ignite the arc. After ignition, the arc voltage decreases with increasing current. At low currents the differential resistance, $R_d = dV/dI$, is negative. This negative arc resistance prohibits direct operation from a voltage source with a low internal impedance. The operating line for the power supply must have a steeper negative slope than the arc characteristic. A very unstable operating situation occurs if the arc characteristic and power supply characteristic have nearly the same slope. A small shift in the arc characteristic would then lead to a large shift in the operating point.

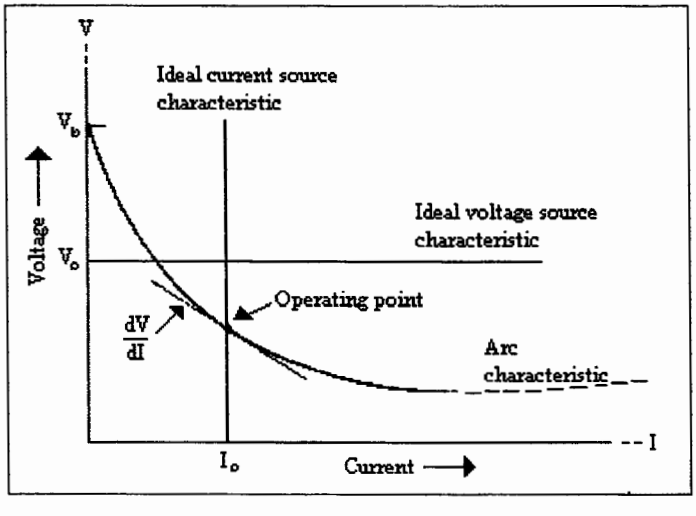

Figure 2.3: Typical voltage-current characteristic of a thermal arc

Another important feature of the plasma arc is the random fluctuations of the arc voltage. These are caused by turbulence in the gas flow around the arc and erratic movements of the attachment points of the arc on the electrodes. The amplitude of these fluctuations depends on the generator design, type of gas, stabilising factors and the operating conditions.

The electric to thermal efficiency of plasma devices can be anything from less than 50 percent to about 95 percent, depending on the geometry and other operating conditions, such as arc length, gas flow rate, gas type, etc. Efficiencies are affected markedly by operating pressure and temperature. Arcs in diatomic or poly-atomic gases operate at higher voltages and efficiencies than arcs in mono-atomic gases. Water-cooling can also have an effect on the thermal-to-process efficiency.

2.1.5 Energy Dissipation in the Plasma Torch[14]

Radiation from the arc is essentially independent of the inside diameter of the generator. The convective losses present a more complicated problem. The thermal conductivity of a gas as a function of temperature can vary by orders of magnitude and is generally much higher at higher temperatures. The same tendency holds for the viscosity. The result is that the most intense turbulence is normally found in the region near the wall. The thermal resistance in this region, which would otherwise be high due to the low thermal conductivity, can thus be reduced considerably by turbulent mixing. A significant part of the thermal resistance between the arc and the plasma generator wall is therefore found in the boundary layer associated with the wall. The convective heat losses are thus partly dependent on the inside diameter of the arc chamber.

The main contributions to the heat dissipation at the cathode come from the kinetic energy of the positive ions hitting the electrode surface and from their recombination energy. The electrons leaving the metal surface absorb a significant amount of energy when they pass through the potential barrier of the work function. At the anode, the electrons enter the conductor, releasing their kinetic energy. When they pass through the work function, they again gain energy, which is also released as thermal energy. Since most of the arc current is carried by electrons, these mechanisms represent large power dissipation. Radiation and convection from the arc further contribute to the heating of the anode spot. In many cases, the anode erosion is much higher than

that of the cathode. Both electrodes are often protected against melting by rapid motion of the connection point of the arc on the electrodes.

2.1.6 The Linear Direct Current Torch[33]

A thermal plasma generator, or plasma torch, is both an electrotechnical and a thermal apparatus. It is a highly flexible instrument, since its thermal, energy and service characteristics cover a wide range. Plasma torches used in technological processes should meet certain requirements:

- they must be able to heat a wide range of gases, from inert to chemically active;
- the apparatus must be able to perform efficiently over a wide range of gas pressures, both below and above atmospheric pressure;
- the working life of the most significant elements, e.g. the electrodes, should exceed 100 hours;
- the arc power (gas enthalpy) should be easy to vary;
- heat losses to the arc chamber should not exceed the values governed by the economics of the process and the physical characteristics of the material;
- the arc should be a stable element of an electric circuit.

In order to design a plasma torch having the required characteristics, it is necessary to be able to predict its electrical, thermal and other parameters. It is therefore important to understand and describe reliably the most characteristic physical processes. These processes occurring in the electric arc chamber are defined by a variety of internal interactions between the arc, the gas and the bounding wall and external factors, such as applied magnetic fields.

2.1.6.1 Features of an electric arc burning in a long channel

The simplest design of a linear plasma torch comprises of a long cylindrical tube with a heated gas flowing through it and two electrodes between which an electrical arc is ignited (see Figure 2.4). One of the most important phenomena in this arc chamber is the interaction between the electric arc and the gas flow, as this determines the gas flow structure and arc character along the channel.

The gas flow structure can be divided into three zones:

1) In the first of these (section 0-1), the arc is stabilised on the channel axis, where the gas is heated rapidly and a low temperature layer forms (1). This layer is characterised by high

2.1.6.2 Shunting

Shunting is an electric breakdown between the arc and the chamber wall (see Figure 2.5). It is the most characteristic physical process in the arc chamber. Large-scale shunting (2) defines the arc length, the length of the failure zone on the surface of electrode A along the discharge chamber, pulsation and other characteristics of the plasma torch.

The arc-electrode surface shunting (4) in the near-wall gas layer and the arc-arc shunting formed in the arc loop are referred to as small-scale shunting. This defines mainly the erosion rate of the electrode material. Small-scale shunting causes additional arc voltage pulsations whose amplitude and frequency differ by an order of magnitude from those caused by large-scale shunting. The arc spot on a cold water-cooled copper electrode moves irregularly in the direction of the gas flow because of small-scale shunting in the near-wall layer. Arc-arc shunting impedes the displacement of the arc spot and thus accelerates electrode failure.

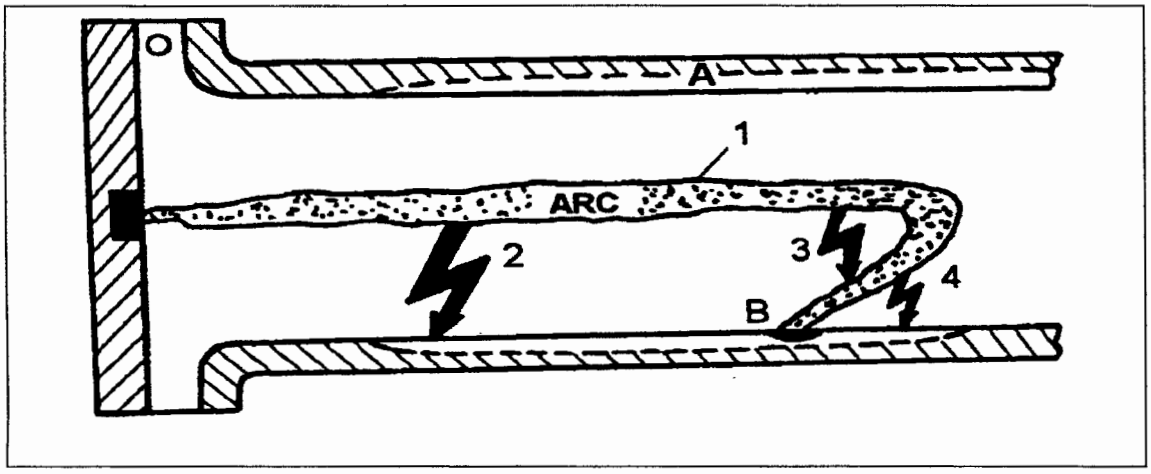

Figure 2.5: Arc shunting in an electric discharge

All types of shunting results not only in length, voltage and current pulsations, but also in changes of temperature and gas flow velocity. Thus, the gas ejected by the nozzle consists of alternating hot and relatively cold regions.

2.1.6.3 Classification of linear plasma torches

Linear plasma torches belong to the widest class of plasma generators, having a great variety of designs. They can be grouped, however, into three main classes according to the physical processes occurring in the arc chamber.

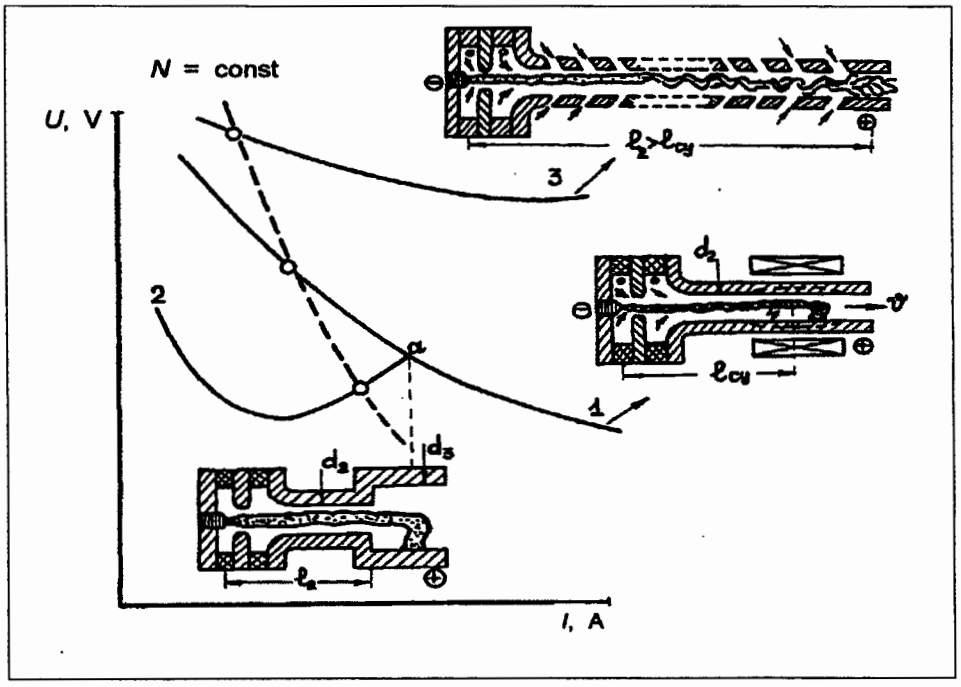

Figure 2.6: V-A characteristic of different linear plasma torches

1. The first class incorporates plasma torches widely used in the industry. They are equipped with a tubular output electrode and have a self-stabilised arc length. Its V-A characteristics fall (see Figure 2.6, curve 1). The mean arc length is the current function if the other parameters are constant. The variation mechanism of the arc length is defined by large-scale shunting occurring in the transient zone of the discharge chamber.

2. The second class consists of plasma torches, whose mean arc length is constant for a rather wide range of currents, providing other parameters are constant. This arc length is always smaller than the self-stabilised arc length. There are several ways of providing a constant arc length. One of the most popular is based on a cascade design of the output electrode, consisting of two cylinders with different diameters, the diameter of the outlet part of the electrode (d_3) being larger than the initial one. The arc length is fixed by this step in electrode diameter as it induces the transient zone of the arc and large-scale shunting prevails in this zone. The V-A characteristic lies below that of the self-stabilised arc and has rising and falling branches. These plasma torches operate steadily on the rising branch of the V-A characteristic (Figure 2.6, curve 2). Fixing the mean arc length substantially expands the range of the V-A characteristics on the V-I plane and provides possibilities of designing plasma torches with a wide spectrum of powers.

3. In the third type of linear plasma torch the mean arc length is also constant, but its is greater than the self stabilised arc length and its V-A characteristics lies above those of the other two (Figure 2.6, curve 3). The mean arc-length is increased using an inter-electrode insert/insulator between a cathode and an anode. A block modular scheme of a plasma torch with inter-electrode inserts is favoured. Each step of the module is an element of an individual segmented plasma torch. When passing from one section to another, the internal diameter of the channel increases.

2.1.6.4 Heat transfer in the arc chamber

Heat losses from the arc to the chamber walls determines the efficiency of the conversion of electrical energy to thermal energy. Heat losses in the initial section of the gas flow are caused mainly by radiation. The heat losses then increase rapidly, due to the increase in the mean gas temperature and the appearance of convective heat exchange between the gas and the wall. Along the fully developed turbulent section, the heat losses due to convective heat exchange continue to increase together with radiant heat fluxes.

2.1.6.5 Electrode erosion

Electrodes are the main units of a plasma torch and therefore largely determine its lifetime. Their erosion is defined by thermal loads, which are directly associated with physical processes in the near-electrode regions of an arc discharge, on the electrode surface and in the crystal lattice of the metal. Erosion is quantified as mass loss per coulomb charge.

A melting zone is often observed at the centre of the cathode. Lengthening the lifetime of the cathode unit remains a problem, but two methods are employed more or less successfully up to 1000 A. The first is based on designing a multi-position electrode unit. This consists of a water-cooled copper drum equipped with circumferentially placed inserts of an emitting material. The distance between the rods and their number are chosen in accordance with the required lifetime of continuous operation. The second method is based on the "splitting" of a near-cathode and, in particular, a radial closing section of the arc into several current-conducting channels. Detailed investigations of both the aerodynamics in an end hollow cylindrical electrode and the V-A characteristics of radial sections of the arc allowed such splitting to be realised.

In linear plasma torches, the output electrode usually serves as the anode. The arc spot displacement over its surface is defined by large- and small-scale shunting and by the circumferential velocity component. The erosion rate of the anode is mostly constant over a wide range of currents, but above a certain critical current, characteristic of each electrode diameter, an abrupt increase in erosion is observed. This is probably caused by the anode jet favouring premature shunting, long-term stay of the arc spot in an immovable state and the variation of the velocity field in the radial direction. Arc spot motion along some rational trajectory over the electrode surface with some fixed frequency results in a considerable decrease in erosion rate.

2.2 Plasma Chemistry

2.2.1 General Introduction[22]

Plasma chemistry is that branch of chemistry concerned with the reactions of the species found in plasmas (that is atoms, free radicals, ions and electrons), both between themselves and with other molecules in the gaseous, liquid or solid state. Early studies of discharges in gases were done by investigators such as Michael Faraday and Sir William Crookes. Crookes was the first to suggest (in 1879) that such gases could be regarded as the fourth sate of matter. Langmuir was the first to use the word *plasma* to denote ionised gases in the early 1930s. The degree of ionisation may range from small to very high. Within this range, gases may show a variety of physical and chemical properties that are entirely different from their normal properties.

In 1920 Wood showed that hydrogen atoms were produced in good yield when hydrogen was passed through a discharge tube. These hydrogen atoms could be pumped out of the discharge in large quantities and carried along for some distance before recombination was complete. The technique introduced by Wood, and modifications thereof, was later also used to study oxygen, halogens and nitrogen atoms and their reactions. The results of the interactions of free radicals that are formed in a discharge were first noted in the late 1920's and early 1930's when a number of workers examined the breakdown of a variety of hydrocarbons. They found polymerisation effects, as well as the formation of new products.

During this earlier period, many studies were also done on the recombination of atoms. These included assessments of the efficiency of various materials and the effects of admixed gases to promote recombination. Investigations were also done on the detection and estimation of the concentration of atoms and radicals. A considerable amount of work has also been done on the stabilisation of free radicals. Under suitable conditions of preparation, free atom and other low molecular weight radicals may be captured and stored for long periods, usually in solidified gases at low temperatures. These so-called matrix isolation studies of trapped radicals extended the knowledge on the interactions of these species with solid lattices, the possibilities of energy storage for purposes of propulsion, the structures of polymers and the role of free radicals in chemical reactions.

2.2.2 Plasma Species and their Reactions

The types of species produced in the plasma and their relative abundance are determined by the conditions that exist within the discharge, especially temperature.[2] The complexity of the system represents a serious problem when investigating reaction mechanisms. Apart from the various forms of atoms and ions (or the molecules produced by their association), radicals may also result when a molecule consisting of two or more different atoms dissociates in a plasma. The mechanism that most frequently gives rise to radicals from gaseous molecules is the removal of an atom. Fragments resulting from these dissociations are usually produced in the ground state.[22]

Processes that may occur between plasma species are as follows:[22]

- At the lowest electron energy, electron addition by electron resonance capture usually occurs to give a negative ion:

$$AB + e \rightarrow AB^-$$

- This ion may dissociate to give a neutral atom and a negative ion:

$$AB^- \rightarrow A + B^-$$

- At higher energies the production of ions may be:

$$AB + e \rightarrow A^+ + B^- + e$$

- At still higher levels of energy the positive molecular ion is formed:

$$AB + e \rightarrow AB^+ + 2e$$

- This may dissociate to give a positive ion together with a radical or atom:

$$AB^+ \rightarrow A^+ + B$$

- Dissociation without ionisation may also occur:

$$AB + e \rightarrow A + B + e$$

After breakdown of a gas has been achieved, a steady state is soon reached in which there is an equilibrium between the rate of formation of ions and free atoms and the rate of their recombination. The recombination occurs mainly on the walls of the containing vessel. Recombination of ions can be either ion-ion recombination or ion-electron recombination.

Three possibilities of ion-ion recombination exist:[22]

i) The energy of the ions is released as heat during recombination:

$$A^+ + B^- \rightarrow AB + h$$

ii) The molecule formed possesses sufficient energy for its own dissociation:

$$A^+ + B^- \rightarrow A^* + B^*$$

iii) The energy carried by the ions is lost due to collision with a third body:

$$M + A^+ + B^- \rightarrow AB + M$$

The first two, being two body collisions, are of most importance at very low pressures, and the last, a third body induced recombination, assumes major importance at higher pressures. It is possible to produce a wide variety of radicals, since the energy required is well within range of those available in plasma discharges. The majority of reaction involving radicals can be designated as breakdown and regrouping.[22]

Collisions between free radicals result in a collision complex with a much greater lifetime than that of atoms. This is because the large number of internal degrees of freedom allows a redistribution of internal energy, so that deactivation usually occurs. The collisional efficiency of recombination is therefore close to unity for simple radicals. For radicals that are more complex the efficiency drops due to steric effects. At a certain pressure, it is thus easier to extract atoms in reasonable concentration from a discharge, than it is to extract radicals. When like radicals combine, two types of reactions are commonly found:

i) Disproportionation, e.g. $2C_2H_5 \rightarrow C_2H_4 + C_2H_6$

ii) Combination, e.g. $2C_2H_5 \rightarrow C_4H_{10}$

Considering the many possible recombination reactions of a number of different radicals, it is obvious that the products may be numerous.[22]

The chemical reactions that occur between ions and molecules have been studied fairly well, using mass spectrometers. The known reactions may be grouped into three classes[22]:

i) *Positive ion and neutral atom transfer*: These often result in new molecular species, e.g.

$$H_2^+ + H_2 \rightarrow H_3^+ + H$$

ii) *Hydride ion transfer*: For example

$$C_3H_5^+ + C_5H_{12} \rightarrow C_5H_{11}^+ + C_3H_6$$

iii) *Condensation reactions*: These involve considerably more molecular rearrangement than the transfer of an atom or atomic bond. In the majority C-C bond formation occurs, e.g.

$$CH_4^+ + C_2H_4 \rightarrow C_3H_5^+ + H_2 + H$$

The study of negative ions is more difficult than that of positive ions and only a limited number of these reactions are known. An example is[22]:

$$H^- + H_2O \rightarrow OH^- + H_2$$

2.2.3 Application of Plasma Chemistry

There are two broad classes of reactions to which plasma processing is applicable. The first consists of reactions that are favoured by high temperatures. These are the strongly endothermic reactions where the free energy decreases with increasing temperature. The temperature range for these reactions is typically from 3000 to 8000 K. The second consists of reactions involving active species that are unstable at normal temperature. The mixture of active species produced by the plasma must be quenched properly in order to produce the desired products. The plasma generated for this class of reaction can be either at a high or relatively low gas temperature.[2]

In evaluating candidates for plasma reactions on an industrial scale, several requirements should be considered to decide on a successful process. First, as discussed above, the reaction must be favoured from either a thermodynamic or a kinetic point of view by the plasma state. Second, the products of the process should have a high unit value as plasma processing is not a cheap method for carrying out reactions. A third requirement is that the reaction step must be important relative

to the separation and purification steps. Other requirements include cheap raw materials, high yields, low capital investment, high production volume and a minimum number of process steps. A process that meets all of these requirements would be very advantageous, but a proper combination of several can offset failure to fulfil the others.[2]

All plasma processes have certain features in common[2]:

- *Plasma generation*: This involves the intense heating of the feed reactants, i.e. the plasma must be generated in or mixed with the raw materials to be processed. For this purpose, any of a number of plasma generators can be used. The generator serves to couple electric energy efficiently into the gas stream.
- *Chemical reaction*: Sufficient time and an appropriate environment must be provided to permit the chemical and physical changes induced by the plasma to take place. A second reactant can also be added to the main reagent stream leaving the plasma generator to induce combination reactions.
- *Quenching*: Finally the reactants must be removed from the plasma state in such a way that the desired products are formed or maintained. Several techniques are available for quenching at rates from 10^5 to 10^8 K/s. These include cold surfaces, cold gas entrainment and fluidised beds.

These three main steps occur typically in times of the order of milliseconds.

A high-intensity thermal arc can be exploited as a chemical reactor by introducing reactants into the high-temperature arc region or into the tail flame of the arc. The reactants may be introduced as a solid, liquid or gas and/or be produced as a result of electrode evaporation. Important advantages of the arc reactor used in chemical synthesis are:

- Extremely high temperatures in the reaction zone resulting in high reaction rates.
- Very high throughputs because of rapid reaction rates and rapid coupling of energy into reactants, resulting in a small reactor volume.
- Production of high concentrations of very reactive species not available at conventional chemical reactor temperatures.
- Simple, versatile, small-scale equipment requirements.[1]
- Utilisation of "waste materials" as feed.
- Not sensitive to impurities in the feeding materials.

Disadvantages are:

- Special materials of construction are needed to handle the high temperatures and corrosive gases.
- Compact layout requires careful mechanical design for scaling due to different thermal expansions of different construction materials.
- Certain components may have a limited lifetime due to the extreme operating conditions.[25]

2.2.4 Specific Application: Production of Tetrafluoroethylene

The advantages of using a plasma system for producing tetrafluoroethylene in comparison with freon based plants, are: (i) less effluent is produced and, (ii) the plasma system can be controlled to produce various different fluorocarbon gases in addition to tetrafluoroethylene.

2.2.4.1 Baddour & Bronfin[1,2]

Tetrafluoroethylene was synthesised by the reaction of carbon tetrafluoride and carbon in a high-intensity carbon arc followed by rapid quenching.

A stable dc arc is sustained easily between carbon electrodes. If the current through the arc is increased after initiation of the arc, the current flux will eventually cover the entire anode face and any further increase in current results in an increase in current density. At anodic current densities between 100 and 400 amperes/cm^2 the energy flux at the anode surface is likely to exceed the radiational and convectional cooling necessary to preserve the anode. Graphite vaporisation occurs, creating a luminous "tail flame" of carbon vapour. To sustain the arc during anode consumption, the anode must be advanced to maintain the small gap between the electrodes. The temperature of this high-intensity arc is well above 6000 K.

The experimental reactor used by Baddour and Bronfin is shown in Figure 2.7. It consisted of four electrically insulated sections. The central section served as the arc reaction chamber. The long anode sections, designed to allow a continuous motor-driven feed of a graphite rod, were mounted at one of the four ports. Two anode configurations were used: (i) the first was a centre-bored anode which fed the reactant gas into the centre of the formed plasma; (ii) the second consisted of a solid graphite rod, with the reactant gas flowing along the outside of the anode, passing through the arc current path and into the hollow cathode.

The stationary graphite cathode was mounted at the opposite port. The gas pressure inside the reaction chamber was stabilised by withdrawing gas continuously through the hollow cathode to a high-capacity vacuum pump. Provision was made at the last insulated section to position a water-cooled hypothermic probe at variable positions down the centreline of the hollow cathode. All metal parts of the reactor were water-cooled. Power was fed through the electrodes from series-operated motor-generators supplying up to 25 kW direct current. The arc was initiated by a high-frequency, high-voltage spark. A magnetic field of approximately 200 gauss was imposed along the electrode central axis to promote mixing of cold reactant gas with the plasma by rapid rotation of the arc column. A continuous quenched gas-product was taken through the probe positioned in the tail flame.

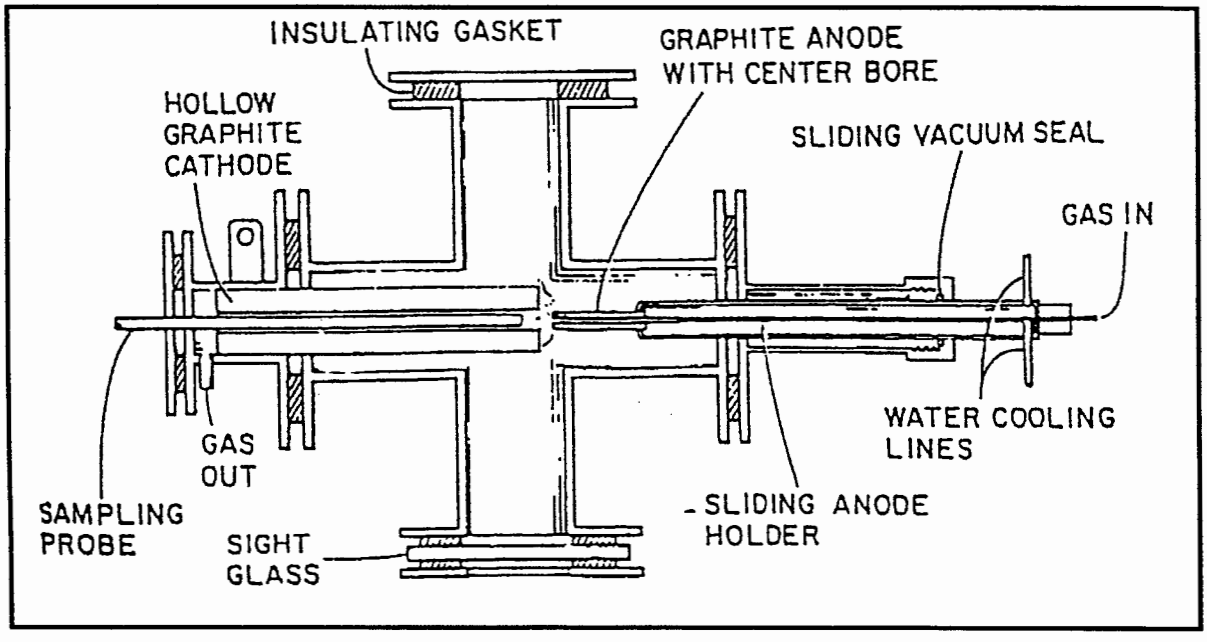

Figure 2.7: Carbon arc reactor used by Baddour and Bronfin

A series of runs were made in which the feed rate of the CF_4, the power and the chamber pressure were varied. Data were collected with the entrance to the quench probe immersed in the tail flame and positioned 1 to 2 inches back from the cathode face. The major constituent of the quenched gas was C_2F_4; the remainder consisted chiefly of CF_4 with small amounts of C_2F_6 and C_3F_8. The highest TFE concentration found was 69 mole %. The TFE yield increased with a decrease in pressure and an increase in power. Variation of the CF_4-reactant feed rate had little effect on the TFE yield.

A reaction mechanism was postulated based on local thermochemical equilibrium in the carbon-fluorine plasma. Full thermochemical equilibrium predicts F, C_2F_2 and various gaseous carbon species as the dominant species in the range 2000 to 5000 K, the temperature of the tail flame of the high-intensity carbon arc. The importance of C_2F_2 as a precursor is increased at lower pressure. The presence of high concentrations of TFE, which is not present in the high-temperature plasma, in the quenched gas, may be a result of the following reactions occurring in the quench probe:

$$C_2F_2 + F \rightarrow C_2F_3$$
$$C_2F_3 + F \rightarrow C_2F_4 \quad ...(1)$$

$$2CF_2 \rightarrow C_2F_4 \quad ...(2)$$

$$2C_2F_2 \rightarrow C_2F_4 + 2C(s) \quad ...(3)$$

The presence of CF_4 in the quenched gas can be attributed to some bypassing of feed reagent, but also to fluorination reactions in the quench probe:

$$C + F \rightarrow CF$$
$$CF + F \rightarrow CF_2$$
$$CF_2 + F \rightarrow CF_3$$
$$CF_3 + F \rightarrow CF_4 \quad ...(4)$$

The gaseous species, C_1, C_2, C_3, ..., can participate in the foregoing reactions or condense on the quench probe walls. Because of the lack of reaction rate data, it is difficult to determine the extent to which each of these competing reactions contributes.

2.2.4.2 Russia[23]

Research was done in Russia between 1965 and 1980 on the plasma-based synthesis of TFE. Three methods were investigated: (i) TFE from CF_4 as plasma gas, using a consumable graphite anode, (ii) TFE from cyclic-C_4F_8 using a graphite cathode and, (iii) TFE from CF_4, carbon and F_2 using a pyrolysis reactor and graphite electrodes.

The first method gave TFE yields of up to 45 mole % for C:F ratios between 0.5 and 0.55. Other by-products formed were CF_4, C_2F_6, C_3F_6 and C_3F_8. Blockages of the quench probe, because of carbon depositing on the cold surfaces, were however a great problem. For the third method, carbon powder was heated first in a carbon-F_2 furnace, which also contained carbon rods. The pyrolysis products entered the plasma reactor, consisting of a V-type plasmatron and a graphite

lined reactor, at temperatures of 1400-1500 K. The plasma product was quenched with CF_4 gas. TFE yields of 35-38 mole % were obtained, but the yield decreased as the carbon rods in the pyrolysis reactor were consumed.

These investigations indicated that the C:F ratio in the reactor should not be lower than 0.5 for optimum TFE yields. The temperature at which the plasma product gas must be quenched should be in the range of 3250 to 3500 K and the quenching rate should be in the order of 10^6 K/s. Graphite electrodes should be made from very pure graphite, while the particle size of carbon particles used should not exceed 0.2 mm.

2.2.4.3 Atomic Energy Corporation of SA[23,25]

The use of dc plasma torches using both consumable and non-consumable anodes has been investigated at the AEC. Experimental work done at the AEC indicated that processes using a consumable anode could not be operated continuously for more than two hours, as the carbon that evaporated from the carbon anode deposited on the cooler areas of the reactor and the quench probe, which resulted in blockages. The use of a carbon bed as quenching medium resulted in very low TFE yields. A process utilising a non-consumable anode was therefore developed, using carbon particles injected into the plasma tail flame as the carbon source. This process can be subdivided into a plasma torch, a reactor and a quench probe. The advantages of this process in comparison with the process using a consumable anode are: (i) carbon particles are cheaper than graphite electrodes, (ii) recycling of by-products is possible and, (ii) the different process steps can be controlled and optimised separately.

The plasma torch consists of a copper cathode, with a small graphite insert, and a cylindrical hollow copper anode. The plasma is initiated with a high-voltage starter, initially using argon as the plasma gas, but after initiation the plasma is operated with CF_4 as the plasma gas. Carbon particles are fed into the plasma tail flame just below the anode, using CF_4 as carrier gas. After a short residence time in the reactor lined with graphite, the resulting product gas is quenched with the aid of a water-cooled quench probe. The quench rate should be of the order of 10^6 K/s and the gas should be quenched to temperatures lower than 1500 °C to obtain reasonable TFE yields. Unreacted carbon is removed with the aid of two filters. All of the components are water-cooled.

Maximum TFE yields of about 40 mole % have been obtained in a laboratory scale reactor, utilising electric power in the region of 30 kW and pressures in the region of 10 kPa. The yield decreases with increasing pressure, but increases with increasing plasma enthalpy.

Thermodynamic data used by Bronfin and Baddour[1,2] were only estimations. In 1993 Swanepoel of the AEC redid the thermodynamic study of the dissociation of CF_4 using new available data. The calculations were done by using the technique of direct minimisation of the Gibbs free energy. The main difference between Swanepoel's and Bronfin and Baddour's results was that Swanepoel found CF_2 to be a more important precursor than C_2F_2, whereas the latter was found by Bronfin *et al.* to be the main precursor. Trunov[23] also found CF_2 to be an important precursor and suggested the following reaction in the place of reaction (3) shown in Section 2.2.4.1:

$$C_2F_2 + C(s) \rightarrow CF_2 + 2C(s)$$

A more detailed discussion of the work done at the AEC is found in Section 2.4.

2.3 Patents Pertaining to Plasma Production of TFE

Since 1955 quite a number of patents has been filed on the plasma production of tetrafluoroethylene (TFE) and other associated fluorocarbons. A brief summary of some of these patents is given in Table 2.1.

Table 2.1: Patents pertaining to the plasma production of TFE and other fluorocarbons

Ref. No.	*Inventors*	*Process description*	*Feeding materials*	*Products*	*Method*	*Operating Conditions*
9	J.T. Denison F.E. Edlin G.H. Whipple	Gaseous organic or inorganic fluoride compounds are heated to 1700 °C and higher. The resultant gaseous products are reacted with an excess of fine carbon particles and then quenched rapidly to enhance TFE formation. The reaction rate is increased greatly when fluidised carbon, at a temperature lower than 500 °C, is used as a quenching medium.	Any organic or inorganic fluorine compound that will decompose to give fluoro-carbon radicals or mono-atomic fluorine or will react with carbon in the pyrolysis zone to form these compounds. Any form of carbon with a large surface area is suitable for quenching.	Primarily the starting material or its de-composition products and fluorocarbons, the most dominant of which are CF_4 and TFE. **TFE yields of 30-80 mole%** were obtained, depending on the quenching medium.	Preferred: The gaseous fluorine compound is passed through an arc between two concentric graphite or carbon electrodes. For uniform heating a magnetically rotating arc is used. It rotates in a gap, supplied by a hollow electrode, through which all the gas must pass to leave the arc chamber. These product gases are then brought into contact with carbon particles at temperatures lower than 500 °C, small enough to be drawn into the gas stream. The gas can also be heated by passing it through a graphite tube heated to 1700-2500 °C by an electrical resistance furnace.	-Temperature of pyrolyzed gas must be higher than 1600 °C before quenching. -Operation at atmospheric pressure is possible, but better conversions are ob-tained at lower pressures -The weight ratio of carbon to the reactant gas should be 10 : 1 or higher. -The temperature of the quenching carbon must be as low as possible.
10	M.W. Farlow	TFE is prepared when a perfluorocarbon of the formula C_xF_y, which is a liquid at room temperature or lower, is pyrolyzed by heating at a temperature of at least 1500 °C.	Perfluorocarbons of the formula C_xF_y, where x and y are positive whole numbers with x being at least three and the ratio of y to x is less than 2.7:1.	A mixture of fluoro-carbons, containing TFE, CF_4, C_3F_6, C_3F_8, and C_2F_6 and minor amounts of other per-fluorocarbons that can also be converted to TFE if recycled. A **50 mole% TFE yield** was obtained.	For pyrolysis of the fluorocarbons it must be passed through a reaction zone heated to at least 1500 °C and preferably 2000-4000 °C. The reaction zone can be a hollow tube of refractory material heated externally or the reactant can be exposed to an electric arc. A carbon arc is especially suitable. Practical conversions to TFE are obtained only if the hot pyrolysis gases are cooled in 0.001 to 01 second to below 400 °C.	-The reactor pressure can range from vacuum to superatmospheric. Low pressures are preferred for operating the carbon arc. -Optimum flow rate of reactant depends on the electric power of the arc or the capacity of the external heater.

11	M.W. Farlow	TFE is synthesized by passing a saturated fluorocarbon, such as CF_4, through a carbon arc, after which the resulting gaseous products are passed at 2700-2000 °C through a carbon bed and then quenched rapidly to a temperature below 500 °C.	Saturated fluorocarbons that, when heated to arc temperatures, decomposes into fluorocarbon and fluorine radicals that are only stable at these high temperatures.	On rapid quenching C-rich radicals form TFE; the others form CF_4 and other F-rich compounds. **48-87 % TFE yields** were obtained depending on reactor design.	The reactor comprised of an electric arc rotated magnetically between two electrodes, through which the reactant is passed, a carbon bed in which the carbon-rich radicals, like CF and CF_4 are formed and a quenching mechanism where these are allowed to combine to form TFE, without forming radicals which lead to the formation of saturated fluorocarbons.	-A dc arc is preferred, the operating conditions of which can vary, depending on the reactant's flow rate and the arc's temperature. -The pressure in the process is preferably maintained below 50 kPa.
12	M.W. Farlow E.L. Muettertles	Fluorocarbons, including TFE, are synthesized by reacting carbon, at the temperature of a carbon arc, with a binary fluoride of silicon and rapidly cooling the resultant reaction mixture to below 400 °C. The fluorocarbons can be separated from the cooled mixture and the unreacted silicon fluoride recycled.	Binary fluorides of silicon of which the best known are SiF_4 and Si_2F_6, both gases under normal conditions. Metal fluosilicates, like barium or sodium fluosilicate, can also be used in anhydrous form which dissociates at relatively low temperatures to give SiF_4.	Unreacted silicon fluorides and fluorocarbons, containing TFE and CF_4 and minor amounts of others, like C_2F_6. Elemental silicon that reacts with O_2 to give silica, is also obtained. **TFE yields were 1.4 - 7 mole%.**	A gaseous silicon fluoride is passed through an arc produced between two carbon electrodes, or a finely divided, anhydrous metal fluosilicate is blown through the arc. The carbon for the reaction is preferably from the graphite electrodes, but fine carbon can also be blown through the arc. The reaction mixture obtained is quenched rapidly (in 0.001 to 0.1 second) to below 400 °C to minimize the decomposition of the TFE.	-Temperatures must be very high, typically that of a carbon arc (~6000 °C) -Low reaction pressures are preferred since this eases operation of the arc. -The optimum reactant gas flow rate depends on the arc's electric power input (the higher the power, the higher the rate).
13	M.W. Farlow E.L. Muettertles	TFE is prepared by bringing elemental fluorine in contact with carbon at a temperature of at least 1400 °C and then cooling the reaction product to below 500 °C in less than a second.	Any form of carbon, amorphous or crystalline, is suitable (graphite electrodes for the arc and either graphite or active carbon for the heated tubular reactor).	Mainly CF_4 and TFE, with minor amounts of other saturated fluorocarbons, like C_2F_6 and C_3F_8. **TFE yields were 4 – 10 mole%.**	i) $F_2(g)$ with inert carrier gas, is passed through a carbon column in an electrical furnace. ii) $F_2(g)$ is passed through a carbon arc and reacts with the carbon electrodes. In both cases the reaction product is cooled rapidly and unreacted fluorine removed quickly to prevent further reaction with the TFE.	-Preferred reaction pressure is less than 60 kPa. -Minimum reaction temp. is 1400 °C; preferably higher than 2000 °C. -Quenching must be done in 0.001 to 0.1 second.

21	B.S. Malone	TFE is prepared by heating a C_1 to C_{10} compound containing fluorine and hydrogen in the presence of an inert gas, like N_2, Ar, etc. to a temperature of at least 2000 °C. The reaction mixture is then cooled to below 800 °C in less than a second.	A C_1 to C_{10} hydrofluoro-carbon, of which the F:H as well as the F:C ratios should be ≥ 1. C_2HF_5 and/or CHF_3 are preferred. The preferred inert gas is argon.	A mixture of fluoro-carbons and hydro-fluorocarbons. The **TFE yield varied from 43 up to 83 mole%** with more rapid quenching.	The inert gas is heated by passing it through an arc. The gas is allowed to relax, i.e. it may contain excited ions, but no free electrons, before coming into contact with the C-H-F compound. The temperature of the gas is controlled by the power input of the plasma source and the contact time between the gas and the carbon compound by quenching.	-A dc arc is preferred. -Preferably no organics must be present at starting. –Reaction pressures may range from 10-1000 kPa, but preferably 10-100 kPa -Contact time: 0.002-0.1 s -Quench time: 0.001-0.1 s
27	I.G. Sayce	This invention presents a direct process for preparing fluorine or volatile fluorine compounds by the electrolysis of molten fluoride, e.g. calcium fluoride, using a plasma electrode as the anode. An arc can also be struck between a consumable carbon electrode and the electrolyte.	Any electrically conducting molten fluoride can be used as electrolyte. The plasma electrodes are usually opera-ted on an inert gas. The electrode material must be unreactive to the melt and the electrolysis products.	Fluorine or volatile fluorine compounds, including TFE, are produced at the anode and a metal is formed at the cathode.	The plasma anode can be a dc plasma jet in the laminar mode. This electrode can also be used to heat the electrolyte initially to obtain a melt. During electrolysis electrons proceed from the plasma torch to the arc root on the surface of the fluoride electrolyte, enter the electrolyte and neutralise cations. The circuit is completed through a second electrode - a plasma or a conventional cathode - and a power source.	
32	J.K. Wolfe N.C. Cook	Fluorocarbons are prepared by reacting a fluoride of a group IIA element of the periodic table and carbon at high temperatures. If mixed chlorofluorocarbons are desired, a metal chloride can be added to the reaction mixture.	Fluorides of the elements of group IIA on the periodic table, preferably in the anhydrous form. Carbon can be added by way of a carbon arc or as part of the container. Pure carbon is preferred as it results in fewer by-products.	A mixture of fluoro-carbons or chloro-fluorocarbons, depen-ding on the reactants used.	Electric furnaces can be used to produce the high temperatures necessary for the reaction. The arc furnaces is preferred and for this invention a carbon arc is used. Either a transferred arc, where the current passes from one electrode to the reaction mixture, or an indirect arc between two electrodes may be used. The reaction should be carried out in an inert atmosphere to reduce the amount of by-products, such as oxides of carbon.	-The ratio of reactants is not critical, but an excess of carbon is usually used. -For high melting reactants a reaction temperature at which the mixture is molten, is advantageous.

2.4 Research done at the AEC[23,25]

Research on the plasma-based synthesis of fluorinated compounds was started at the AEC in 1991. Initial chemical thermodynamic equilibrium calculations suggested a simple synthesis method for producing TFE: (i) obtain the required C/F ratio in the plasma phase at the correct temperature and pressure, (ii) quench the plasma product as fast as possible and, (iii) separate the resulting mixture. Homogeneous kinetics simulation has indicated that operation of the plasma at 10 kPa should give a maximum TFE yield of 50 mole % at a temperature of 2600 K. Yields of TFE from experiments done on the system described in Section 2.4.3 are however, typically less than 35 mole %.

Moore[23] continued the thermodynamic studies done by Swanepoel (see Section 2.2.4.3). She did a complete thermodynamic study on the reaction between CF_4 and carbon at plasma temperatures to determine the optimum operating conditions, using the computer package, ASTRA, that was developed by B.G. Trusov in Russia. This package simulates heterogeneous systems at chemical equilibrium, based on the fundamental principal that the entropy of an isolated system reaches a maximum at equilibrium, and contains a extended database that can be adapted by the user. Complete thermodynamic equilibrium (CTE) in the plasma was assumed for the calculation of the equilibrium composition. The reaction mechanism used for the calculations was that of Alexeev[23]:

$$CF + F \rightarrow CF_2 \quad ...(1)$$

$$CF_2 + 2F \rightarrow CF_4 \quad ...(2)$$

$$CF_3 + F \rightarrow CF_4 \quad ...(3)$$

$$CF_2 + CF_2 \rightarrow C_2F_4 \quad ...(4)$$

$$2C_2F_2 \rightarrow C_2F_4 + 2C(s) \quad ...(5)$$

The thermodynamic calculations were done for different C:F ratios and reactor pressure for every 20 K over a temperature range of 1000 to 6000 K. Output from ASTRA consists, among other things, of the concentrations in [moles/kg feeding material] of all the species present and an enthalpy value that can be used to calculate the total energy needed for the reactions. The maximum TFE yield possible was also calculated. Some of the results obtained from these calculations were:

- The enthalpy of the reaction system can rise sharply for only a small increase in reaction temperature.
- Less energy is needed for higher C:F ratios to reach the same reaction temperature.
- The concentration of the precursor C_2F_2 increases sharply with an increase in the C:F ratio, while the enthalpy needed to obtain the maximum concentration of this precursor decreases.
- The concentration peaks of the three intermediate species, C_2F_2, CF_2 and CF broadened for an increase in the C:F ratio.

The thermodynamic results obtained were compared to experimental results and were found to correspond well within a statistical significance standard of 5%.

The TFE yield was optimised with the use of an experimental simplex that is based on the mathematical principle that the optimum of a linear programming problem is associated with an extreme value in the solution space. The most sensitive parameters in the process were identified with the use of correlation analysis as: (i) particle size of the carbon, (ii) reactor length, (iii) plasma-enthalpy, (iv) mixing enthalpy, (v) quenching enthalpy, (vi) momentum of the carbon particles and (vii) the C:F ratio. Of these parameters the plasma enthalpy, the reactor length and the flow rate of the CF_4 carrier gas (on which the momentum of the particles is dependent) were chosen as the three factors for the experimental simplex. All other parameters were kept constant. Four iterations of the simplex indicated a maximum TFE yield of 38.6% at a related energy cost of 22 kWh/kg TFE. Better results could be obtained by optimising more parameters, but then the experimental space would also be larger. It is also possible that the TFE yield is more sensitive to other parameters than the chosen three.

A quadratic polynomial was fitted to the experimental data in order to obtain mathematical curves to summarise the data and to observe possible trends. The following polynomial was used (n = 3):

$$Y = C_o + \sum_{i=1}^{n} C_i X_i + \sum_{i=1}^{n} \sum_{j=1}^{i} C_{ij} X_i X_j$$

where Y is the response parameter (either TFE yield or specific enthalpy in kWh/ kg TFE), X_1 the flow rate of the CF_4 carrier gas, X_2 the reactor length and X_3 the plasma enthalpy. The cross terms were included to determine whether or not the parameters influence the system independently. After the constants were determined by minimising the sum of the square of the differences between the calculated and experimental values, graphs were plotted to describe the

behaviour of the response parameters. The graphs cannot be extrapolated and only describe trends within the experimental space. The graphs indicated that the TFE yield is assisted by high specific enthalpies and low CF_4 carrier gas flow rates.

A global empirical model was also fitted to the system. Parameters that showed a high correlation with the TFE yield were the temperature of the reaction mixture after the particles had been injected into the plasma tail flame, the quenching temperature, the reactor length, reactor pressure, total CF_4 fed and the plasma enthalpy.

The process was described best by an equation of the form:

$$\%TFE = 0.2908 \times T_{mix}^{0.64} \times \tau^{-0.79}$$

where τ is the residence time of the reactants in the reactor. (τ is a function of reactor length, CF_4 flow rate and reactor pressure.) Again the above equation is only valid in the experimental space that was investigated. The standard deviation between calculated and experimental values was 4.1 % TFE.

Research was also done on the utilisation and effect of the recycling of by-products. The plasma torch was therefore also tested with the use of C_2F_6, SF_6, CHF_3 and SiF_4 as plasma gas. TFE yields were obtained for all of these gases. The recycling of C_2F_6 and C_3F_6, two of the main by-products, should therefore be possible.

Some of the main principles on the plasma synthesis of TFE established through the research at the AEC can be summarised as follow:

- TFE yields of more than 30 mole % is possible for a product cost of about 20 kWh/kg TFE and production rates of ~ 1.5 kg TFE/h.
- The product gas consists mainly of CF_4, C_2F_4, C_2F_6 and small amounts of C_3F_6.
- The mixing temperature after the particles have been injected into the plasma tail flame is lower than the evaporation temperature of carbon. Chemical evaporation, therefore, has to occur, because of the reaction of the highly reactive fluorine radicals with the carbon particles.
- The quenching rate of the plasma product gas has to be at least 10^6 K/s to obtain reasonable TFE yields.
- A high quenching enthalpy enhances the TFE yield.

- Descending V/A characteristics are obtained when the 30 kW plasma torch is operated on CF_4 gas as the plasma gas. The power source must be able to accommodate these descending V/A characteristics.
- The C:F ratio should be more than 0.65 according to the thermodynamic study.

2.5 Plasma-particle Interaction

In the thermal processing of powders under plasma conditions, whether for spheroidisation, melting, plasma spraying of protective coatings, plasma decomposition of toxic waste or chemical synthesis, the proper control of the trajectories of the particles and of their temperature history in the plasma is one of the most crucial aspects on which the overall success of the operation depends.[3,14,24,28] Plasma-particle interaction has consequently been well-studied.

2.5.1 Particle Injection

A number of techniques can be used for particle injection into a plasma jet. These techniques vary mostly with regard to the location of the point of injection and the angle of injection with respect to the axis of the jet. One configuration is to inject the particles in the anode constriction region with a slight inclination towards the upstream side of the jet. Another is to inject the powder at right angles to the plasma jet at the downstream end of the anode. A lower carrier gas flow rate is necessary for the tilted injector than for the orthogonal one in order to obtain similar trajectories. In spite of a higher velocity with the tilted injector, the particles reach a higher surface temperature due to their longer residence time in the hottest zone of the plasma jet. However, due to injection in a hotter zone of the plasma, sticking problems arise with this type of injection.[3,14] A water-cooled injection probe can be used to inject the powder right at the edge of the plasma jet to insure that the particles penetrate the plasma. This, however, can have a cooling effect on the temperature field of the plasma flow around the point of injection and can also cause serious asymmetry of the flow field in the plasma.[31]

In either case, the proper control of the injection velocity of the particles in the plasma jet is crucial to ensure that they penetrate the hot region of the plasma and acquire as close as possible

an axial trajectory. For a given plasma jet, the momentum of the particles have to be adapted to that of the jet in order to ensure that their residence time is as long as possible in the hot zones of the jet. When the flow rate of the carrier gas is too low, the particles do not penetrate the plasma jet; if it is too high, they pass through it. For a given powder and a given injector geometry, the smaller the particles, the higher must be the carrier gas flow rate.[3.14] Even a powder with a very narrow particle size distribution can still have a wide range of trajectories, resulting in a spread of particles over a large region of the plasma.[31]

An increase in the plasma gas flow rate results in an increase in particle velocity and a more uniform distribution of the particle flux number density in the plasma jet. The particle temperature decreases, however, due to the lower specific enthalpy of the plasma at these conditions and to the shorter residence time of the particles in the higher flowing plasma jet.[31]

The pneumatic transport of powders in small diameter tubes suffers from an excessive loss of particle kinetic energy through particle-wall interactions. This results in a large slip between the gas and the particle transport velocities. For a 2 mm diameter tube, the average particle velocity in the transport line can be as low as one third that of the carrier gas velocity. The slip between the particle and gas velocities is reduced with an increase in the diameter of the particle transport line. The average particle velocity reaches typical asymptotic values of 0.6 to 0.8 that of the carrier gas for tubes with an inside diameter larger than 6 to 8 mm. The collisions between the particles and the injector wall also result in high radial velocity components. Smaller particles, due to their broader velocity distributions, as they follow the motion within eddies in the plasma flow more closely, have a much broader trajectory distribution than large particles for which the velocity distribution is narrower.[3,14,24,31]

Another important factor that can have quite a substantial influence on the efficiency of the powder heating, is the effect of the carrier gas on the flow and temperature of the plasma. The higher the flow rate of the carrier gas and the smaller the inside diameter of the injector, the higher will be the disturbance and cooling of the plasma. Research has shown that, especially for small particles which need a high carrier gas flow, it is advantageous to use two powder injectors opposing to each other. In this case, the particle distribution within the plasma exhibits a cylindrical symmetry.[3.14]

2.5.2 Plasma-particle Mass, Momentum and Heat Transfer

Correlations pertaining to mass, momentum and heat transfer between the plasma and particles are summarised in Table 2.2. The correlations deal mainly with interactions between the plasma and a single, spherical particle. Attention is also given to internal heat conduction in the particle as well as particle melting and evaporation. An explanation of the symbols is found at the end of this chapter.

Considerable attention has been given to the study of the flow and temperature fields around single spheres. Typical flow patterns as a function of the particle Reynolds number are given in Figures 2.8 and 2.9.[3,14] These are limited to values of the particle Reynolds number smaller than 100, which are normally encountered under plasma conditions. The particle Reynolds number is defined as:

$$Re = \frac{\rho\, U_R d_p}{\mu} \qquad (5.1)$$

U_R is the relative velocity between the particle and its surroundings, defined as :

$$U_R = \sqrt{(U - U_p)^2 + (V - V_p)^2} \qquad (5.2)$$

As seen in Figure 2.8(a) an increase in the particle Reynolds number results in a gradual shift of the flow pattern from the typical symmetric Stokes flow regime for $Re < 0.01$ to the viscous, but slightly non-symmetric (upstream versus downstream) flow pattern represented by the Oseen approximation for $0.01 < Re < 1.0$ (Fig. 2.8(b)). As the Reynolds number increases, the flow pattern, though still in the laminar region, becomes increasingly non-symmetric with the eventual development of a separation bubble behind the particle at Reynolds numbers higher than 50 (Figure. 2.9).[3,14]

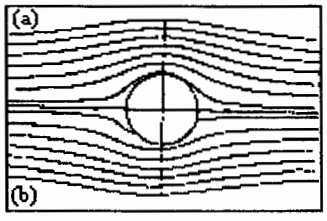

Figure 2.8: Streamlines relative to a spherical solid particle at low *Re*
(a) Stoke's solution; (b) Oseen approximation

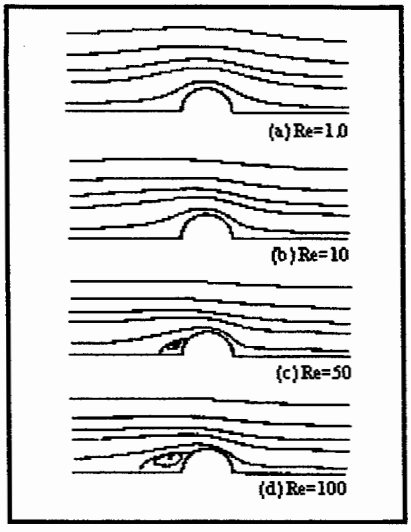

Figure 2.9: Streamlines for flow past a solid sphere for $1 \leq Re \leq 100$

Obviously, these changes in the flow pattern around the particle will have a direct influence on the drag coefficient, C_D, and the heat transfer coefficient, h, between the particle and its surrounding. The drag coefficient is defined as:

$$C_D = \frac{2F_D}{A\rho U_R} \tag{5.3}$$

The heat transfer coefficient between the plasma and the particle is expressed in terms of the Nusselt number defined as:

$$Nu = \frac{h\, d_p}{\kappa} \tag{5.4}$$

A typical correlation for the Nusselt number as a function of the Reynolds and Prandtl numbers at low temperature difference, is[3.14]:

$$Nu = 2 + 0.6\, Re^{0.5}\, Pr^{0.33} \quad \text{for } Re < 200 \text{ and } 0.5 < Pr < 1.0 \tag{5.5}$$

The principal characteristics of momentum and heat transfer under plasma conditions, however, are the presence of charged particles and of steep temperature gradients across the boundary layer, with possible temperature ratios as high as 10 between the plasma and particle temperatures.[4,20] These can have a substantial effect on the flow and temperature fields around the sphere through its influence on the local fluid properties. Corrections to the correlations for calculating the drag coefficient and the Nusselt number have therefore been suggested to account for these and are summarised in Table 2.2. Because of strong non-linear variations of κ with temperature, one of the main problems in calculating the Nusselt number is to determine which

temperature to use. Different temperatures at which the fluid properties used in the correlations should be obtained, were suggested in the literature. These are also summarised in Table 2.2.

Other corrections which might be necessary when dealing with the transport and heating of very fine powders ($d_p < 10$ μm) under plasma conditions are due to non-continuum effects when the Knudsen number (Kn) is greater than 0.001, where $Kn = \lambda / d_p$. This is especially important when the mean free path of the plasma is of the same order of magnitude as the diameter of the particle. Of particular importance is the temperature jump (slip flow) regime, when $0.01 < Kn < 1.0$. This implies more corrections to the transport correlations as shown in Table 2.2.[3,14,24]

The particle temperature is governed by a balance between conduction and convection heat transfer between the plasma and the particle and radiative heat losses from the particle to the surroundings. In most cases, the radiative heat transfer from the plasma can be neglected because the plasma is optically thin. The net heat transfer from the plasma to the particle is given by:[3,14]

$$Q = h\ a_p(T_\infty - T_s) - a_p \varepsilon\ \sigma\ (T_s^4 - T_a^4) \qquad (5.6)$$

A problem when calculating trajectories and temperature histories of particles injected into a plasma is to decide whether internal conduction in the particle should be taken into account. The difference between the temperature of the surface of the particle and that of its centre depends on the temperature of the plasma and the thermal conductivity of the material of the particle. The assumption of a uniform particle temperature implies that the thermal conductivity of the particle material is much higher than that of the gas, i.e. $Bi = \kappa / \kappa_p < 0.03$.[3,4]

When heat propagation has to be taken into account, the time evolution of the temperature field within the particle is given by the following conduction equation:[3,4,15]

$$\frac{1}{r^2}\frac{\partial}{\partial r}\left(\kappa_p r^2 \frac{\partial T}{\partial r}\right) = \rho\ c_p \frac{\partial T}{\partial t} \qquad (5.7)$$

Spherical symmetry of the particle is assumed. The initial temperature distribution is:

$$T(r, 0) = f(r)$$

and the symmetry condition is:[4,15]

$$\left.\frac{\partial T}{\partial r}\right|_{r=0} = 0$$

The remaining boundary conditions for the particle depend on its state.

(a) For a particle in a one-phase state the condition of the outer boundary is determined from the heat balance: [15]

$$\kappa_p \left.\frac{\partial T}{\partial r}\right|_{r=d_p/2} = Q \qquad (5.8)$$

(b) For a two-phase sphere: [15]

$$\kappa_p \left.\frac{\partial T}{\partial r}\right|_{r=r_m-0} = \kappa_p \left.\frac{\partial T}{\partial r}\right|_{r=r_m+0} + \lambda_m \rho_p \frac{dr_m}{dt} \qquad (5.9)$$

and $T|_{r_m-0} = T|_{r_m+0} = T_m$

The velocity propagation of a melting front is given by:[3,15]

$$\left(\frac{\partial r}{\partial t}\right)_{r_m} = \frac{1}{\rho_l \lambda_m}\left[\kappa_{pl}\left(\frac{\partial T}{\partial r}\right)_{r_m} - \kappa_{ps}\left(\frac{\partial T}{\partial r}\right)_{r_m}\right] \qquad (5.10)$$

(c) Vaporisation and evaporation of the particles also occur. Vaporisation is defined as a mass transfer process driven by vapour concentration gradients existing between the free stream and the particle surface and can thus occur below the boiling point of the particle matter. Evaporation of the particle will start to take place when the particle surface temperature approaches its boiling point. In either case, the generated vapour cloud will surround the particle, affecting the heat transfer rates between the plasma and the particle. Thus the net heat flux between the particle and its surroundings are affected due to absorption of heat by the vapour: [3]

$$Q_v = 2\pi\, d_p \lambda_v \ell n\left(1 + \frac{h_\infty - h_s}{\lambda_v}\right)\left(\frac{\bar{\kappa}}{c_p}\right) \qquad (5.11)$$

During evaporation of the sphere the outer boundary of the sphere moves due to evaporation of the outer layer of the particle: [15]

$$\kappa_p \left.\frac{\partial T}{\partial r}\right|_{r=r_v} = Q_v + \lambda_v \rho_p \frac{dr_v}{dt} \qquad (5.12)$$

and $T(r_v, t) = T_v$.

The evaporation rate depends on the mass transfer coefficient of the particle material. This is expressed in terms of the Sherwood number, defined as:

$$Sh = \frac{h_m d_p}{D} \tag{5.13}$$

The Sherwood number is calculated using similar correlations as for the Nusselt number:

$$Sh = 2 + 0.6\, Re^{0.5}\, Sc^{0.33} \tag{5.14}$$

If necessary the same correction factors used for the Nusselt number are applicable to the Sherwood number.[3,14,24] A numerical method is usually best employed to solve this non-stationary heat and mass transfer problem. [15]

During the displacement of a particle in a plasma stream, it is subjected to a number of forces which act simultaneously on it and have an influence on its trajectory and the residence time in the plasma. Among the most important to be taken into account are the inertia forces, F_i, and the viscous drag forces, F_D, which are defined as:

$$F_i = m\frac{dU_p}{dt} \tag{5.15}$$

$$F_D = \tfrac{1}{2}\, \rho\, A\, C_D\, U_R^2 \tag{5.16}$$

The gravity force, $F_g = mg$, can also be important in low-velocity flows. Other forces, which may have an influence on the trajectory of the particle in particular situations, are the pressure gradient force in the presence of steep pressure gradients in the flow field, the Basset history under very high acceleration conditions, thermophoresis effects for very fine particles ($d_p < 0.1$ μm) in the presence of steep temperature gradients and Coriolis forces which results from the rotation of the particles about an axis parallel to the direction of relative motion.[3,14,24]

In most cases the last named four forces are negligible and a force balance around a single particle in motion in plasma flow can be written simply as:

$$F_i = F_D + F_g \tag{5.17}$$

Substitution of equation (5.15), (5.16) and the gravity force into equation (5.17) gives the following:[3]

$$\frac{dU_p}{dt} = -\frac{3}{4} C_D (U_p - U)|U_p - U|\frac{\rho}{\rho_p d_p} \pm g \tag{5.18}$$

$$\frac{dV_p}{dt} = -\frac{3}{4}C_D(V_p - V)|V_p - V|\frac{\rho}{\rho_p d_p} \qquad (5.19)$$

(The + or - sign in front of "g" depends on whether the positive direction for the velocity of the particles is chosen as being downwards or upwards.) The magnitude of acceleration exerted on a spherical particle is inversely proportional to the particle density, inversely proportional to the square of the diameter of the particle and proportional to the relative velocity.[24]

A number of other factors can also influence momentum and heat transfer between the plasma and the particles. The particles injected into the plasma are not necessarily spherical. The shape of the particle and its drag coefficient can be correlated by the sphericity factor in a limited range of shape effects. Particle charging can also have a limited effect on its trajectory since a particle injected into a plasma assume a negative charge due to the difference between the thermal velocities and mobilities of electrons and ions. This is however of minor importance under LTE conditions. Deviations from LTE conditions can also be important, especially near the particle surface. Radiative heat losses from particles also become important for large particles, high particle surface temperature and emmisivity and low enthalpy difference between the surfaces of particles and the plasma.[3,14,24]

The diffusion of the particle vapour in the plasma surrounding also has an effect on the plasma transport properties. When chemical reactions between the vapour and the plasma or between the particle and the plasma have to be considered, a source term, representing the variation of the mole numbers of the different chemical species in the conservation equations, has to be introduced into the calculation.[3.14]

The equations summarised in Table 2.2 and discussed above, deal with the calculation of individual particle trajectories and temperature histories. Under the dense loading conditions used in the application of plasma technology, local cooling of the plasma due to the presence of the particles, as well as radiative exchange between particles, can cause substantial deviations from model predictions. The problem of treating all three sources of gas-particle interaction, i.e. mass, momentum and energy coupling between phases, causes the modelling to be much more complex.

A mathematical model was developed by Boulos and his collaborators,[3] which, through an interactive procedure, continuously up-dates the computed plasma temperature, velocity and

concentration fields. The interactions between the stochastic single particle trajectory and those of the continuum, temperature and concentration fields are incorporated using appropriate source-sink terms in the respective transfer equations. These are estimated using the so-called particle-source-in-cell model (PSI-Cell) developed by Crowe, Sharma and Stock.[8]

This model is founded on the idea of treating particles as sources of mass, momentum and energy to the gaseous phase. Firstly, the flow field is subdivided into a series of cells. Each cell is regarded as a control volume for the gaseous phase. As particles pass through a given cell, they may be: (i) evaporating or condensing, resulting in a source (or sink) of gaseous mass to the fluid in the cell; (ii) accelerating or decelerating , resulting in a momentum increase or decrease in the fluid in the cell in the direction of particle motion; (iii) conducting heat or convecting enthalpy, resulting in a source (or sink) of thermal energy to the fluid in the cell. Finite-difference equations for mass, momentum and energy conservation are written for each cell. The particle trajectories, sizes and temperature history are obtained by integrating the equations of motion for the particles in the flow field and utilising equations for the particle-gas mass and heat transfer rates.[8]

For the purpose of this study only a one-dimensional model will be implemented to predict overall trends. The three-dimensional modelling of the 36 possible reaction equations falls outside the scope of this study, and is indeed beyond the capability of commercial CFD work stations currently available.

Table 2.2: Summary of heat, mass and momentum transfer equations

Ref. No.	Heat Transfer between the plasma and the particle	Mass Transfer / Phase change	Momentum Transfer	Reference Temperature	Assumptions	Accuracy
3, 14	a) Same as Reference 28, 29 b) $Nu = \left(2 + 0.515\sqrt{Re}\right)\left(\frac{\nu_f}{\nu_\infty}\right)^{0.15}$ c) $Nu = (2 + 0.6\sqrt{Re}\,Pr^{0.33})(\frac{\rho_\infty \mu_\infty}{\rho_s \mu_s})^{0.6}$ d) $Nu = (2 + 0.6\sqrt{Re}\,Pr^{0.33})(\frac{\rho_\infty \mu_\infty}{\rho_s \mu_s})^{0.6}(\frac{c_{p_\infty}}{c_{p_s}})$ e) $Nu = 2\left[1 + 0.63Re_\infty \left(\frac{Pr_\infty^{0.38}}{Pr_s^{0.42}}\right)\left(\frac{\rho_\infty \mu_\infty}{\rho_s \mu_s}\right)^{0.52} C^2\right]$ $C = \frac{1-(h_s/h_\infty)^{1.1}}{1-(h_s/h_\infty)^2}$ Correction for non-continuum effect: $q = q_{continuum}\,[1 + (2Z^*/d_p)]^{-1}$	Melting ($T=T_m$): $\frac{dy}{dt} = \frac{Q_v}{m\lambda_m}$ Evaporation ($T=T_v$): i) Pseudo steady state: $\frac{dm}{dt} = S\rho_g h_m M\ell n\left(\frac{p}{p-p_v}\right)$ ii) Heat transfer controlled $\frac{dm}{dt} = \frac{Q_v}{\lambda_v}$ iii) Particle size: $\frac{dd_p}{dt} = \frac{-2Q_v}{\pi d_p^2 \rho_p \lambda_v}$	Correlations for C_{Di} the same as that of Reference 30, except for: $20 \le Re < 200$: $C_{Di} = \left(\frac{24}{Re}\right)\left(1 + 0.189Re^{0.62}\right)$ $Re \ge 200$: $C_{Di} = \frac{24}{Re} + \frac{6}{1+\sqrt{Re}} + 0.4$ Correction for steep temp. gradients: (i) $C_D = C_{Di}\,(\nu_f/\nu_\infty)^{0.15}$ (ii) $C_D = C_{Di}\,(\rho_\infty \mu_\infty/\rho_s \mu_s)^{0.45}$ Correction for non-continuum effect: $C_D = C_{Di}\left[1 + \left(\frac{2-a}{a}\right)\left(\frac{\gamma}{1+\gamma}\right)\left(\frac{4}{Pr_s}\right)Kn\right]^{-0.45}$	-Mean film temperature, T_f, for C_{Di}. -Integral mean of physical properties when calculating C_D direct. -$T_{0.19}$ (see ref. 28, 29) for Re of heat transfer equation (a). -T_f for Pr and Re of heat transfer equations (c) and (d)	-For heat transfer equations (a) to (e) a negligible internal temp. gradient. -A low particle-gas loading ratio.	For heat transfer, equation (e) was found to be the most accurate.
4	$Nu = 2$ after 2 μs (i) Particle at uniform temperature: $\frac{dT_s}{dt} = \frac{-12\overline{\kappa_p}(T_s - T_\infty)}{\rho_p c_p d_p}$ (ii) Internal heat propagation in particle dealt with in main part of section 2.5.2.			Integral mean of physical properties is used.	-Low particle-gas loading ratio. -Spherical particles with constant c_p -Heat transfer limited to conduction.	
15	$Nu = \left(2 + 0.6\sqrt{Re}\,Pr^{1/3}\right)\left(\frac{\rho_\infty \mu_\infty}{\rho_s \mu_s}\right)^{0.6}$	$Sh = 2 + 0.6Re^{0.5}Sc^{0.33}$	Axial particle velocity: $\frac{dU_p}{dt} = U_p\frac{dU_p}{dx} = 0.75C_D\frac{\rho}{\rho_p d_p}(U - U_p)^2$ Drag coefficient: $C_D = \frac{24}{Re}$ for $Re < 2$ $C_D = 18.5Re^{-0.6}$ $2 < Re < 500$ $C_D \approx 0.44$ $Re > 500$		-Spherical particles -Spherical symmetry of temperature field in particle.	

24	$Nu = 2 + 0.6Re^{0.5}Pr^{0.33}$ Correction for non-continuum effect: $q = q_{continuum}\,[1 + (2Z^{*} / d_p)]^{-1}$	Vaporisation ($T<T_v$): $\dot{m} = \rho\ h_m M\ \ell n\left(\frac{p}{p - p_v}\right)$ $Sh = 2 + 0.6Re^{0.5}Sc^{0.33}$ Evaporation ($T=T_v$): $\frac{dm}{dt} = \frac{Q_v}{\lambda_v}$	$C_{Di} = \frac{24}{Re} + \frac{6}{1+\sqrt{Re}} + 0.4$ Correction for variable property effects: (i) $C_D = C_{Di}\,(\rho_\infty / \rho_f)\,(\nu_f / \nu_\infty)^{0.15}$ (ii) $C_D = C_{Di}\,(\rho_\infty\,\mu_\infty / \rho_s\,\mu_s)^{-0.45}$ Correction for non-continuum effects: Same as reference 3	- Mean film temperature for C_{Di}	-Plasma flow conditions are uniform and specified in terms of temp.	
28, 29	$Nu = 2f_o + 0.473\,Pr^{m}\,Re^{0.552}$ $m = 0.78\,Re^{-0.145}$ $2f_o = 2\left(1 - T_o^{1+x}\right) / \left[(1+x)(1-T_o)T_o^{x}\right]$			-$T_{0.19}=T_s+0.19(T_\theta-T_s)$ for ν(Re) - T_s for κ(Nu)		Accurate for single stationary sphere.
26			Trajectory far downstream of particle injection point: $\frac{\bar{y}}{\ell_m} = 1.34\left(\frac{x}{\ell_m}\right)^{0.22}\left(\frac{\rho_j}{\rho_o}\right)^{0.25}$ where the characteristic length, ℓ_m, is: $\ell_m = d_j\left(\frac{\rho_j}{\rho_o}\right)^{0.5}\frac{V_j}{U_o}$		-The solid-gas jet is homogeneous, i.e. the solid phase remains with the jet. -Properties vary only along the axis of the jet.	
30	Particle temperature ($T_s<T_v$, $T_m<T_s<T_v$): $\frac{dT_s}{dt} = \frac{Q}{mc_p}$ $Nu = 2 + 0.514\,Re^{0.5}$	Melting ($T=T_m$): $\frac{dy}{dt} = \frac{Q}{m\lambda_m}$ Evaporation ($T=T_v$): $\frac{dd_p}{dt} = \frac{-2Q_v}{\pi d_p^2 \rho_p \lambda_v}$	Axial particle velocity: $\frac{dU_p}{dt} = 3C_D(U_p - U)\,\lvert U_p - U\rvert\left(\frac{\rho}{4\rho_p d_p}\right)$ Drag coefficient: $C_D = \frac{24}{Re}$ for $Re < 0.2$ $C_D = \left(\frac{24}{Re}\right)(1+0.187Re)$ $0.2 \le Re < 2$ $C_D = \left(\frac{24}{Re}\right)(1+0.11Re^{0.81})$ $2 \le Re < 21$ $C_D = \left(\frac{24}{Re}\right)(1+0.189Re^{0.62})$ $21 \le Re < 500$	The integral mean of the properties between the particle surface and the plasma free stream temperatures is used, e.g. $\bar{\kappa} = \int_{T_s}^{T_\infty}\frac{\kappa}{(T_\infty - T_s)}\,dT$	- 1 D flow in which particles maintain an axial trajectory. - Spherical particles - Negligible internal temp. gradient. - Low particle loading ratio. -Plasma in LTE and optically thin.	Accurate for particle velocity, but not for particle temperature history.

List of Symbols

A	- particle projected surface area perpendicular to the flow = $\pi d_p^2/4$ [m^2]
a	- thermal accommodation coefficient
a_p	- particle surface area = $\pi\, d_p^2$ [m^2]
Bi	- Biot number
C_D	- drag coefficient
C_{Di}	- drag coefficient initially calculated
$\overline{c_p}$	- intergral mean of fluid specific heat in the range T_s to T_g [J/kg.K]
c_p	- specific heat of particle [J/kg.K]
D	- diffusion coefficient [m^2/s]
d_j	- particle injector nozzle diameter [m]
d_p	- particle diameter [m]
f	- effect of variable properties on limiting *Nu* number defined in references 28,29
F_D	- total drag force exerted by the fluid on the particle [N]
F_g	- gravity force [N]
F_i	- inertia forces [N]
g	- gravitational acceleration [m/s^2]
h	- heat transfer coefficient [$W/m^2.K$]
h_m	- mass transfer coefficient [m/s]
Kn	- Knudsen number
m	- exponent of *Pr* in heat transfer equation of references 28, 29
m	- particle mass [kg]
$\dot{m}$	- rate of mass loss [kg/s]
M	- molecular weight [kg/kmol]
Nu	- Nusselt number
p	- saturation vapour pressure [kPa]
p_v	- vapour pressure at the surface temperature of the particle [kPa]
Pr	- Prandtl number
Pr_s	- Prandtl number of the gas at the surface temperature of the particle
q	- net heat flux to particle [W/m^2]
Q	- net heat transfer to the particle [W]

Q_v - net heat transfer to the particle when heating of vapour surrounding the particle is brought into account [W]

r - radial distance from the centre of the particle [m]

r_m - radius of the melting front [m]

r_v - radius of particle during evaporation [m]

Re - Reynolds number

S - particle surface area [m^2]

Sc - Schmidt number = $\mu / \rho D$

Sh - Sherwood number

T_a - ambient temperature of surfaces receiving the particle radiation [K]

T_f - mean film temperature = $(T_s + T_\infty)/2$ [K]

T_g - temperature of plasma next to particle surface [K]

T_m - melting temperature [K]

T_o - ratio of particle surface to free-stream temperatures (T_s/T_∞)

T_r - reference temperature [K]

T_s - temperature of the particle surface [K]

T_v - boiling temperature [K]

T_∞ - free stream temperature of the plasma [K]

U - gas velocity component in the axial direction [m/s]

U_o - (Ref. 26): velocity component in axial direction at main flow inlet [m/s]

U_p - particle velocity component in the axial direction [m/s]

U_R - relative velocity between the particle and its surroundings [m/s]

$\overline{v_s}$ - average molecular speed at T_s [m/s]

V - gas velocity component in the radial direction [m/s]

V_j - (Ref. 26): velocity component in radial direction at injector inlet [m/s]

V_p - particle velocity component in the radial direction [m/s]

x - (Ref. 28): exponent on T in the expression relating the kinematic viscosity and the thermal conductivity to the absolute temperature

x - distance in axial direction [m]

y - mass fraction of particle in the liquid state

$\bar{y}$ - (Ref. 26): centre line of injected particle jet in radial direction [m]

z - temperature jump distance [m]

Z^* - non-continuum heat-conduction potential jump distance

ε - particle emmisivity

γ - specific heat ratio (c_p/c_v)

κ - thermal conductivity of the gas [W/m.K]

κ_p - thermal conductivity of the particle [W/m/K] (subscript l $\Rightarrow$ liquid, s $\Rightarrow$ solid)

λ - mean free path of the plasma constituents [m]

λ_m - latent heat of melting [J/kg]

λ_v - latent heat of vaporisation [J/kg]

μ - fluid viscosity [kg/m.s]

ν - kinematic viscosity of fluid [m^2/s]

ρ - fluid density [kg/m^3]

ρ_g - vapour density in the boundary layer around the particle [kg/m^3]

ρ_j - fluid density at inlet conditions of particle injector [kg/m^3]

ρ_o - fluid density at main flow inlet conditions [kg/m^3]

ρ_p - density of the particle [kg/m^3]

σ - Stephan-Boltzmann constant = 5.67×10^{-8} $W/m^2.K^4$

Subscripts:

f - corresponding to film temperature

s - corresponding to surface temperature

∞ - corresponding to plasma free stream temperature

References

1) Baddour, R.F. & Bronfin, B.R., **Production of Tetrafluoroethylene by Reaction of Carbon with Carbon Tetrafluoride in an Electric Arc**, *Industrial and Engineering Chemistry: Process Design and Development*, Vol. 4, No. 2, pp. 162-166, (April 1965)
2) Baddour, R.F. & Timmins, R.S. (editors), *The Application of Plasmas to Chemical Processing*, Massachusetts Institute of Technology (M.I.T.) Press, USA, (1967)
3) Boulos, M.I.; Fauchais, P.; Vardelle, A. & Pfender, E., *Plasma Spraying: Theory and Applications* (editor: R. Stamanarayanan), Chapter 1: **Fundamentals of Plasma Particle Momentum and Heat Transfer**, World Scientific Publishing Company, (1993)
4) Bourdin, E.; Fauchais, P. & Boulos, M.I., **Transient Heat Conduction under Plasma Conditions**, *International Journal of Heat and Mass Transfer*, Vol. 26, No.4, pp. 567-582, (1983)
5) Chen, F.F., *Introduction to Plasma Physics*, Plenum Press, New York, (1977)
6) Chen, X. & Pfender, E., **Effect of the Knudsen Number on Heat Transfer to a Particle Immersed into a Thermal Plasma**, *Plasma Chemistry and Plasma Processing*, Vol. 3, No. 1, pp. 97-113, (1983)
7) Chen, X. & Pfender, E., **Effect of Pressure on Heat Transfer to a Particle Exposed to a Thermal Plasma**, *Journal of Engineering for Gas Turbines and Power*, Vol. 107, pp. 147-151, (January 1985)
8) Crowe, C.T.; Sharma, M.P. & Stock, D.E., **The Particle-Source-In Cell (PSI-Cell) Model for Gas-Droplet Flows**, *Journal of Fluids Engineering*, pp. 325-332, (June 1977)
9) Denison, J.T., Edlin, F.E. & Whipple, G.H., **US Patent 2 852 574**, *Preparation of Tetrafluoroethylene*, Patented: 16 September 1958
10) Farlow, M.W., **US Patent 2 709 182**, *Process for producing Tetrafluoroethylene from perfluorocarbon having at least three carbon atoms*, Patented: 24 May 1955
11) Farlow, M.W., **US Patent 3 081 245**, *Method for the preparation of Tetrafluoroethylene*, Patented: 12 March 1963
12) Farlow, M.W. & Muettertles, E.L., **US Patent 2 709 191**, *Preparation of Tetrafluoroethylene by reacting carbon with a binary silicon fluoride*, Patented: 24 May 1955
13) Farlow, M.W. & Muettertles, E.L., **US Patent 2 732 411**, *Preparation of Tetrafluoroethylene*, Patented: 24 January 1956

14) Feinman, Jerome (Editor), *Plasma Technology in Metallurgical Processing*, AIME, USA, (1987)

15) Fiszdon, J.K., **Melting of Powder Grains in a Plasma Flame**, *International Journal of Heat and Mass Transfer*, Vol. 22, pp. 749-761, (1979)

16) Kennard, E.H., *Kinetic Theory of Gases*, McGraw-Hill Book Company, Inc., USA, (1938)

17) Lee, Y.C. & Pfender, E., **Particle Dynamics and Particle Heat and Mass Transfer in Thermal Plasmas. Part I. The Motion of a Single Particle without Thermal Effects**, *Plasma Chemistry and Plasma Processing*, Vol. 5, No. 3, pp. 211-237, (1985)

18) Lee, Y.C.; Chyou, Y.P. & Pfender, E., **Particle Dynamics and Particle Heat and Mass Transfer in Thermal Plasmas. Part II. Particle Heat and Mass Transfer in Thermal Plasmas**, *Plasma Chemistry and Plasma Processing*, Vol. 5, No. 4, pp. 391-414, (1985)

19) Lee, Y.C. & Pfender, E., **Particle Dynamics and Particle Heat and Mass Transfer in Thermal Plasmas. Part III. Thermal Plasma Jet Reactors and Multiparticle Injection**, *Plasma Chemistry and Plasma Processing*, Vol. 7, No. 1, pp. 1-27, (1987)

20) Lewis, J.A. & Gauvin, W.H., **Motion of Particles Entrained in a Plasma Jet**, *AIChE Journal*, Vol. 19, No. 5, pp. 982-990, (September 1973)

21) Malone, B.S., **US Patent 4 973 773**, *Production of Tetrafluoroethylene*, Patented: 27 November 1990

22) McTaggart, F.K., *Plasma Chemistry in Electrical Discharges*, Elsevier Publishing Company, Netherlands, (1967)

23) Moore, A.M.C., *Die sintese van Tetrafluoroetileen - 'n omgewingsvriendelike alternatief*, Masters Thesis, PU vir CHO, South Africa, (1997)

24) Pfender, E., **Particle Behavior in Thermal Plasmas**, *Plasma Chemistry and Plasma Processing*, Vol. 9, No. 1 (Supplement), pp. 167S-194S, (1989)

25) Ponelis, A.A., Crouse, P.L., Moore, A.M.C. & Swanepoel, J., **Plasma-based Production of Tetrafluoroethylene**, *AEC Article*, South Africa, (1997)

26) Salzman, R.N. & Schwartz, S.H., **Experimental Study of a Solid-Gas Jet Issuing Into a Transverse Stream**, *Journal of Fluids Engineering*, pp. 333-339, (September 1978)

27) Sayce, I.G., **Patent 1 278 495**, London Patent Office, *Production of fluorine or volatile fluorine compounds by melt electrolysis*, Application filed: 8 August 1969

28) Sayegh, N.N. & Gauvin, W.H., **Numerical Analysis of Variable Property Heat Transfer to a Single Sphere in High Temperature Surroundings**, *AIChE Journal*, Vol. 25, No. 3, pp.522-534, (May 1979)

3. EXPERIMENTAL

3.1 Experimental Set-up and Apparatus

A schematic of the overall experimental set-up is shown in Figure 3.1. The experimental apparatus that was used, can be divided into a number of sections, namely the power supply, the plasma torch, the carbon feeder, the reactor, the quench probe, the filtering system and the analytical loop. The plasma torch, reactor and quench probe is shown in some detail in Figure 3.2. Other apparatus in the set-up include the high-frequency starter, measuring instrumentation and rotameters. An enthalpy probe was used for diagnostics.

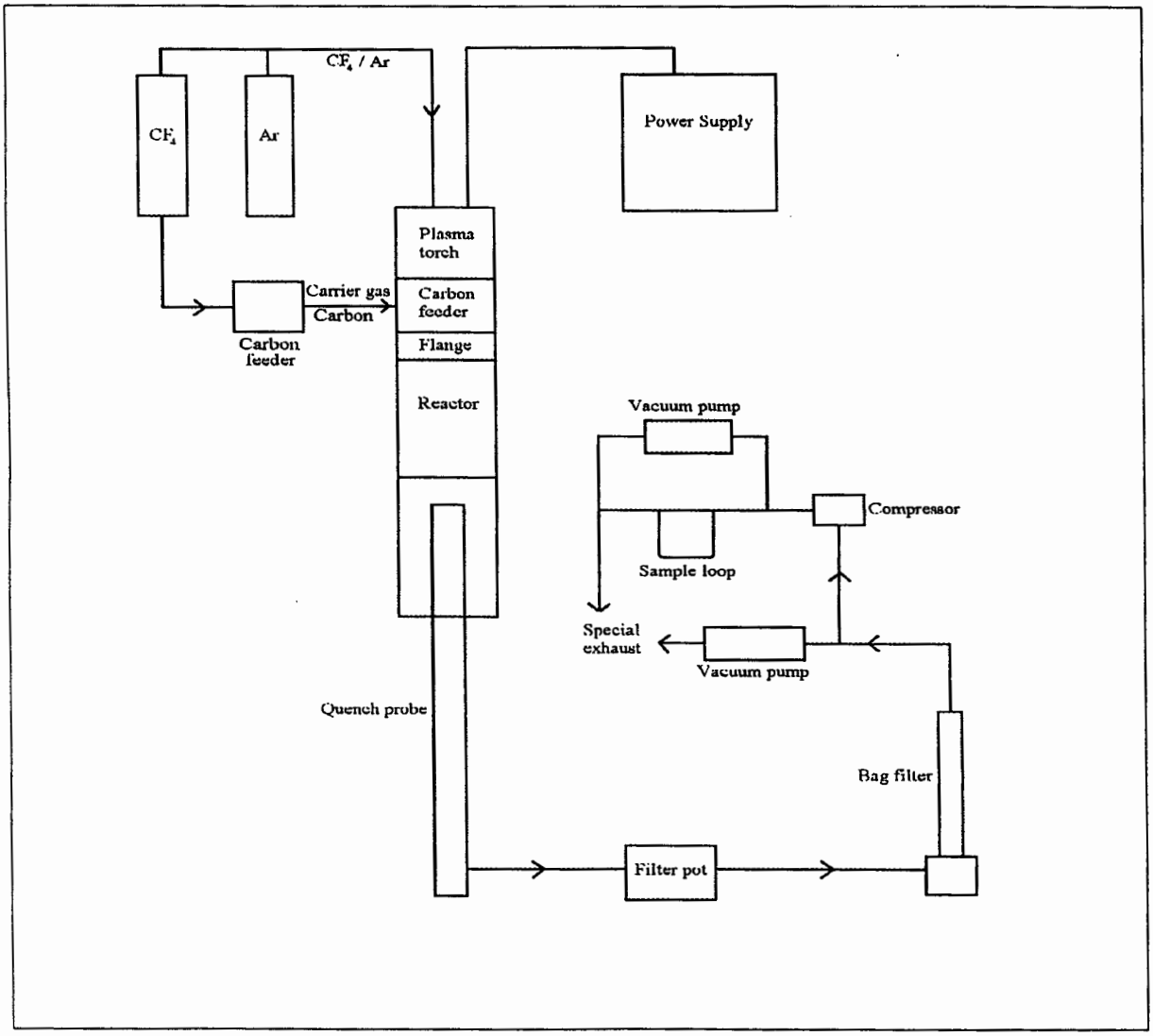

Figure 3.1: Schematic of the experimental set-up

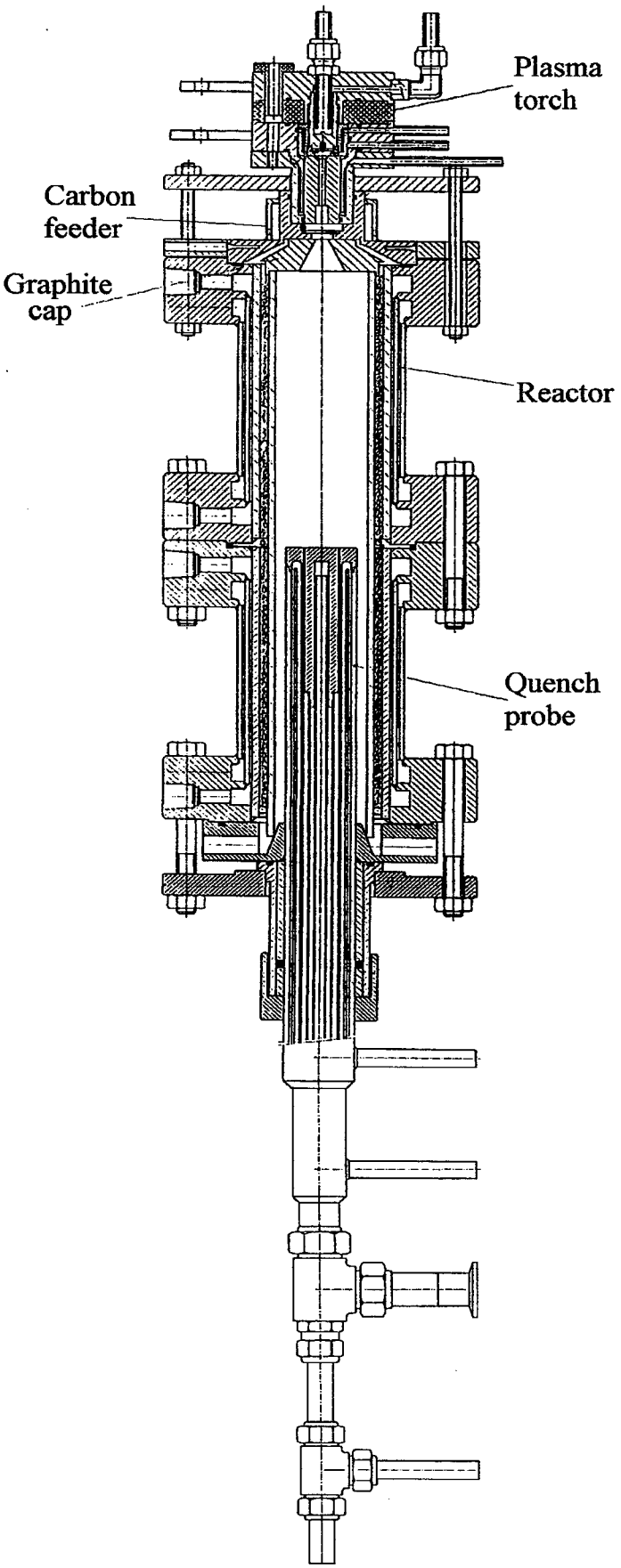

Figure 3.2: Reactor System

3.1.1 Power Supply

The power to the plasma torch was supplied by a locally manufactured DC power supply. The two main components of the power supply are a thyristor-controlled rectifier and an inductor with a laminated iron core. The power supply has an operating window of 250 A and 250 V and can therefore deliver a maximum power of 62.5 kW. The power supplied to the plasma torch, however, is usually in the region of 28 to 30 kW. The power supply is current controlled.

The input to the rectifier is three phase, with a voltage of 380 V. The rectifier consists of six phase-controlling thyristors that switch sequentially, producing six pulse rectified direct current as output. The purpose of the inductor is twofold. (i) More energy is necessary to initiate the plasma than to operate it. This energy is stored in the inductor. (ii) During the operation of the plasma, the arc attachment point shifts at a frequency of about 1.7 kHz. This exceeds the 50 Hz controlling bandwidth of the power supply. The inductor supplies the necessary energy to prevent the plasma from being extinguished when the point of attachment shifts.

3.1.2 Plasma Torch

The AEC designed plasma torch consists of a copper cathode with a graphite insert and a concentric annular copper anode (see Figure 3.3). The arc chamber is situated inside the tubular anode. The arc length is kept as near as possible to constant by employing a cascade design[7] for the anode. The anode can be described as consisting of two consecutive cylinders, the first having an inner diameter of 4 mm and the second an inner diameter of 8 mm. The linear direct current plasma arc is established between the graphite insert in the cathode and the "step" in the anode between the two cylinders of different diameter.

The cathode and anode are separated by an insulator made from polycarbonate which fits inside the top of the anode and a gas spinner made from pyrophyllite which fits into the bottom of the insulator. The plasma gas enters the plasma torch through four small holes in the top of the anode, moves downward between the anode and the insulator and is fed into the plasma arc through four 1-2 mm^2 holes in the gas spinner. The plasma is vortex stabilised. Both the anode and cathode are water-cooled during operation.

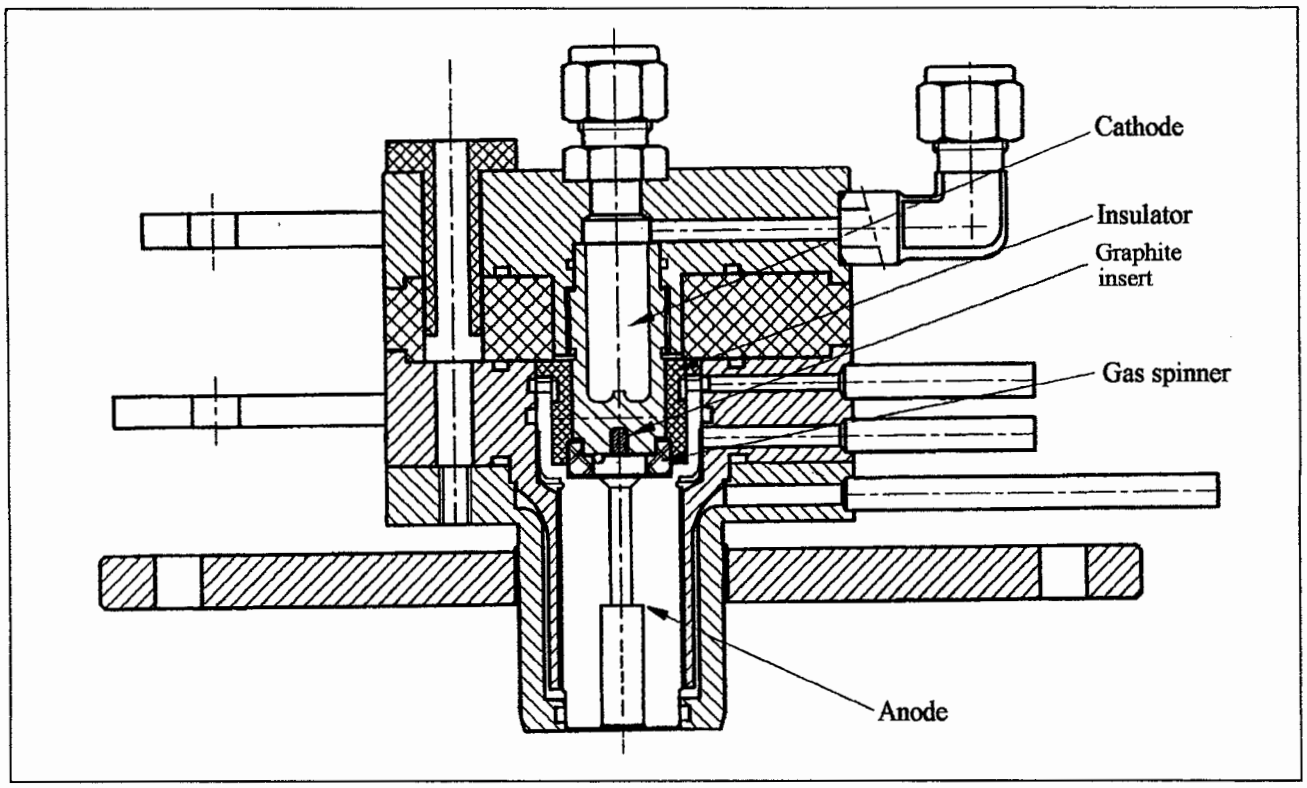

Figure 3.3: AEC designed plasma torch

3.1.3 Carbon Feeder

The carbon feeder consists of a water-cooled flange with the feeder head welded onto its top. The plasma torch fits into this head and carbon is injected into the plasma tail flame just below the anode. The carbon enters the feeder head by means of a 2 mm inside diameter pipe and is fed into the tail flame by an injector, which consists of a circular disk with three evenly spaced V-shaped grooves. The main purpose of the injector is to distribute the carbon particles more evenly and to inject the particles in a radial direction into the plasma tail flame.

For most of the experimental runs, the carbon was supplied by a piston feeder. This feeder consists of a vertical cylinder filled with carbon powder. A piston moves slowly upwards in this cylinder to push the carbon into the CF_4 carrier gas stream, while a rotating comb at the top of the feeder prevents the carbon from compacting. The carbon mass flow rate depends on the pressure difference between the piston feeder and the reactor, the upward speed of the piston feeder and the mass flow rate of the carrier gas. The carbon mass flow rate for each experiment was determined by placing the piston feeder on a scale and noting the mass loss with time. The feed

rate was kept as constant as possible by manually adjusting the upward speed of the piston when necessary.

For some of the earlier experimental runs, the carbon was supplied from a hopper inside a vacuum-tight container. The carbon was fed into the carrier gas line by means of a rotating screw at the bottom of the hopper. The carbon mass flow rate depends on the pressure difference between the hopper container and the reactor, the rotating speed of the screw feeder and the mass flow rate of the carrier gas. It was very difficult to maintain a constant carbon feed rate with this feeder system and blockages of the carbon feeding line also occurred frequently. This necessitated the installation of the piston feeder, which is more dependable, although its capacity is much smaller than that of the hopper.

Carbon, supplied by SASOL, was screened and only carbon particles less than 53 microns in diameter were used for the experiments, as the smaller particles have a bigger surface area for heat transfer. The mass flow rate of the carbon usually varied between 0.9 and 1.15 kg/h. The carrier gas flow rate was kept at about 0.4 kg/h.. The pressure in the carbon container was typically 5 to 10 kPa higher than that in the reactor.

3.1.4 Reactor

The reactor consists of a cylinder divided into top and bottom halves. These halves are individually water-cooled. The effective length of the reactor, can be changed by varying the height to which the quench probe is pushed up into the cylinder. For most of the experiments conducted, the quench probe was kept at a distance of 220 mm under the torch outlet, as this was the optimum length determined by Moore.[3] The outside of the reactor is made of stainless steel, while the inside is made of Inconel. Four 12.7 mm holes were drilled through the top half of the reactor, at 50, 100, 150 and 200 mm below the torch outlet, for diagnostic purposes, e.g. inserting the enthalpy probe into the plasma tail flame.

The cylinder has an inside diameter of 75 mm. The inside of the reactor is lined with graphite linings which usually consists of an outside lining with an outside diameter of 68 cm and an inside diameter of 48 cm and an inside lining, with an inside diameter of 25 mm, which just fits into the

outside lining. A graphite cap, which fits into the bottom of the carbon feeder, is placed on top of the cylindrical linings. During an experimental run, the top part of the graphite lining is "consumed", while the bottom part tends to "grow" due to carbon deposits. Holes were drilled through the lining when necessary for enthalpy probe measurements.

3.1.5 Quench Probe

The quench probe is essential for rapidly quenching the hot reactant gas to prevent the TFE formed from disassociating again. It can best be described as an annulus heat exchanger, consisting of an inner water-cooled finger made of copper surrounded by a water-cooled stainless steel cylinder. The gas that needs to be quenched flows between the "finger" and the cylinder. The quenching of the gas mainly takes place in the first few centimetres of the quench probe - the rest of the probe serves as a heat exchanger to cool down the gas to temperatures lower than 100 °C. It is essential that the rate at which the gas is quenched exceed 10^5 K/s to obtain the desired products.

3.1.6 Filtering System

A filtering system is necessary to remove all the excess carbon from the product gas stream. The system consists of a filter pot, in which gravity is used to remove most of the larger particles, followed by a bag filter, which removes the rest of the carbon powder.

3.1.7 Analytical Loop

A sample line is connected just after the bag filter to the main line between the vacuum pump and the reactor system. This line is connected to a small compressor that ensures a constant flow of gas through the line, as well as an absolute pressure of about 100 kPa of product gas in the line. Samples are taken in a sample loop connected to the analytical line. When a sample is not being taken, the gas in the analytical loop is vented to the special exhaust. The samples taken are analysed gas chromatographically.

3.1.8 High frequency - high voltage spark generator

A HF450 high frequency – high voltage spark generator is used to initiate the plasma. The high voltage, typically 20 kV, is necessary to initially ionise the gas in the plasma torch in order to initiate the plasma arc between the cathode and the anode. The high frequency of the spark makes the generator safer to operate as it prevents the high voltage of the generator of penetrating the skin.

3.1.9 Measuring Instrumentation

Pressure measurement

The pressure in the gas rotameter, in the gas line to the plasma torch, in the carrier gas line, inside the carbon container, inside the reactor, after the quench probe and before and after the compressor in the analytical loop (Section 3.1.7) are measured with **WIKA** *Tronic Line* pressure sensors. The ranges of the pressure sensors used, vary between 0 to 1 bar absolute and 0 to 10 bar absolute. They have an accuracy of $\pm$ 0.5 %.

Temperature measurement

The water temperatures of the various water-cooled components are measured in order to determine the energy losses from the reactor system. The temperature of the gas in the gas rotameter and temperature of the product gas stream just after the quench probe are also measured. PT-100 Resistance Temperature Detectors (RTDs) from **Thermocouple Products** are used for the temperature measurements. The ranges of the RTDs used, vary between 0 to 100 °C and 0 to 500 °C. They have an accuracy of $\pm$ 0.01 %.

Both the pressure sensors and the RTDs give an output signal of between 4 and 20 mA, according to the value being measured and the range of the instrument. These signals are received by a PC-81 Multiplexer card, where they are converted to millivolt signals which serves as input to a PC-30 Analog-digital communication card in a personal computer. Despite the good accuracy of the measuring instruments, standard deviations of up to 4 % were found in the temperature and pressure readings. The main cause of this scatter in data run is probably due to the inherent instability of the overall conversion of the signals from the sensors.

A special program written in Visual C co-ordinates the reading of the output signals from the measuring instruments, calculates the correct temperature and pressure readings with the use of calibration curves and logs the readings to a spreadsheet. This program also controls the pneumatic valves used in the analytical loop.

3.1.10 Water Flow Meters

Most of the water flow meters used to measure the water flow rate through the reactor components, are ICC water rotameters from **Ascoreg**, except on the water line to the anode and the inner part of the quench probe. On these lines **Krohne** flow meters, which can interact with a control loop on the reactor system, are used. The water flow meters have an accuracy of ± 2 %.

3.1.11 Gas Flow Rotameters

The gas flow to the plasma torch and the carrier gas flow are controlled with **Fisher & Porter** rotameters, which have an accuracy of ± 1 %. Their maximum design conditions are 1600 kPa absolute and 90 °C. The rotameter used for the plasma gas has a range of 0 to 16.5 l/min at standard temperature and pressure. The carrier gas rotameter has a range of 0 to 4.5 l/min at standard temperature and pressure.

3.1.12 Enthalpy Probe

The chief diagnostic tool used in the experiments performed, was the enthalpy probe. This is a robust tool, capable of measuring temperature, velocity and species concentration in thermal plasmas directly and simultaneously. A very important feature of this technique is its efficiency in measuring temperatures below the practical limit for the use of emission spectroscopy, but too high for measurement with thermocouples or thermometers.[1,4,5] It has been shown that the enthalpy probe technique is slightly less accurate than emission spectropic measurements for temperatures above 10 000 K, but below 10 000 K, the enthalpy probe is generally more accurate.[4]

The probe measurement is based on a two step energy balance on the cooling water circulating in the enthalpy probe. The first step is the tare measurement of the heat taken from the probe when no gas sample is flowing through the probe. The second step is the measurement of the heat taken from the probe when a known amount of gas is extracted from the plasma through the probe. The difference between these two measurements represents the energy associated with the extracted gas sample. Measurement of the flow rate of the gas sample through the enthalpy probe, as well as the probe exit temperature, enables the calculation of the gas enthalpy at the inlet of the probe.[4,5] When no gas flows through the probe, it can be used as a water-cooled pitot tube for determining the stagnation pressure at the probe tip to enable the calculation of the free stream velocity of the hot plasma gas.[5]

The performance of the enthalpy probe depends largely on its sensitivity factor, which represents the contribution of the gas sample to the overall heat load on the probe cooling water circuit. Since the sensitivity factor is proportional to the amount of the gas sample, it benefits from an increase in the gas mass flow rate. However, increasing the gas mass flow rate through the probe, may cause an increasing deviation from the isokinetic sampling conditions, i.e. that the velocity of the gas sample inside the probe is as close as possible to the free stream velocity. There is also a physical limitation to the amount of gas that can be withdrawn, especially when operating under low pressures.[4]

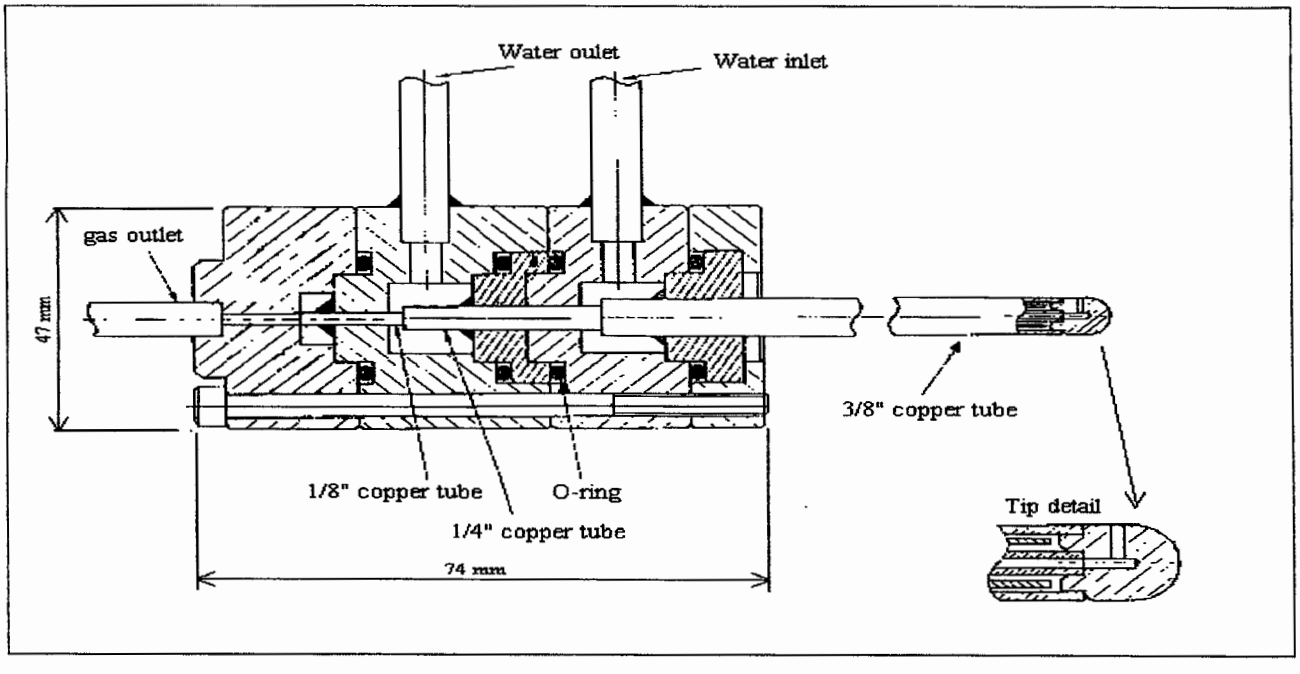

Figure 3.4: Enthalpy probe

The enthalpy probe employed consists of three concentric copper tubes (see Figure 3.4). The innermost tube, with an inside diameter of 3 mm, is used for the gas sampling, while the other two tubes guide the cooling water to and from the tip of the probe. The system further includes a gas sampling line, connected to a mass flow controller, and a PC data acquisition and control unit with Labview software. A **Tylan** (2900 series) mass flow controller enables the control and direct measurement of the mass flow rate of the gas sample. A vacuum pump at the outlet of the mass flow controller ensures gas flow through the sampling line. A sintered metal filter between the probe and the mass flow controller prevents any carbon particles that is drawn through the probe from clogging the controller. The gas sampling line is also connected to one end of a differential pressure sensor; a line from the reactor is connected to the other side of the sensor. The sensor is a **Fuji Electric** FC series instrument with a range of 0 to 10 kPa. The water inlet and outlet temperatures, as well as the outlet temperature of the gas sample, is measured with Type J thermocouples.

3.2 Calibration of Instruments

3.2.1 Gas Flow Rotameters

The gas flow rotameters were calibrated using **Gilian®**'s *Gibrator-2 Primary flow calibrator.* The output of this calibrator is volumetric flow rate in litre per minute at the ambient temperature and pressure. The gas flow through each rotameter was incremented and the mean of 10 to 12 calibrator readings was obtained for each setting of the rotameter.

The flow rates obtained with the calibrator were converted to the flow rates (in m^3/h) at the reference conditions (chosen as T_o = 300 K and P_o = 385 kPa) by using equation (1) given below. Linear regression was done on each data set, obtaining a linear expression for the volumetric flow rate as a function of the rotameter setting at the reference conditions. The mass flow rates of the gases at the reference conditions were calculated using the ideal gas equation. (The compressibility factor for CF_4, the gas used to calibrate the flow meters with, was calculated to be near to unity at the reference conditions, so that the deviation from the ideal gas equation was deemed to be minimal.) The error margins for the flow rates were also calculated.

For a given operating condition, where the reference conditions are labelled ***0***, the temperature and pressure in the rotameter ***1*** and the temperature and pressure in the reactor ***2***, the flow rate through the rotameter is given by:[6]

$$V_1 = V_0\sqrt{\frac{P_0 T_1 M_0}{P_1 T_0 M}} \qquad \ldots(1)$$

where M_0 is the molecular flow rate of the gas used to calibrate the rotameter, V_0 is the reference or calibration flow rate and T_0 and P_0 are the temperature and pressure at which V_0 were obtained. The volumetric flow rate through the reactor, is given by:[6]

$$V_2 = V_0\frac{T_2}{P_2}\sqrt{\frac{P_0 T_1 M_0}{P_1 T_0 M}} \qquad \ldots(2)$$

3.2.2 Water Flow Meters

The water rotameters were calibrated by connecting a pipe to the outlet manifold. The inlet to the rotameters were then opened one by one and the mass of water captured in a bucket in exactly one minute was determined for at least four settings on each of the rotameters. A regression line was calculated through the data points collected for each rotameter. An error analysis was also done on each data set and the error margins on all of the rotameters were found to be less than 9%.

3.2.3 Thermocouples

The Resistance Temperature Detectors (RTDs) were calibrated with the aid of a water bath of which the temperature can be set to a specific value. The RTDs were immersed in the water bath and the millivolt signals received by the computer for five different temperature settings were noted. Linear regression was done on each data set to obtain the necessary calibration curves. These were then entered into the control program.

3.2.4 Pressure Sensors

The pressure sensors were connected to the reactor and the millivolt signals at different reactor pressures noted for each of the sensors. The correct reactor pressure was determined from a

pressure sensor connected to a calibrated readout. Linear regression was done on each data set and the calibration curves supplied to the control program.

3.3 Characterisation of the Plasma Torch

3.3.1 V-A Characteristics

Two anodes were characterised – in the first (onwards called the 33/15 anode) the first, smaller diameter, cylinder was 33 mm in length with the second cylinder 15 mm in length, while both cylinders were 24 mm in length for the second anode (onwards called the 24/24 anode).

The torch was characterised by determining the V-A characteristics of the torch, the plasma enthalpies and the torch efficiencies at different pressures for different plasma gas flow rates. The torch efficiency is the efficiency of converting electrical energy into thermal energy inside the torch and is calculated by subtracting the heat losses in the torch from the electrical energy supplied by the power source and dividing this by electrical energy supplied by the power supply. The plasma enthalpy is defined as the energy supplied by the plasma torch (i.e. the energy supplied by the power source minus the heat losses in the torch) divided by the mass flow rate of the plasma gas.

Results

Graphs of voltage versus current show a decrease in the voltage across the torch with an increase in current. The V-A characteristics of the torch are in general similar to the typical V-A curves of an electrical linear arc plasma. The higher the plasma gas flow rate, the higher the voltage across the plasma torch. The efficiency of the plasma torch increases with an increase in current and plasma gas flow rate. The plasma enthalpy increases with an increase in current, but a decrease in plasma gas flow rate. Figures 3.5 – 3.10 illustrates these trends. A more complete summary of the data obtained is given in Appendix A.1.

At a given current setting, pressure and plasma gas flow rate, the 24/24 anode showed 3 to 6 V higher voltages across the plasma torch, as well as higher torch efficiencies and plasma enthalpies than the 33/15 anode. Plasma enthalpies of up to 7.8 kWh/kg CF_4 are possible at low gas flow

rates with the 33/15 anode, while enthalpies of more than 9 kWh/kg CF_4 were obtained with the 24/24 anode. The torch efficiencies with the 33/15 anode varied between 45 and 68 % and between 60 and 80 % with the 24/24 anode. Changing the operating pressure of the torch did not have a large influence on the performance of the 33/15 anode, with possibly a small decrease in voltage, efficiency and plasma enthalpy with an increase in pressure. At very low gas flow rates the plasma became unstable, especially at low pressures. The 24/24 anode showed substantial increases in voltage with an increase in pressure. The torch efficiency decreases and plasma enthalpy increased slightly with an increase in pressure.

Figure 3.5: V-A characteristics of 33/15 anode
(Reactor Pressure: 75 kPa)

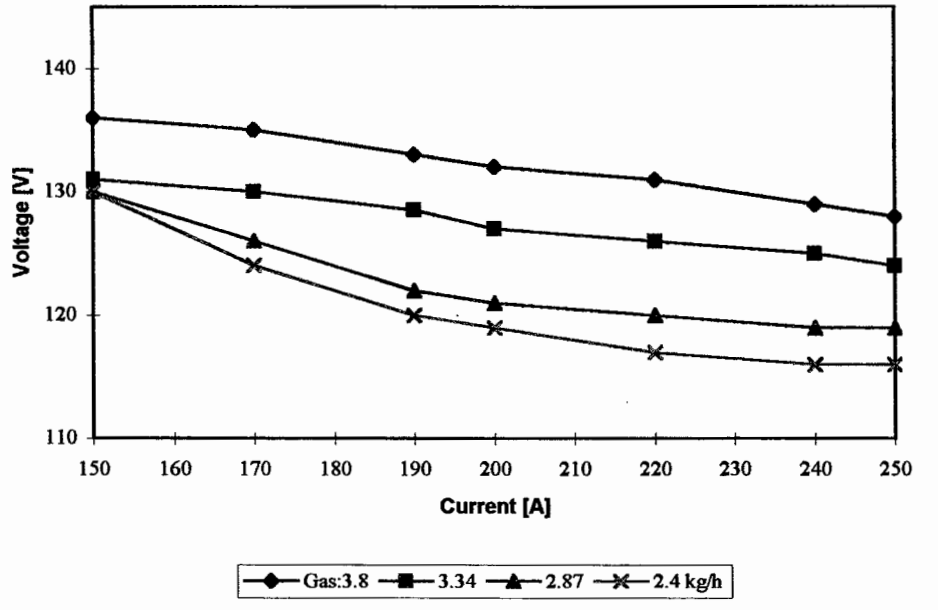

Figure 3.6: V-A characteristics of 24/24 anode
(Reactor Pressure = 75 kPa)

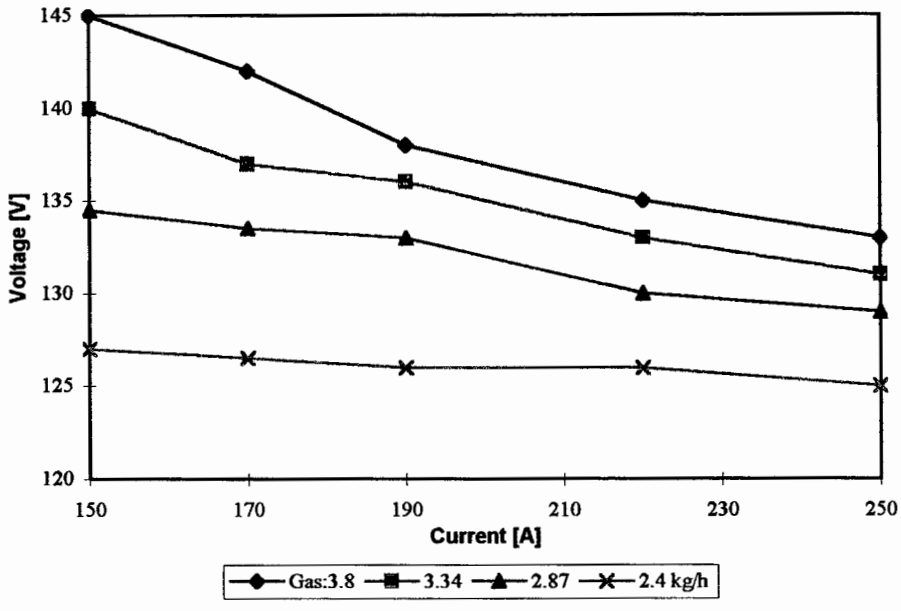

Figure 3.7: Efficiency of 33/15 anode
(Reactor Pressure: 20 kPa)

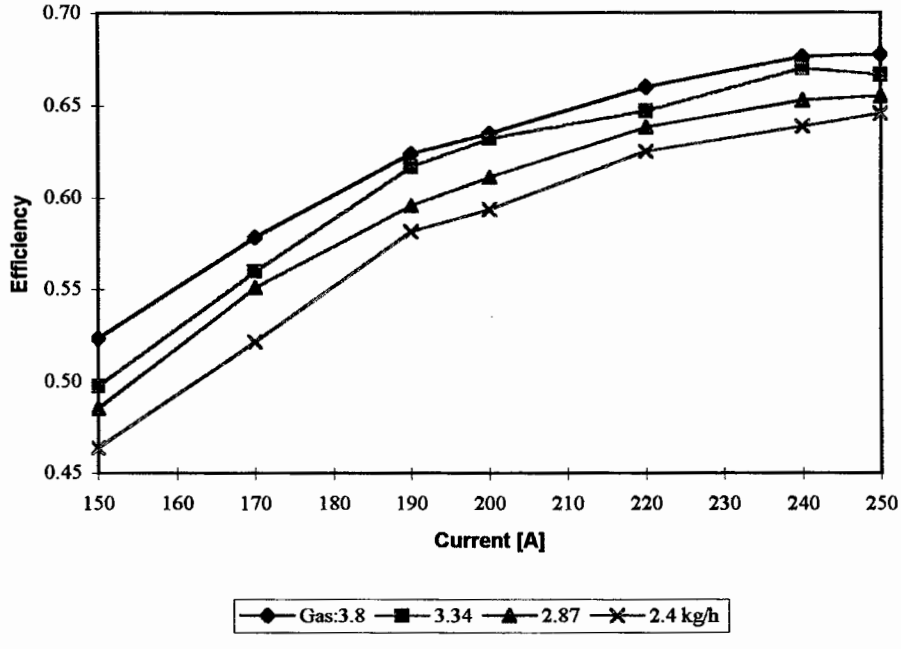

Figure 3.8: Efficiency of 24/24 anode
(Reactor Pressure = 20 kPa)

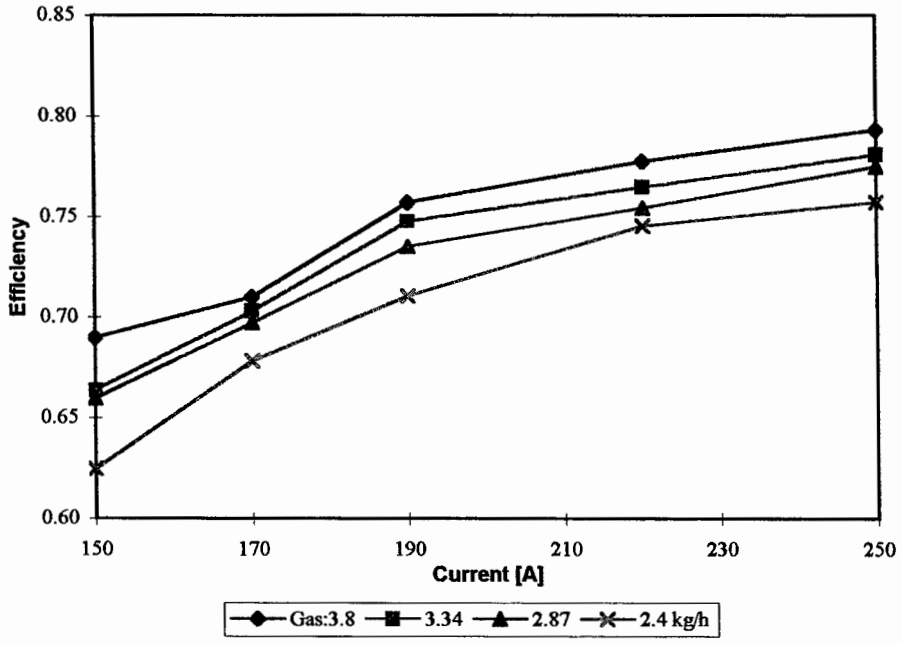

Figure 3.9: Enthalpy of 33/15 anode
(Reactor Pressure: 75 kPa)

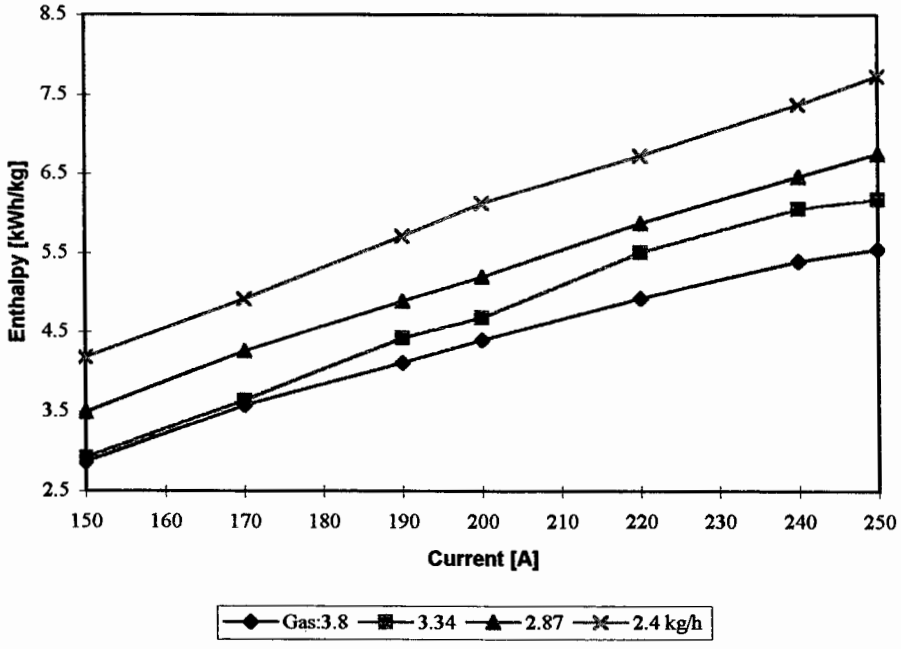

Figure 3.10: Enthalpy of 24/24 anode
(Reactor Pressure = 75 kPa)

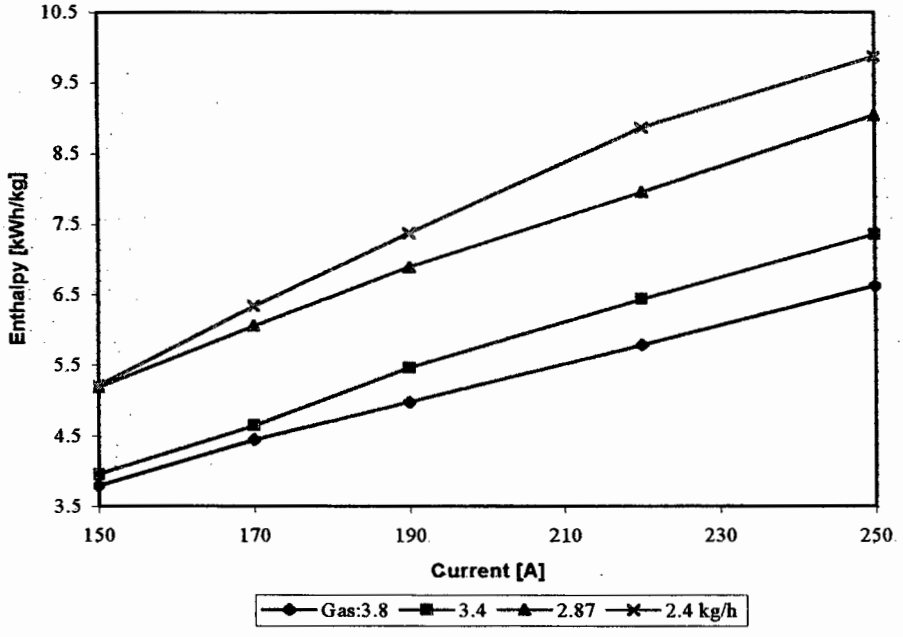

3.3.2 Empirical correlations

A power function was fitted to the experimental data in order to summarise the dependency of the voltage, torch efficiency and plasma enthalpy on the current, the reactor pressure and the gas flow rate for the two anode geometries. The function fitted was of the form:

$$Y = \alpha P^{\beta} I^{\gamma} \dot{m}^{\delta}$$

where Y = the dependent variable, i.e. the voltage, torch efficiency or plasma enthalpy

α = a constant

β,γ,δ = exponents

P = reactor pressure [kPa]

I = current [A]

$\dot{m}$ = gas flow rate [kg/h]

The best fitting parameters are summarised in Table 3.1.

Table 3.1: Best fitting parameters

33/15 Anode					
Y	α	β	γ	δ	R^2
Voltage [V]	143.5	-0.0153	-0.0847	0.314	0.972
Efficiency	0.0258	-0.0230	0.572	0.165	0.934
Enthalpy [kWh/kg]	0.00418	-0.0371	1.47	-0.552	0.989
24/24 Anode					
Y	α	β	γ	δ	R^2
Voltage [V]	134.03	0.0188	-0.0665	0.228	0.941
Efficiency	0.149	-0.0315	0.287	0.147	0.906
Enthalpy [kWh/kg]	0.019	0.0246	1.227	-0.708	0.972

The voltage of the torch should increase with an increase in pressure, as this results in an increase in the resistivity of the plasma arc.[2] Reactor pressure should therefore have a positive coefficient in the equation for the voltage. The negative coefficient for the 33/15 anode probably indicates that some shunting occurs in this anode. The V-A characteristics of the 30 kW AEC torch are determined at relatively low currents and therefore the voltage decreases with an increase in current (Figure 2.3). The negative coefficient for the current in the voltage equation was therefore to be expected. An increase in the mass flow rate of the plasma gas, would result in an increase in voltage[2], as indicated by the positive coefficient on mass flow rate in the voltage equation.

Torch efficiency shows a decrease with an increase in pressure as indicated by the negative coefficient on pressure in the efficiency equation. This corresponds to a general equation for efficiency that was derived by Russian researchers[2]. The increase in efficiency with an increase in mass flow rate of the plasma gas also corresponds to the Russian equation, but the increase in efficiency with an increase in current contradicts the Russian equation. The cause of this anomaly is probably the current ranges for which the two equations were derived – the Russian equation was derived for higher current regions, where the V-A characteristics of the plasma have a positive slope, while the equation for the AEC torch was derived in the lower current regions where the V-A characteristics display a negative slope.

As with the dependency of the voltage on the reactor pressure, there is again a discrepancy in the dependency of the enthalpy on the reactor pressure between the two torch geometries. This is

probably associated with the disparity between the two geometries with regard to the voltage dependency on the pressure, as the enthalpy is proportional to the voltage. As the positive coefficient for the current in the equation for plasma enthalpy indicate, the plasma enthalpy increases with an increase in current. The reason is that the energy that is put into the plasma gas increases with an increase in current, therefore the enthalpy also increases. The plasma enthalpy decreases with an increase in plasma gas mass flow rate, because the more gas is fed into the plasma, the more the plasma is cooled down, thus decreasing the enthalpy.

3.3.3 Torch lifetime

The running times of the torch were noted, together with the power supplied to the torch. The maximum time recorded for operating the torch totalled about 17 hours, corresponding to about 480 kWh of energy supplied by the power source. In general, however, the torch is only run for about 4 hours (~ 120 kWh) in total, before it has to be dismantled and some of its components replaced. (It should be kept in mind that the torch is not run continuously for 4 hours, but with frequent stoppages depending on the length of the experiments conducted on the reactor system. Every time the torch is started, it is subject to a high voltage spark and thermal shock, which is detrimental to the torch lifetime.)

The component with the shortest lifetime is the pyrophyllite gas spinner. The anode also have quite a short life span, as the "cascade step" is eroded with time by the plasma arc and this results in a decrease in the plasma voltage. At the plasma gas flow rate of about 3 kg/h normally used, the voltage would typically decrease from about 130 V for a new anode and gas spinner to less than 105 V, which is too low to maintain the plasma enthalpy at the desired level. The cathode and the polycarbonate insulator very seldom have to be replaced. If no carbon is fed into the plasma flame, the graphite insert in the cathode erodes and needs replacing after a while. When carbon is fed,however, this graphite insert tends to "grow" and the cathode is thus preserved.

3.4 Thermal Conductivity of Graphite Lining

To enable heat transfer calculations, it was necessary to determine the thermal conductivity of the graphite lining used in the reactor. The experimental set-up used for this determination was

exactly the same as that described in Section 3.1, except for the reactor. For these experiments a reactor consisting of eight segments, each about 27 mm in length, was used. A drawing of this reactor is shown in Figure 3.11. Each of the segments contained two RTDs, with a range of 0 to 100 °C, to measure the temperature of the cooling water as it flows through that specific segment. The heat losses between segments could therefore be calculated individually. RTDs with a range of 0 to 1350 °C in each segment measured the outside temperature of the graphite lining inserted in the reactor. Each segment was also provided with a 9.5 mm hole for diagnostic purposes.

For the thermal conductivity experiments, two type S thermocouple were inserted into the graphite lining through the diagnostic holes. The first was inserted 7.25 mm into the outer lining in the fourth segment, while the other was inserted 6.2 mm into the outer lining in the sixth segment. The S type thermocouples have a ceramic casing and can measure temperatures of up to 1760 °C. The plasma system was then operated under the conditions most often employed and the temperatures measured with the type S thermocouple were recorded as a function of time. The various water temperatures and reactor lining outside temperatures measured with the RTDs were also logged with the aid of the data logging program on the PC (described in Section 3.1.9).

A summary of the experimental results obtained is given in Appendix A.2. The thermal conductivity of the lining was calculated with the following equation:

$$k = \frac{q_s \ell n(r_2 / r_1)}{2\pi (T_1 - T_2) L}$$

The two parts of the graphite lining were taken as one during the calculation of the thermal conductivity and no contact resistance to heat transfer was taken into account. The heat loss from a specific segment was taken as the average of the heat losses between that segment and the previous segment and that segment and the next segment.

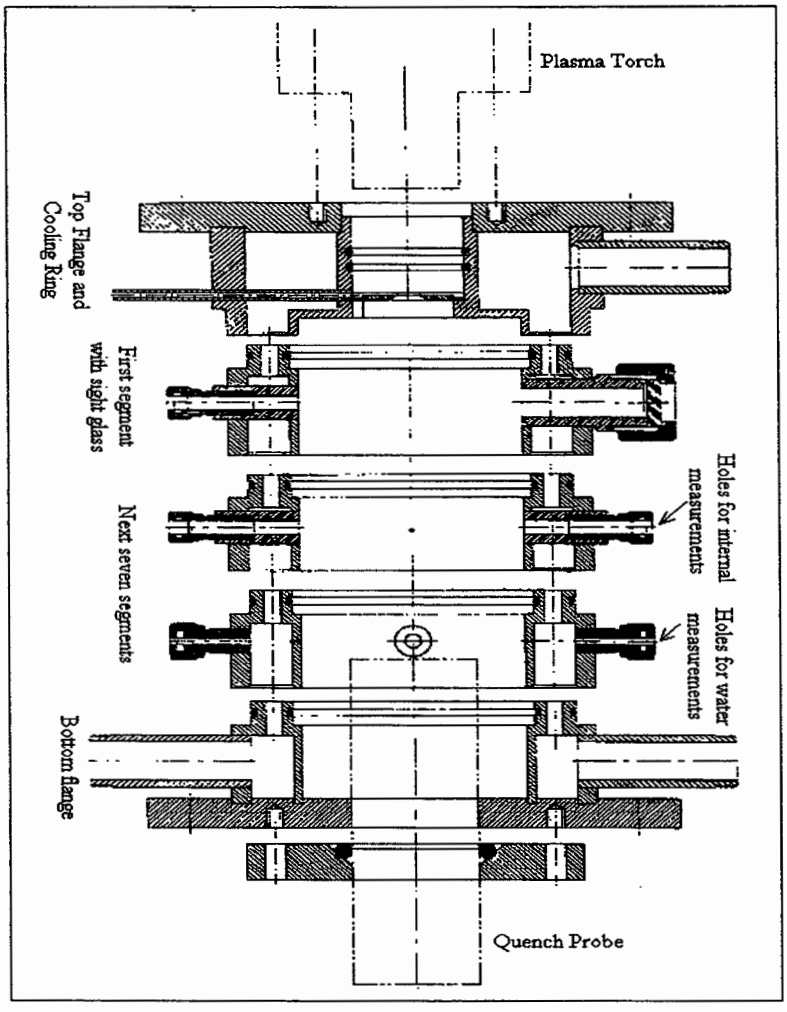

Figure 3.11: Segmented reactor

The change of thermal conductivity with temperature is shown in Figure 3.12. The thermal conductivity increases with an increase in lining temperature and the profile tends to flatten out in the region where the lining temperature stabilises. The calculations show the thermal conductivity in this temperature region to be in the order of 6 to 8 W/m.K.

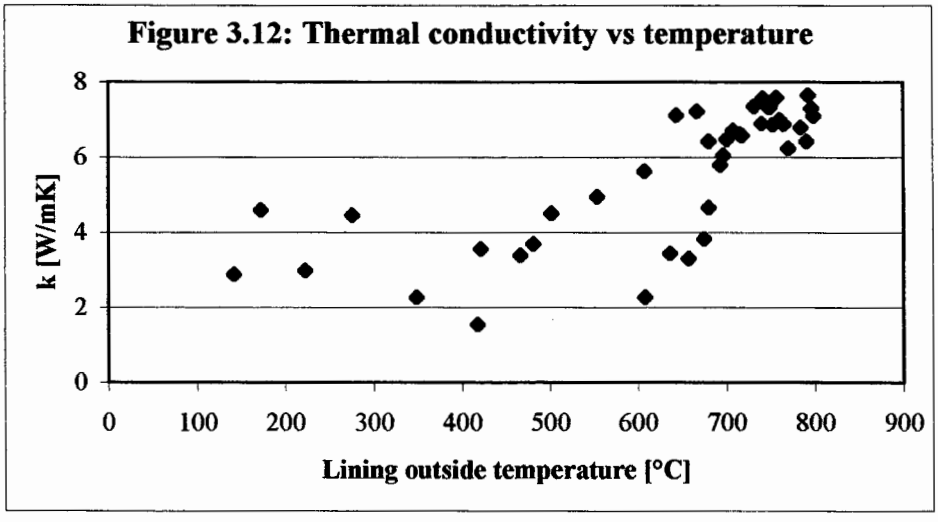

3.5 Experimental Procedure

Reactor System

The whole reactor system is vacuum tight. Before an experimental run, the system is put under vacuum by means of a vacuum pump connected to the outlet of the bag filter. Argon is then fed as plasma gas to the torch. An open circuit voltage of about 350 V is applied across the cathode and the anode and then the arc is struck with the high voltage spark generator. After the arc is initiated with argon, which is more easily ionised, CF_4 replaces the argon as plasma gas. The mass flow rate of CF_4 is typically about 2.9 kg/h. This results in a voltage of about 120 V at a current setting of 240 A for the 24/24 anode, depending on the condition of the torch.

After the CF_4 plasma arc has been established and the reactor pressure set to the required value by means of a control valve just before the vacuum pump, the feeding of carbon powder to the system can be started. The carbon mass flow rate is typically in the order of 1 kg/h, with the CF_4 carrier gas flow rate about 0.4 kg/h. The reactor length is usually set at 220 mm. In most cases the product gas is vented to a special exhaust and then released into the atmosphere after passing through a scrubber.

Samples of the product gas are taken periodically via the analytical loop and analysed with a gas chromatograph. The volume percentages of the different components of the product gas are normalised after deducting the air in the sample. The cooling water inlet and outlet temperatures, the product gas temperature, as well as the various pressures, are monitored and recorded with the computerised logging system. The water flow rates to the various water-cooled components as well as the exact plasma and carrier gas flow rates and the carbon mass flow rate are also recorded. Experimental runs varied between 15 to 60 minutes.

Measurement of graphite lining wall temperatures

The inner and outer wall temperatures of the graphite lining were measured with the use of a **Minolta/Land** *Cyclops 52* pyrometer. For the measurements optical glass windows were placed on the four diagnostic holes in the reactor in order to view the lining with the pyrometer during plasma operation. For the inner wall temperature measurements, holes were also drilled through the lining on the viewing side in order to view the opposite inner wall. As the plasma tail flame is

considered to be optically thin, it should not have too great an influence on these inner measurements.

Enthalpy probe measurements

Enthalpy measurements were made for three radial positions at each of the four axial positions provided in the reactor, i.e. immediately inside the lining, at a position half the inner radius of the lining in from the side and in the middle of the reactor. This was done with and without the feeding of carbon particles. The measurements were taken more than once to ensure better accuracy. The inside lining was replaced regularly to prevent erosion of the lining from having too big an influence on the obtained experimental data.

At the start of each measurement with the enthalpy probe, the probe was rotated until the inlet hole is at an angle of 90° with the direction of plasma gas flow. The pressure difference between the reactor and the probe was recorded. The probe was then rotated so that the inlet faced the plasma gas stream and the pressure difference again recorded. The next step was the tare measurement of the heat taken from the probe when no gas sample is flowing through the probe. This was done by recording the inlet and outlet probe cooling water temperatures. After this, the valve to the vacuum pump was opened and the inlet and outlet water temperatures again recorded to determine the heat taken from the probe with gas flow. The mass flow rate of the gas and the outlet gas temperature were also recorded. The acquisition of data was controlled by a Labview program and the data logged to a spreadsheet. Each of the different measurements done was repeated for a at least a minute at half-second intervals. Gas samples through the enthalpy probe could also be taken via the analytical loop for GC analysis.

3.6 Processing of Results

For each experimental run the data necessary to do a complete mass and energy balance was recorded. A typical mass and energy balance is shown in Appendix B. From these balances, a number of important gas enthalpies and the torch efficiency can be calculated, as shown in some detail in Appendix C. The data obtained with the enthalpy probe is used to determine the gas temperature and velocity inside the reactor, as illustrated in Appendix D.

Mass balance

It is difficult to determine the mass of carbon particles fed to the system that reacts experimentally. A fluorine balance is therefore done to determine the flow rate of the product gas, of which the composition is known. Once the flow rate of the product gas is established, it is possible to determine the rate at which carbon, as a component of the product gases, leaves the reactor in the gas phase. The rate at which gaseous carbon as a component of CF_4 enters the reactor is known, therefore the rate at which the carbon reacts and the rate at which unreacted carbon powder leaves the reactor can be deducted.

Energy balance

Steady state conditions are assumed for the energy balance, i.e. energy put into the reactor system should equal energy taken from the system. The energy put into the system equals the electric energy supplied to the torch by the power supply, since both the carbon and the CF_4 gas enter the system at room temperature, which is taken as the reference temperature. The energy taken from the system is the sum of the energy losses to the cooling water of the various components and the energy of the product gas and the unreacted carbon leaving the system. The accuracy of the energy balance is calculated as the energy out as a percentage of the energy in. About five to ten minutes after start up, in which time the reactor system approachs steady state, the energy balance is usually found to be 90 to 110 % accurate.

Enthalpies and Torch efficiency

The following calculations are only done on data that corresponds to an energy balance with an accuracy between 90 and 110%.

$$\text{Torch efficiency} = \frac{q_{in} - q_{anode} - q_{cathode}}{q_{in}} \qquad \ldots(3)$$

$$\text{Plasma enthalpy} = \frac{q_{in} - q_{anode} - q_{cathode}}{\dot{m}_{CF_4(plasma)}} \quad [\text{kWh/kg } CF_4] \qquad \ldots(4)$$

$$\text{Mixing enthalpy} = \frac{q_{in} - q_{anode} - q_{cathode} - q_{Cfeeder}}{\dot{m}_{CF_4(plasma)} + \dot{m}_{CF_4(carrier)} + \dot{m}_{Carbon}} \quad [\text{kWh/kg } CF_4 + C] \qquad \ldots(5)$$

$$\text{Quenching enthalpy} = \frac{q_{in} - q_{anode} - q_{cathode} - q_{Cfeeder} - q_{Reactor}}{\dot{m}_{CF_4(plasma)} + \dot{m}_{CF_4(carrier)} + \dot{m}_{Carbon}} \quad [\text{kWh/kg } CF_4 + C] \qquad \ldots(6)$$

Enthalpy probe

The average and standard deviation of each measurement is determined. These averages are used for calculation of the plasma gas enthalpies, while the standard deviation is used to calculate the overall error margin. The enthalpy of the plasma gas at the inlet of the probe can be determined by an energy balance:[1,4,5]

$$\dot{m}_g (h_i - h_e) = \dot{m}_w c_{p,w} [(\Delta T_w)_{sampling} - (\Delta T_w)_{tare}] \qquad \ldots(7)$$

The mass flow rate of the sample gas, $\dot{m}_g$, is known from the readings of the mass flow controller and the mass flow rate of the cooling water, $\dot{m}_w$, from the reading on a calibrated rotameter. The enthalpy of the gas sample at the exit of the enthalpy probe, is calculated from the gas exit temperature:

$$h_e = c_{p,s} (T_{exit} - T_{ref}) \qquad \ldots(8)$$

where the reference temperature is taken as the ambient temperature.

The temperature of the plasma gas at the inlet of the probe is determined by means of a program, **CFP**, written in-house by A.M.C. Moore. CFP extracts the thermodynamic properties of a C and CF_4 gas mixture at different pressures and C:CF_4 ratios from tables constructed with the thermodynamics program, ASTRA (see Section 2.4). CFP also calculates the temperature of the gas given its enthalpy, or *vice versa*. The necessary input to CFP is the reactor pressure, the enthalpy of the gas in units of kWh/kg and the C:CF_4 ratio of the gas mixture that is sampled through the enthalpy probe. To obtain this ratio, it is necessary to know the mass flow rate of carbon particles through the enthalpy probe. This is determined by weighing the carbon that is retained on the sintered metal filter in the gas sampling line and by noting the exact time that the gas is extracted through the enthalpy probe. Gas-phase carbon is determined from GC analyses.

In ASTRA the enthalpy at the temperature of interest is determined for the equilibrium species composition, using the equilibrium composition at 298 K as reference. When the gas is quenched through the enthalpy probe during measurements, however, the product composition differs from the equilibrium composition due to the sudden cooling of the gas down to room temperature. Instead of forming only CF_4 and carbon, the equilibrium composition at room temperature that

would have formed if the gas were cooled slowly, the following (unbalanced) reaction takes place:

$$CF_4(g) + C(s) \rightarrow CF_4(g) + C_2F_6(g) + C_2F_4(g)$$

This is an endothermic reaction and therefore reduces the enthalpy measured with the enthalpy probe. The heat of reaction for this reaction must therefore be added to the measured enthalpy before the temperature of the gas at the inlet of the enthalpy probe is determined with CFP. The correct mole fractions for balancing the above reaction equation is determined from GC analyses of the gas extracted through the enthalpy probe.

Gas velocities can only be calculated for enthalpy probe measurements when no carbon is fed into the reactor, as the carbon particles cause a serious instability in the differential pressure reading. The velocity is normally deduced from Bernoulli's equation:[1,4,5]

$$U = \sqrt{\frac{2(dP_{axial} - dP_{radial})}{\rho_{CF_4}}} \quad [m/s] \qquad \ldots(9)$$

The density of the gas is obtained from **CFP**. In practice the measurement of velocities turned out to be problematic, as will be discussed later.

The gas velocity at the inlet of the probe is also calculated to determine whether the gas sample was extracted under isokinetic conditions:

$$U_{probe} = \frac{\dot{V}_{inlet}}{A_{probe}} \quad [m/s] \qquad \ldots(10)$$

The rate at which the gas flowing through the enthalpy probe is quenched, is approximated:

$$\text{Quench Rate} > \frac{\Delta T_{probe} \times \dot{V}_{probe}}{Volume_{probe}} \quad [K/s] \qquad \ldots(11)$$

List of Symbols

A_{probe} - cross sectional area of the inner tube of the enthalpy probe [m^2]

$c_{p,w}$ - specific heat of water [kJ/kg. K]

$c_{p,s}$ - specific heat of gas sample extracted through the quench probe [kJ/kg.K]

dP_{axial} - pressure difference measures when the inlet of the enthalpy probe was tuned in the axial direction [kPa]

dP_{radial} - pressure difference measured when the inlet of the enthalpy probe was turned in the radial direction [kPa]

h_e - enthalpy of gas at exit of enthalpy probe [kJ/kg]

h_I - enthalpy of gas at inlet of enthalpy probe [kJ/kg]

k - thermal conductivity [W/m.K]

L - length of segment [m]

$\dot{m}_{Carbon}$ - carbon mass flow rate [kg/h]

$\dot{m}_{CF_4(plasma)}$ - mass flow rate of the CF_4 plasma gas [kg/h]

$\dot{m}_{CF_4(carrier)}$ - mass flow rate of the CF_4 carrier gas [kg/h]

$\dot{m}_g$ - gas mass flow rate through enthalpy probe [kg/h]

$\dot{m}_w$ - mass flow rate of the cooling water

q_{in} - rate at which energy is supplied to the plasma torch [kW]

q_{anode} - rate at which energy is lost from the anode [kW]

$q_{cathode}$ - rate at which energy is lost from the cathode [kW]

q_{feeder} - rate at which energy is lost from the carbon feeder [kW]

$q_{reactor}$ - rate at which energy is lost from the combined reactor [kW]

q_s - rate of heat loss to cooling water in specific segment [W]

r_1 - radius to tip of inserted S type thermocouple [m]

r_2 - outer radius of graphite lining [m]

T_1 - temperature of graphite lining at r_1 [K]

T_2 - temperature of graphite lining at r_2 [K]

T_{exit} - temperature of gas sample as it exits the enthalpy probe [K]

T_{ref} - reference temperature [K]

ΔT_w - temperature rise of the cooling water in the enthalpy probe [K]

U - free stream velocity of plasma gas [m/s]

U_{probe} - inlet velocity to the enthalpy probe [m/s]

$\dot{V}_{inlet}$ - volumetric flow rate of the gas at the inlet of the enthalpy probe [m^3/s]

$\dot{V}_{probe}$ - average volumetric flow rate of the gas through the enthalpy probe [m^3/s]

References

1) Brossa, M. & Pfender, E., **Probe Measurements in Thermal Plasma Jets**, *Plasma Chemistry and Plasma Processing*, Vol. 8, No. 1, pp. 75-90, (1988)
2) Crouse, P.L., **A Simple View of the Plasma Arc**, Unpublished notes, AEC, (1998)
3) Moore, A.M.C., *Die sintese van Tetrafluoroetileen - 'n omgewingsvriendelike alternatief*, Masters Thesis, PU vir CHO, South Africa, (1997)
4) Rahmane, M., Soucy, G. & Boulos, M.I., **Analysis of the enthalpy probe technique for thermal plasma diagnostics**, *Review of Scientific Instruments*, Vol. 66, No. 6, pp. 3424-3431, (June 1995)
5) Swank, W.D., Fincke, J.R. & Haggard, D.C., **Modular enthalpy probe and gas analyzer for thermal plasma measurements**, *Review of Scientific Instruments*, Vol. 64, No. 1, pp. 56-62, (January 1993)
6) Vaux, W.G., **Calculating flow through gas rotameters**, *Chemical Engineering*, pp.119-120, (December 1980)
7) Zhukov, M.F., *Thermal Plasmas and New Materials Technology* (editors: O.P. Solonenko & M.F. Zhukov): **Linear Direct Current Plasma Torches**, Cambridge Interscience Publishing, Great Britain, (1994)

4. ONE-DIMENSIONAL MODEL OF THE REACTOR

4.1 Basic Model

Crouse and Moore of the AEC developed and programmed a basic one-dimensional model of the reactor system, using basic heat transfer equations and force balances[3]. The complete mathematical model is shown in Appendix E.1. The reactor was treated as a cylinder with a composite wall consisting of the graphite lining and the metal reactor wall. The plasma gas and particles move downward in the centre of this cylinder, whiles the cooling water flows around the outside of the cylinder.

The following assumptions were made in the development of the model:

- Heat transfer in the system is in steady state.
- The temperature of the cooling water is constant.
- The inner and outer graphite lining was treated as one solid lining.
- No contact resistances to heat transfer were brought into consideration.
- The plasma gas is at local thermodynamic equilibrium (LTE).
- The plasma gas is optically thin.
- The diameter of the carbon particles stays more or less constant.
- Conduction heat transfer in the particles is negligible.

The program code for the model was written in **C** using a *Microsoft Visual C++* editor. The program code is given in Appendix E.2. Comments are shown in green text. The programming was done in such a way that it would be simple to follow and easy to add to when required.

A fourth-order Runge-Kutta method was implemented to solve the set of differential equations numerically. Commonly known empirical correlations were used to calculate most of the required Nusselt numbers. The exception was the Nusselt number used in calculations of the convective heat transfer between the gas and the graphite lining, because of the influence that the carbon particles has on the heat transfer. A correlation for the Nusselt number from Reference 4 that takes the two-phase flow into account was therefore implemented. The drag coefficient for the particles was programmed as a function of the Reynolds number as found in Reference 1.

The radial position of a particle is adjusted during each iteration of the model by taking into account its radial position during the previous iteration as well as the radial velocity and residence time of the particle in the reactor segment in question during the iteration. The middle line of the reactor was assigned the zero radial position and the radial position of the particle is given as either positive or negative with regard to the zero position. The initial radial position of a particle equals the inner radius of the reactor on the positive side of the zero position. When the absolute value of the radial position of the particle equals the inner radius of the reactor, the movement of the particle is adjusted to the opposite direction. Collision of the particle with the wall was assumed to be elastic.

The physical properties of the plasma gas as a function of temperature are read from a table compiled from the computer package ASTRA (see Section 2.4). Variable physical properties for the carbon particles are read from a table constructed from the JANAF Thermochemical Tables[2]. The integrated mean of the physical properties used in calculations was initially taken as the average of the specific property at the two different temperatures in question.

Initial values are assigned to the variables that have to be calculated. The gas inlet temperature is the temperature of a CF_4 plasma at an enthalpy of 7.5 kWh/kg and a carbon to CF_4 mass ratio of 0.327 as these conditions were paramount during experiments. The initial radial velocity of the particles equals the velocity of the carrier gas through the three grooves of the carbon injector. The initial axial velocity of the particles is zero. The particle inlet temperature is taken as room temperature. The initial inner and outer temperatures of the graphite lining and the reactor wall are estimated.

4.2 Expansion of model

In order to be completely relevant to the reactor used in the experiments described in this work, the basic model had to be modified and expanded. These additions to the model are shown in blue text in the program code given in Appendix E.2.

The first step was to modify the cylindrical shape used in the basic model to the actual reactor geometry. A gap between the graphite lining and the reactor wall also had to be incorporated. The gas in this gap was assumed to be immovable and only conduction and radiation heat transfer were taken into account across the gap. The ASTRA text file containing the physical

properties of the plasma gas also had to be recalculated for the reactor pressure and carbon to CF_4 ratio at which most of the experiments were performed. A function was also developed to calculate the integrated mean of the necessary properties by stepwise integration.

The Nusselt number for convective heat transfer to the cooling water was also recalculated to ensure its relevance to the reactor used. This was done with the aid of an empirical correlation from Reference 5 for water flow through an annulus. The complete calculation of this Nusselt number is found in Appendix E.3.

4.2.1 Radiation heat losses from gas

Comparison of the gas temperatures calculated with the model, with the temperatures determined from the enthalpy measured with the enthalpy probe and adjusted with the heat of reaction for the non-equilibrium reaction, showed that the calculated temperatures were much too high. (Comparison of the results obtained from the model and experimental results are discussed in more detail in Chapter 5.) As the physical properties of the plasma gas as used in the model calculations are determined at equilibrium conditions, heat of reaction for the plasma species present is intrinsically included. The only other factor contributing towards lower gas temperatures could therefore be radiation heat losses from the gas to the graphite lining and to the carbon particles. The incorporation of these radiation heat losses constituted the most significant addition to the model and the derivation of the model had to be modified slightly for this purpose – this is shown in blue text in Appendix E.1.

The assumption that the plasma gas is optically thin was observed while adding the gas radiation to the model. The greatest problem in the incorporation of the gas radiation was to find a correlation for the emissivity of the plasma gas as a function of gas temperature. Unfortunately the emissivity of CF_4 and its plasma products is not known. A general equation was therefore fitted to a plot of emissivity for CO_2 versus temperature and the parameters adjusted to fit the model more or less to the obtained experimental results. The equation has the following form:

$$\varepsilon = c_o e^{c_1 T_g}$$

where: ε = emissivity

c_o, c_1 = parameters

T_g = gas temperature [K]

The optimum set of adjusted parameters was obtained with the aid of a simplex. This is an iterative mathematical method based on the principle that the optimum solution in a solution space is associated with a corner point or an extreme value.[6] Only a simple two-factor simplex was necessary in this case. First three different (c_o; c_1) parameter sets were chosen and the response variable associated with each of these three points determined. The response variable was defined as the sum of the absolute values of the differences between the values calculated with the model and the experimental results for the gas temperature, the inner lining temperature and the outer lining temperature, divided by the number of differences calculated.

The purpose of the simplex in this case was to minimise this response variable. This is done by reflecting the parameter set that resulted in the worst value, i.e. the maximum value in this case, for the response variable through the centre of the vector that connects the other two sets with better response variables. A new group of three parameter sets is thus obtained and the process is repeated until the optimum response variable is acquired. The parameter set that resulted in the optimum response variable in this case had to be adjusted slightly as it initially predicted gas emissivities higher than one. The final values for the parameters as used in the model are c_o = 0.0136 and c_1 = 0.00106.

4.2.2 Particle Nusselt numbers

Quite a few Nusselt numbers for the heating of particles in a plasma flame is found in the literature as summarised in Table 2.2. In addition to a basic Nusselt number for convective heat transfer to and from particles, three other Nusselt numbers found in Reference 1 was compared in order to decide on the particle Nusselt number to be used in the model. The temperatures calculated with the use of the four different Nusselt numbers are shown in Figures 4.1 to 4.4. The different Nusselt numbers are identified by the names of the people who derived them. The inlet conditions used were the same as those described in Section 4.1. The initial radial velocity of the particles was taken as 30 m/s. The total gas mass flow rate, i.e. plasma gas plus carrier gas, was 3.3 kg/h and the carbon mass flow rate 1.1 kg/h. The mean particle diameter of the carbon particles was assigned a value of 50 micron and the diameter was assumed constant throughout the reactor.

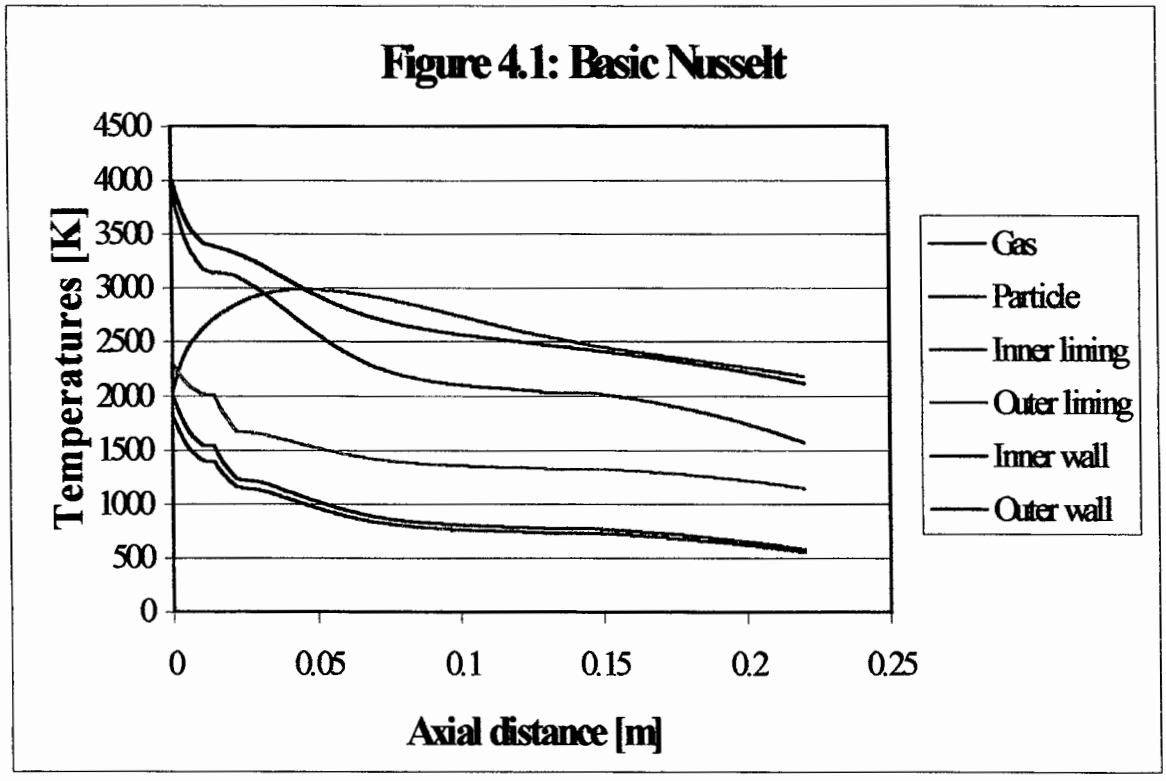

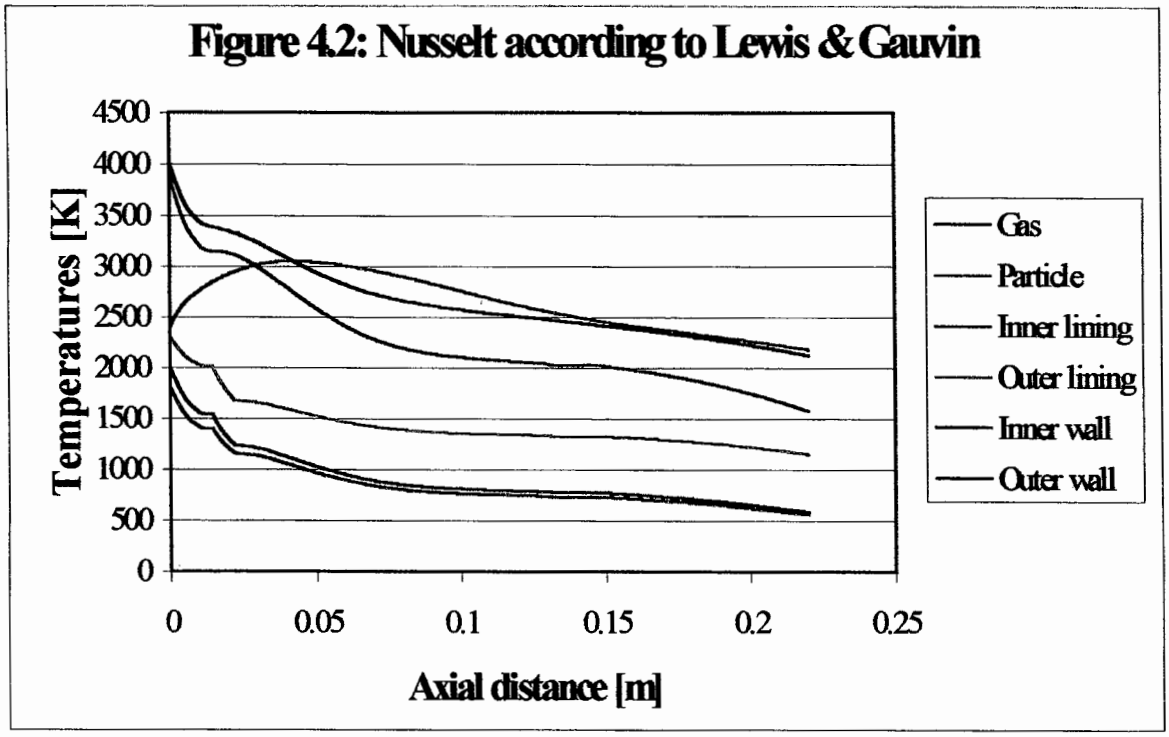

Figure 4.3: Nusselt according to Fizsdon

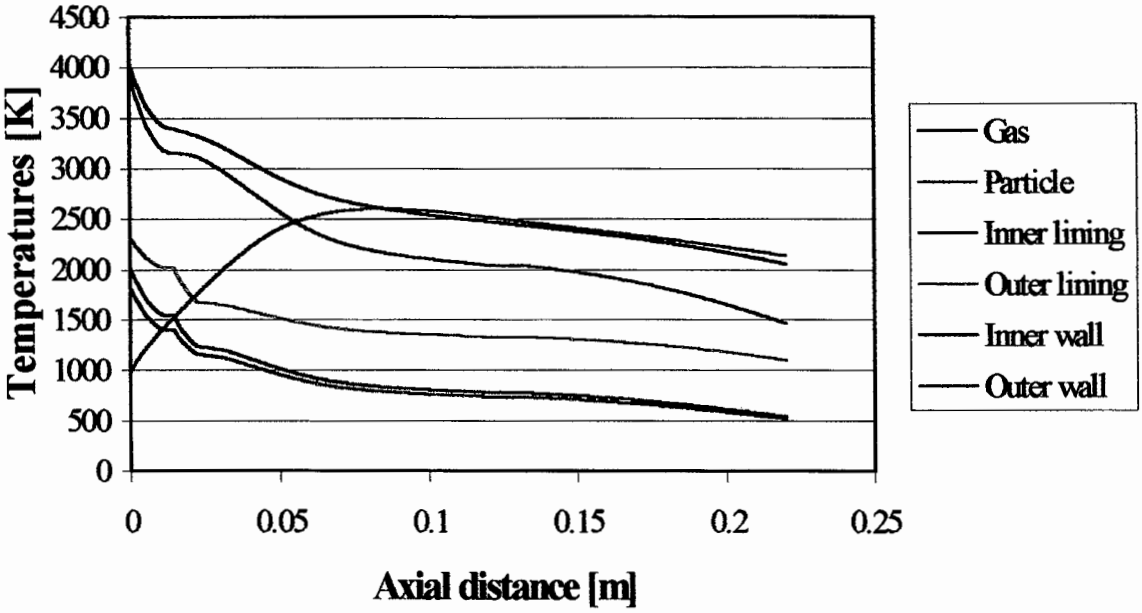

Figure 4.4: Nusselt according to Lee

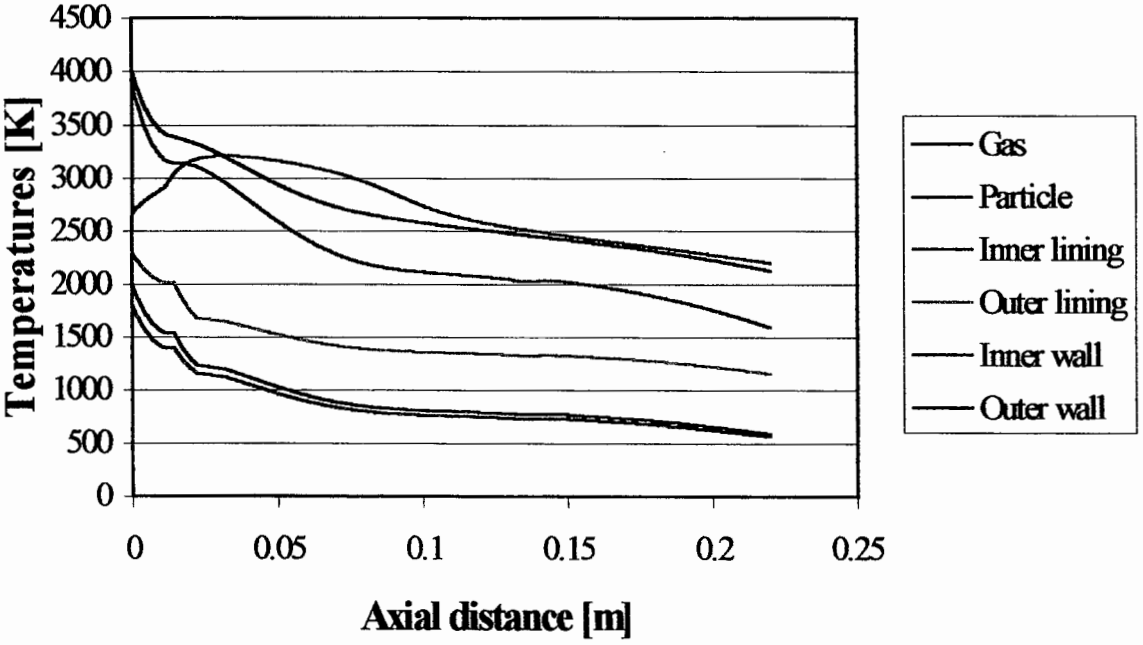

There does not seem to be much of a difference in the results obtained with the use of the different Nusselt numbers, except that the particles take a bit longer to heat up to their peak value when the Nusselt number according to Fizsdon (Figure 4.3) is used. The same response variable that was used to optimise the simplex described in Section 4.2.1 was used to decide on the particle Nusselt number to be employed. The response variable obtained with the use of the Nusselt number according to Lee (Figure 4.4) was marginally smaller than the response variables obtained with the other Nusselt numbers and was therefore decided upon.

References

1) Boulos, M.I.; Fauchais, P.; Vardelle, A. & Pfender, E., *Plasma Spraying: Theory and Applications* (editor: R. Stamanarayanan), Chapter 1: **Fundamentals of Plasma Particle Momentum and Heat Transfer**, World Scientific Publishing Company, (1993)
2) Chase, M.W., Davies, C.A., Downey, J.R., *et. al.*, *JANAF Thermochemical Tables*, 3rd edition, Journal of Physical and Chemical Reference Data, Vol. 14, Supplement No. 1, American Institute of Physics, USA, (1985)
3) Crouse, P.L. & Moore, A.M.C., Unpublished notes, AEC, (1998)
4) Gorbis, Z.R., Spokoyny, F.E., *Momentum and Heat Transfer in Turbulent Gas-Solid Flows*, Begell House, Inc., USA, (1995)
5) Jakob, M., *Heat Transfer*, Vol. 1, 6th edition, John Wiley & Sons, USA, (1958)
6) Moore, A.M.C., *Die sintese van Tetrafluoroetileen – 'n omgewingsvriendelike alternatief*, Masters Thesis, PU vir CHO, South Africa, (1997)

5. RESULTS AND DISCUSSION

Unless otherwise stated the results discussed in this chapter were obtained under the following conditions:

- A reactor pressure of 10 – 15 kPa.
- A total gas flow rate – plasma plus carrier gas – of 3.3 kg/h.
- A carbon mass flow rate of 1 – 1.1 kg/h with a particle size of less than 53 micron.
- A plasma gas enthalpy of 7 – 7.5 kWh/kg CF_4 at the inlet to the reactor.
- The quench probe at a position of 220 mm under the outlet of the plasma torch.
- An inside reactor diameter, i.e. with the graphite linings in place, of 25 mm.

5.1 Carbon injectors and particle mixing

The depth of the V-shaped grooves in the carbon injector (Section 3.1.3) was varied to determine the influence of the injection speed on the mixing of the particles with the hot plasma gas. The TFE yield was used as a measure of the mixing obtained, because the better the mixing the higher the yield. The plasma enthalpy and the mass flow rate of the carbon was kept constant as far as possible throughout the series of experiments, the plasma enthalpy varying between 6.8 and 7.2 kWh/kg, while the carbon mass flow rate was about 0.85 kg/h. The results obtained are summarised in Figure 5.1. Again the top and bottom of the vertical lines denote the minimum and maximum values, while the horizontal line indicate the mean value. The data can be found in Appendix A.4.

There is no clear trend emerging, with the yields resulting from the use of the different injectors for the most part overlapping between 30 and 35 mole % TFE. The conclusion that was reached, therefore, is that the injection speed in this case does not have a notable influence on the particle distribution and mixing. This is probably due to the presence of three evenly spaced grooves and the fact that the inner diameter of the graphite lining in the reactor system is only 25 mm, which could result in the particles "bouncing" off the lining a number of times before exiting the reactor.

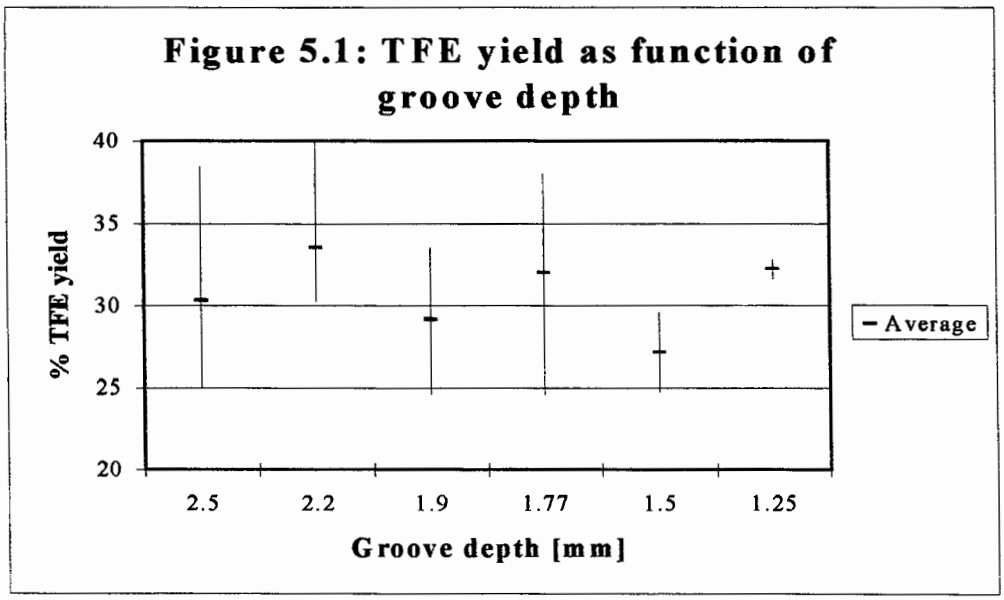

The above finding is supported by the C:CF_4 ratios determined from enthalpy probe measurements taken during carbon feeding (see Section 3.6). The C:CF_4 ratios calculated at the different axial and radial positions were sometimes less and sometimes more than the ratio of between 0.3 and 0.35 for the total reactor system, as portrayed in Figure 5.2. (The radial positions are indicated in the legend: r = Ro is immediately next to the lining, while r = 0 is in the middle of the reactor.) Again there were no real trends, which seems to indicate that the particle mixing is quite uniform, with a possible exception at 50 mm below the torch, where the particles seem to be concentrated more toward the middle of the reactor. (The enthalpy probe results are tabulated in Appendix A.5.)

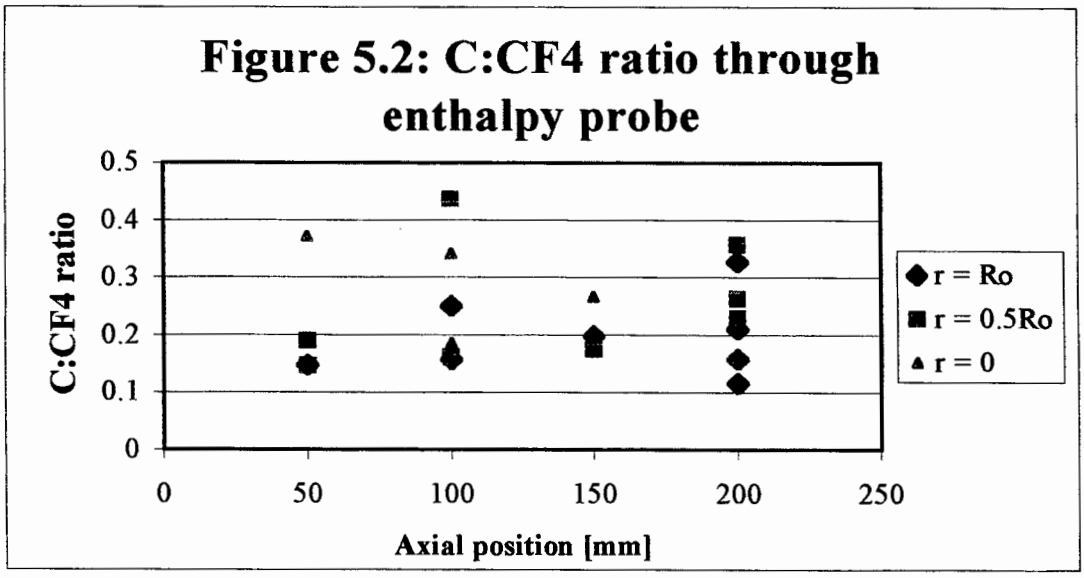

The radial movement of a particle as predicted by the one-dimensional model also supports the idea of uniform particle distribution. The model calculations were done for three different particle sizes. As shown in Figure 5.3, if elastic collisions of the particles with the wall of the reactor are assumed, a particle would cross the inside of the reactor at least once before leaving the reactor. This means that most of the particles are well exposed to the plasma tail flame during their sojourn in the reactor. The centre of the reactor is taken as the zero radial position in Figure 5.3.

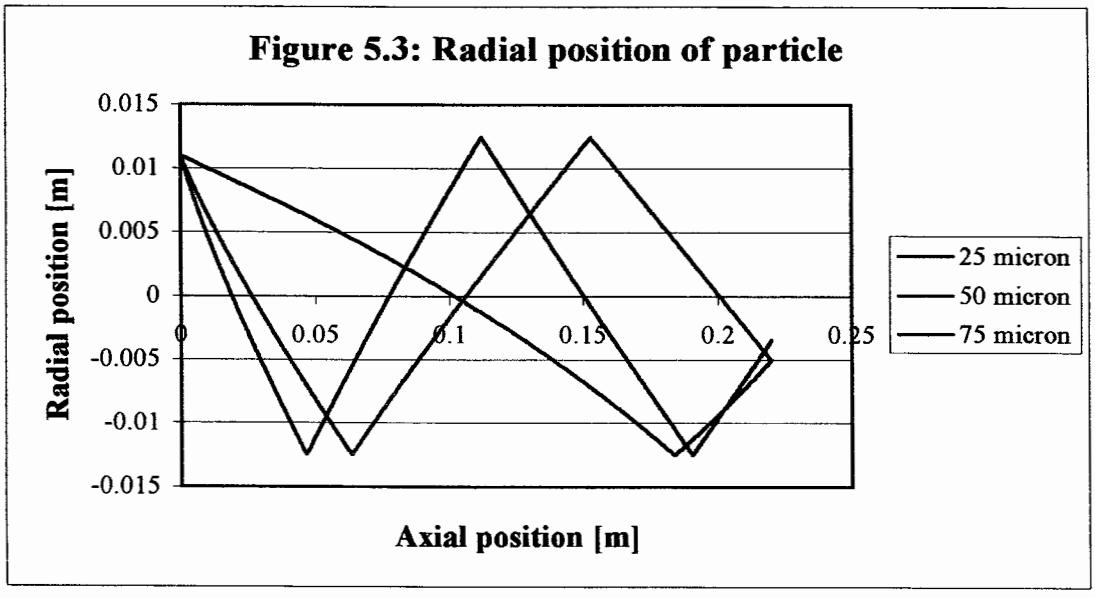

5.2 Graphite lining wall temperatures

A table containing all the graphite lining wall measurements, as well as some descriptive statistics, is given in Appendix A3. The measurements are summarised in Figures 5.4 and 5.5. The top and bottom of the vertical lines indicate the maximum and minimum temperatures measured at a certain axial position, while the horizontal lines indicate the average of the measurements at that position. The temperature distribution in the axial direction has a slightly parabolic profile for both the inner and the outer wall temperatures. The inner wall temperature decreases from about 2300 K at 50 mm below the torch to about 1450 K at the 200 mm axial position, while the outer wall temperatures decrease from about 1700 K to 1200 K over the same axial range.

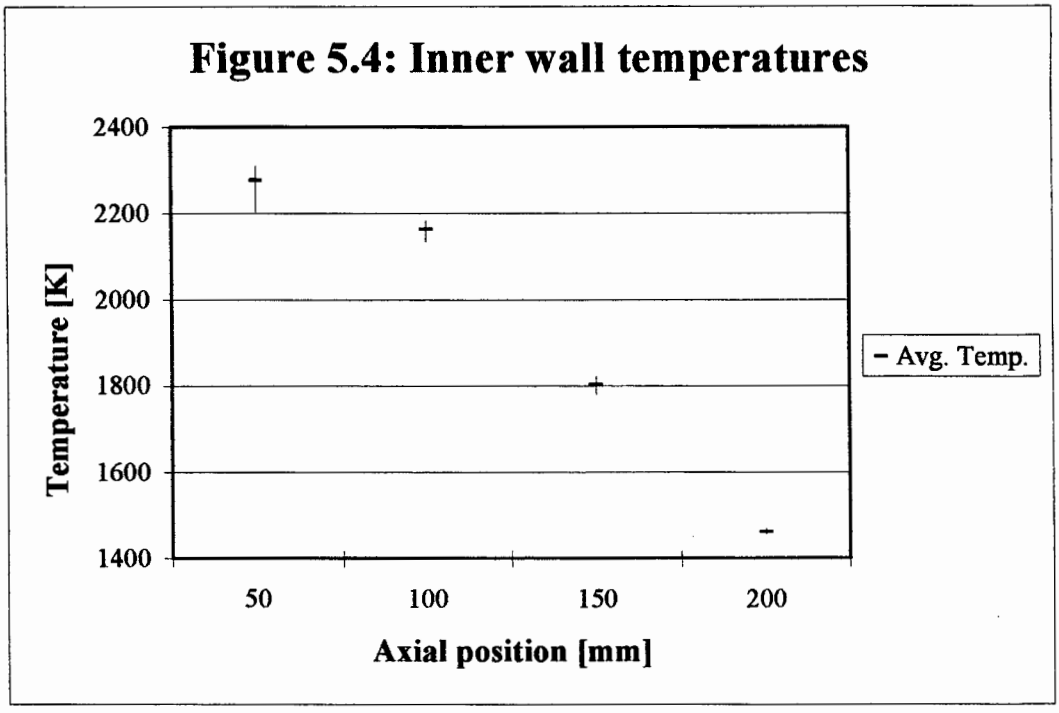

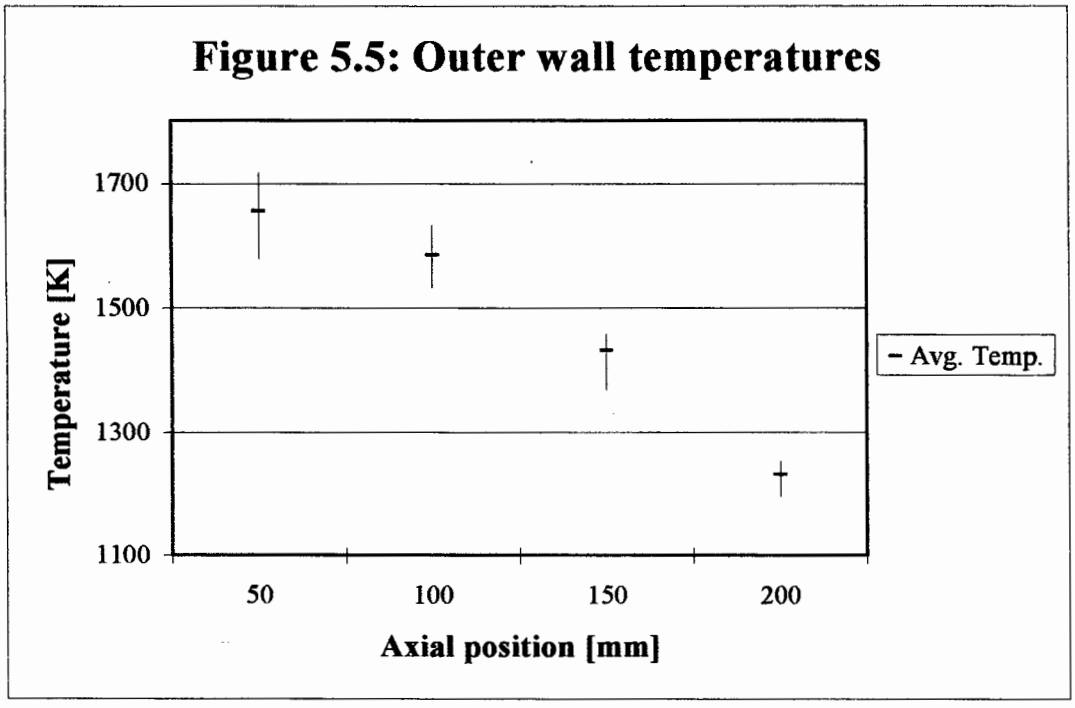

In Figure 5.6 the inner and outer lining temperatures obtained with the one-dimensional model are compared to the average experimental values. The values obtained with the model compare quite well with the experimental values, although the inner lining temperatures obtained with the model tend to be too high, while the outer lining temperatures calculated with the model tend to be too low.

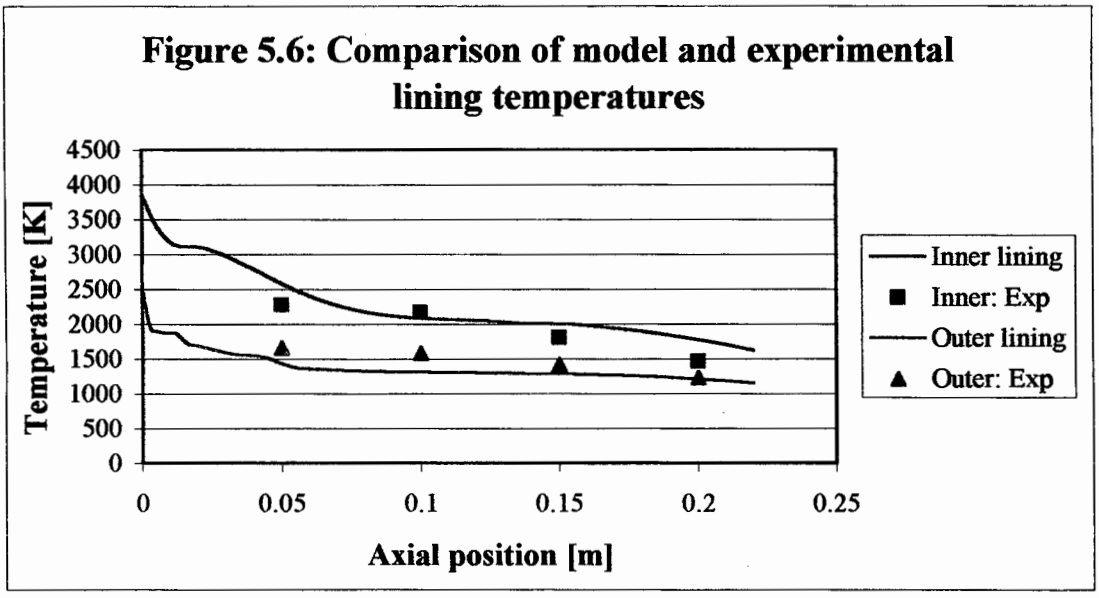

5.3 Gas radiation

The differences in the gas and lining temperatures as calculated with and without radiation heat losses from the gas to the lining and particles with the aid of the one-dimensional model, are illustrated in Figure 5.7.

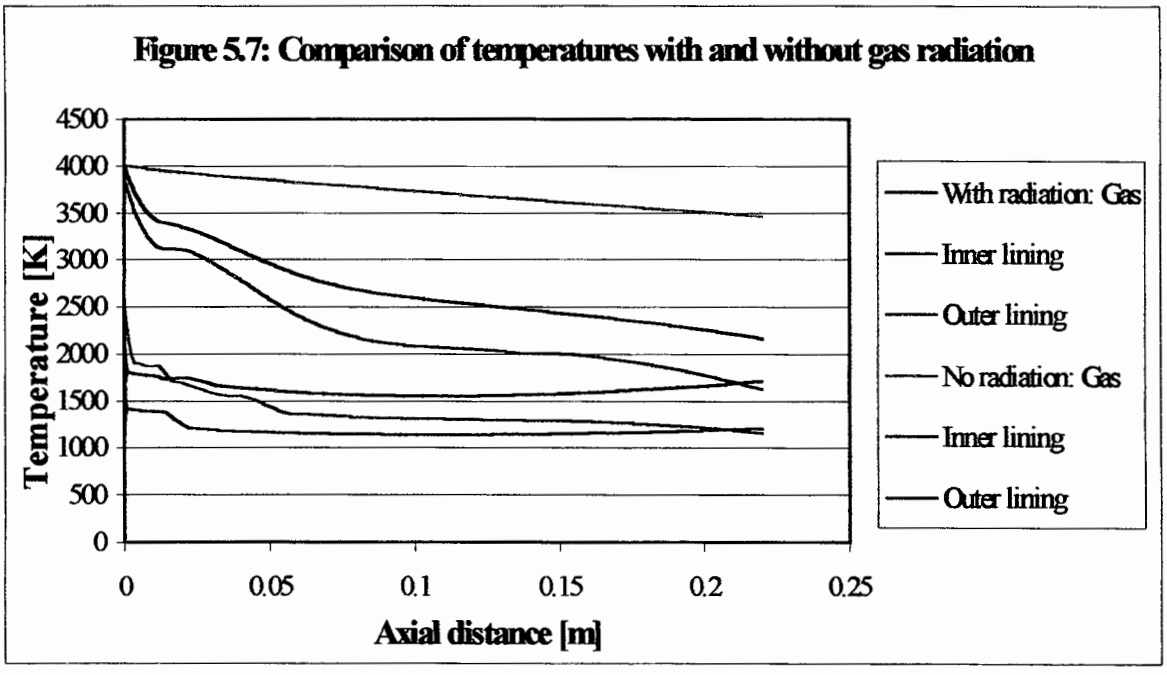

The gas temperature calculated without gas radiation being taken into account is much higher than when the radiation heat losses from the gas is incorporated into the model. In turn the lining temperatures is higher due to the gas radiation. It is clear from Figure 5.7 that incorporating the radiation heat losses from the gas into the model has a profound influence on the calculated temperatures and is therefore an important parameter in the model.

5.4 Gas temperature profile in reactor

The gas temperature profile in the reactor was derived from the enthalpy probe measurements. These measurements were done with and without carbon feed. The gas extracted with the enthalpy probe when no carbon particles were fed, essentially consisted only of CF_4. As this is the same as the equilibrium composition that would have been obtained if the gas had been cooled slowly, no reaction heat had to be added to the measured enthalpies for the measurements during which no carbon was fed. The heat of reaction for the non-equilibrium gas composition had to be added to the enthalpies measured with carbon feed, however. The reaction heat constituted 3 to 20 % of the measured enthalpy in these cases.

The temperature results obtained from these enthalpies are depicted in Figures 5.8 and 5.9. The conditions under which the enthalpy probe measurements were done, were kept as constant as possible throughout the experiments. The plasma enthalpy varied between 7 and 8 kWh/kg, the torch efficiency between 0.75 and 0.81 and the reactor pressure between 10 to 14 kPa. The mass flow rate of the CF_4 plasma gas was kept at 2.9 kg/h. The carbon feed rate, when applicable, was between 0.96 and 1.2 kg/h, while the CF_4 carrier gas flow rate was 0.4 kg/h. The C:CF_4 ratio when carbon was fed therefore varied between 0.29 and 0.36.

The gas temperature in the reactor ranges from about 2400 K at 200 mm below the torch, up to about 2700 K an axial position of 50 mm. The temperature in the centre of the reactor appears to be a bit higher than near the wall. Except at the top of the reactor, the temperatures measured with carbon feed is 30 – 50 K lower than those measured at the same position without carbon feed. This is due to the heat loss from the gas to the particles and carrier gas.

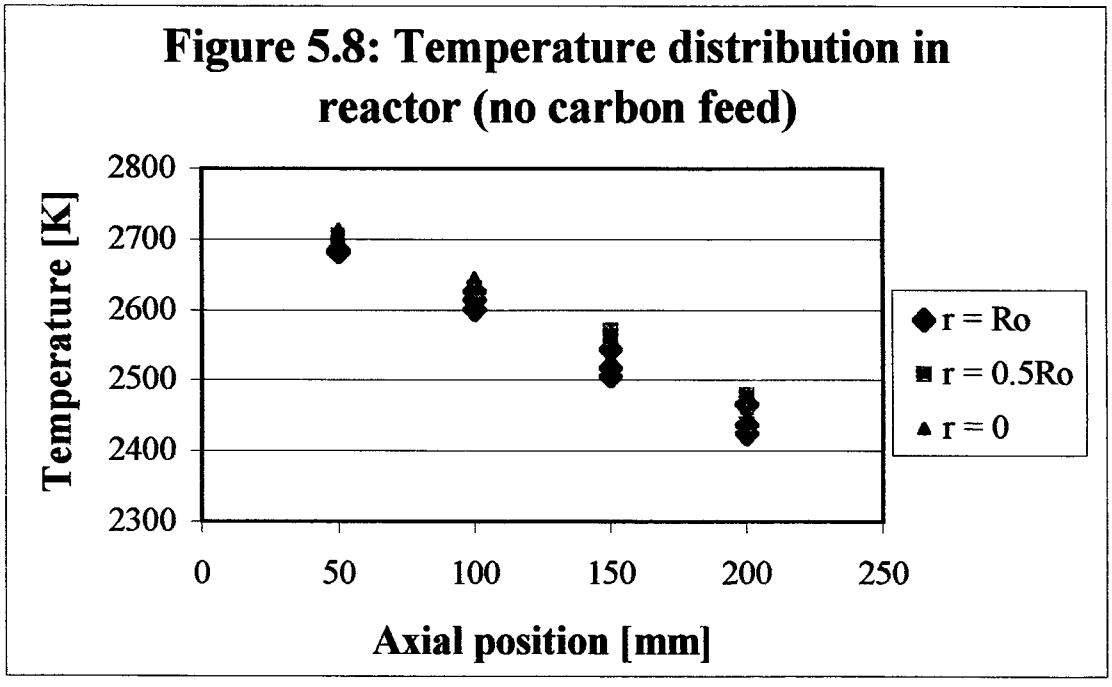

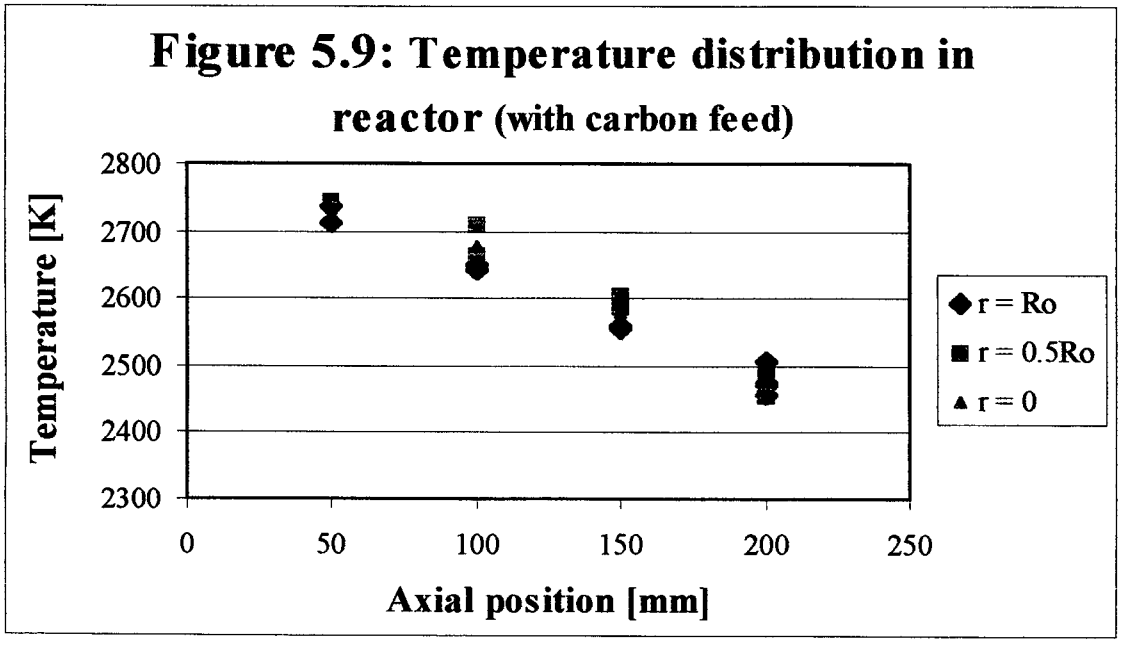

This difference in gas temperature when different amounts of carbon is fed into the plasma tail flame is also illustrated in Figure 5.10. This plot was constructed with data obtained by running the simulation program ASTRA (see Section 2.4) for different mass percentages (noted in legend) of carbon feed. At lower enthalpies, the temperature at a specific enthalpy is lower the more carbon is included in the feed material. At higher enthalpies, however, more carbon is vaporised and reactions with plasma species increases. As these reactions are exothermic, the temperature in this enthalpy region is higher when there is more carbon in the feed material. A

mass percentage of 25% carbon results in a C:CF_4 ratio of 0.3 which is about the same as the ratio fed to the experimental reactor system. It is clear that the 25% carbon line crosses the no carbon line just above 2600 K. This corresponds well with the experimental results where the gas temperature with and without carbon feed at the top of the reactor is virtually equal at about 2700 K, while the temperatures without carbon feed is higher than those with carbon feed lower in the reactor.

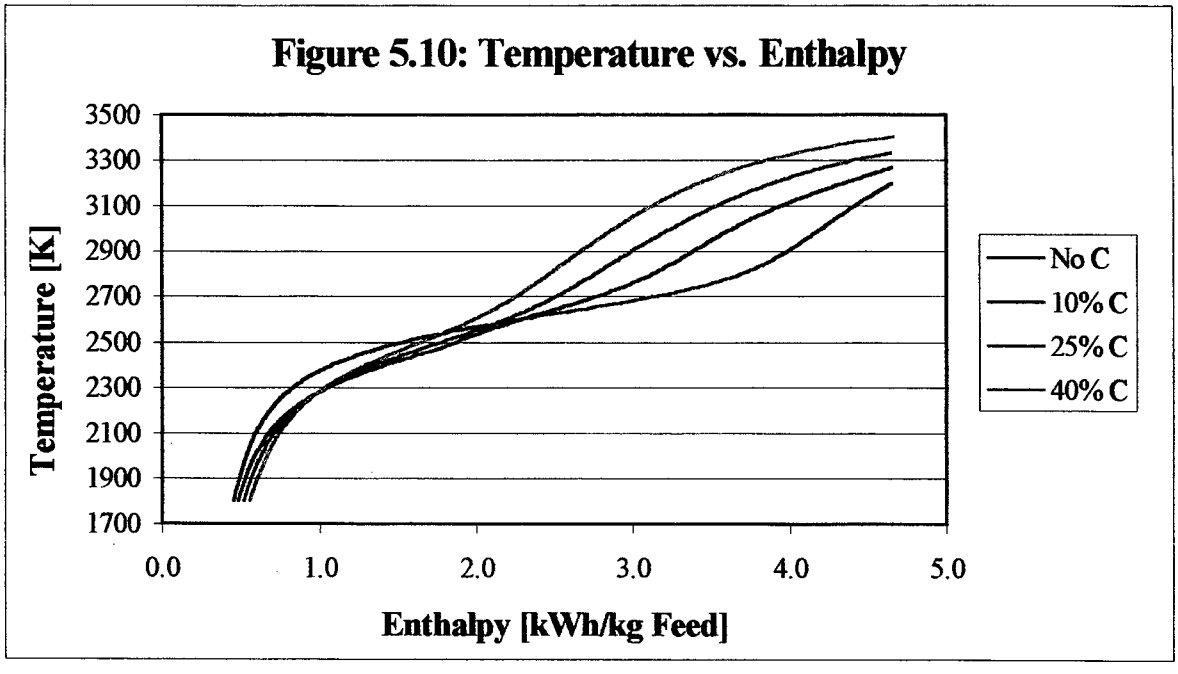

Figure 5.11 is a comparison of the average gas temperature with carbon feed as determined with the enthalpy probe and the gas temperatures predicted by the one-dimensional model. The temperatures predicted with the model correspond quite well with the experimental values. The lower experimental value at an axial position of 0.05 m is possibly due to the cooling effect of the enthalpy probe on the hot plasma gas leaving the plasma torch. The differences can also be ascribed to the assumptions made in the derivation of the model, especially the one of local thermodynamic equilibrium. The gas emissivity used for the plasma gas is also a bit suspect. It should also be kept in mind that this is only a one-dimensional model; radial effects are therefore not taken into account.

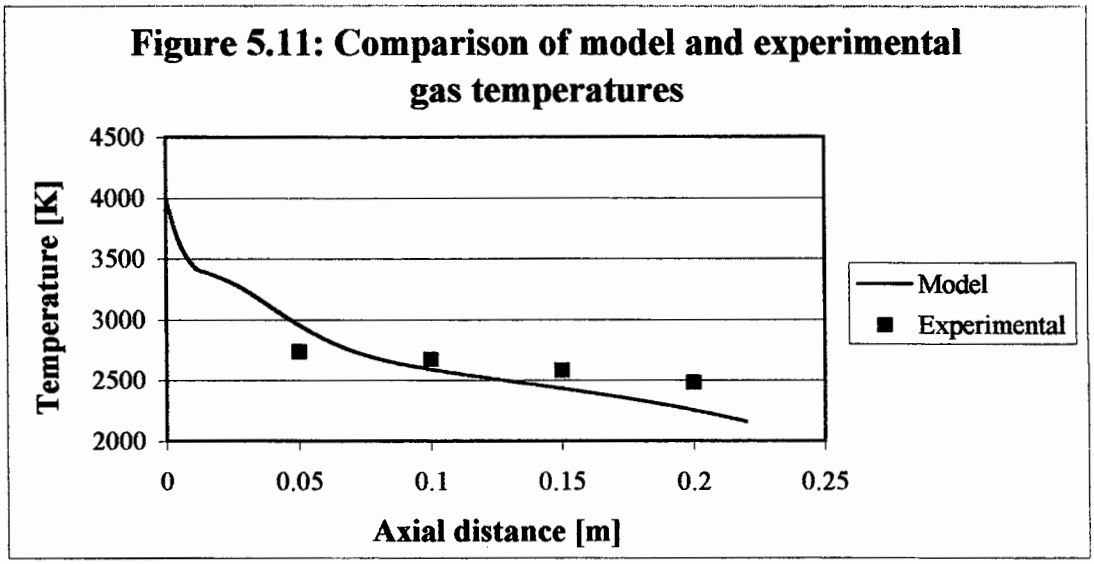

5.5 Gas velocity profile in reactor

An attempt was made to determine gas velocities in the reactor by using the enthalpy probe as a pitot tube. The variance of the results obtained were very large, however. The velocities determined at a certain location could for example vary between 200 and 400 m/s. A summary of the enthalpy probe velocity results is given in Appendix A.5. The velocities obtained were also as a rule much higher than what was expected. This caused suspicion about the accuracy of the enthalpy probe as pitot tube and it was therefore decided to do some experiments under atmospheric conditions.

This was done by blowing air with a known volumetric flow rate through an open pipe supplied with an opening for insertion of the enthalpy probe. Three pipes, with diameters of 12.4, 21.5 and 43 mm, were used for this purpose. Results obtained with the enthalpy probe were compared with those obtained with an ordinary pitot tube and a 3.2 mm capillary tube also used as pitot tube. (These results are tabulated in Appendix A.6) Comparison of the results showed clearly that the bigger the ratio of pipe inside diameter to diameter of the device used as pitot tube, the nearer the gas velocity calculated from the measured pressure differences get to the average velocities determined from the volumetric flow rate. It seems, therefore, that if the ratio of pipe inside diameter to diameter of the device used as pitot tube is too small, there is a build-up of pressure upstream of the pitot tube.

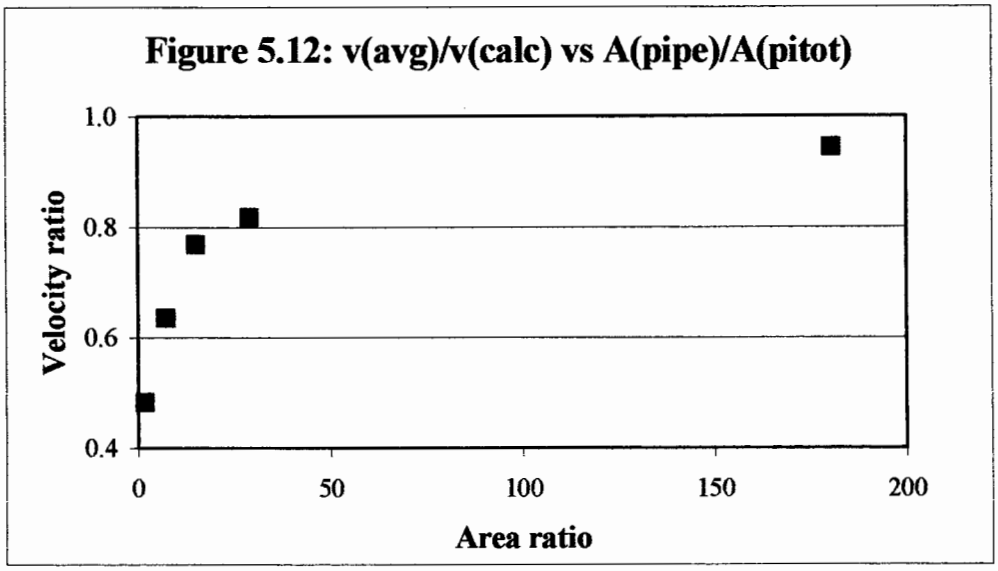

The conclusion is also illustrated in Figure 5.12. In this figure, "v(avg)" is the average velocity determined from the volumetric flow rate, while "v(calc)" is the velocity calculated from the measures pressure difference. "A(pipe)" is the cross-sectional area of the pipe used as flow channel and "A(pitot)" is the projected area of the device used as pitot tube that is "visible" to the oncoming gas flow. It is clear from the plot that the area ratio has to be at least more than fifty for pitot tube results to be at all reliable. The area ratio when the enthalpy probe is used in the reactor is at most twenty. Velocity measurements with the enthalpy probe in the reactor would therefore not give a true picture. Instead the velocities were calculated from the known gas mass flow rate through the reactor, with the density of the plasma gas determined at the average temperature with carbon feed as measured with the enthalpy probe. These results are summarised in Table 5.1.

Table 5.1: Gas velocity as function of axial distance

Ax. dist. [m]	T_{avg} [K]	$\rho(T_{avg})$ [kg/m^3]	v [m/s]
0.05	2733	0.0266	70.2
0.1	2670	0.0312	59.9
0.15	2581	0.0365	51.2
0.2	2480	0.0458	40.8

In Figure 5.13 these experimentally derived velocities are compared with the velocities predicted by the one-dimensional model. The agreement between the experimentally derived values and

the model values is acceptable, given the agreement between the experimental and model temperatures.

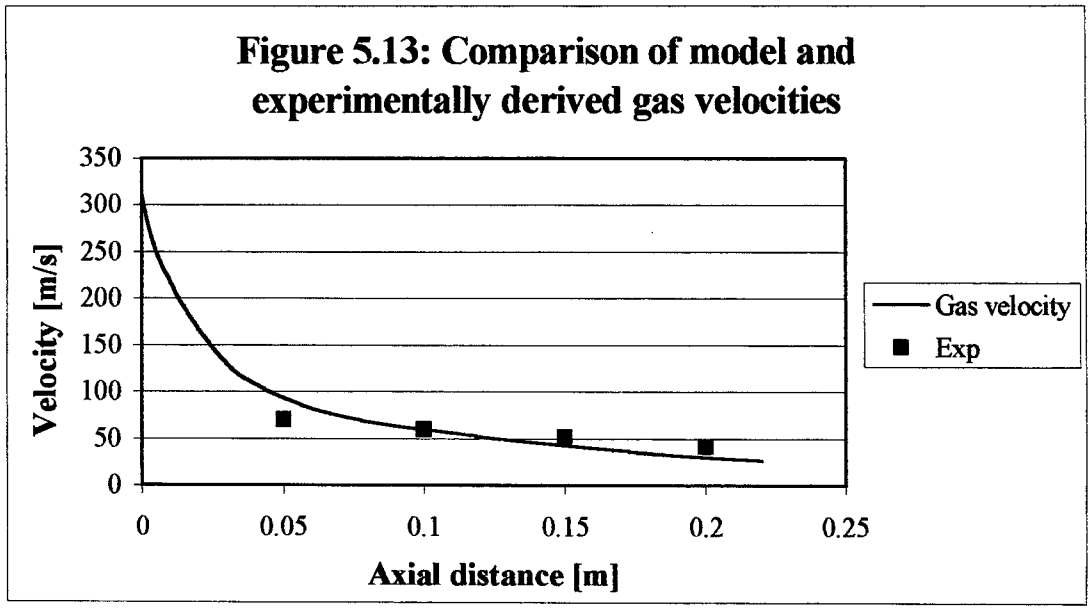

5.6 Temperature distribution through composite wall

Figure 5.14 give an illustration of the temperature distribution predicted by the one-dimensional model through the composite wall of the reactor consisting of the graphite lining, the gas gap between the lining and the reactor wall and the Inconel reactor wall.

There is very little difference between the outer and inner reactor wall temperatures. This is expected as the metal reactor wall has quite a high thermal conductivity and the wall is only 5 mm thick. The temperature difference between the inner and outer wall of the graphite lining is much higher, as the total lining is 43 mm thick and the graphite has a lower thermal conductivity. The inside of the lining is also exposed to radiation from the gas and the particles. The difference between the outer lining temperature and the inner reactor wall temperature is also large as the gas in between has a low thermal conductivity and radiation heat transfer from the colder outer lining wall is not high.

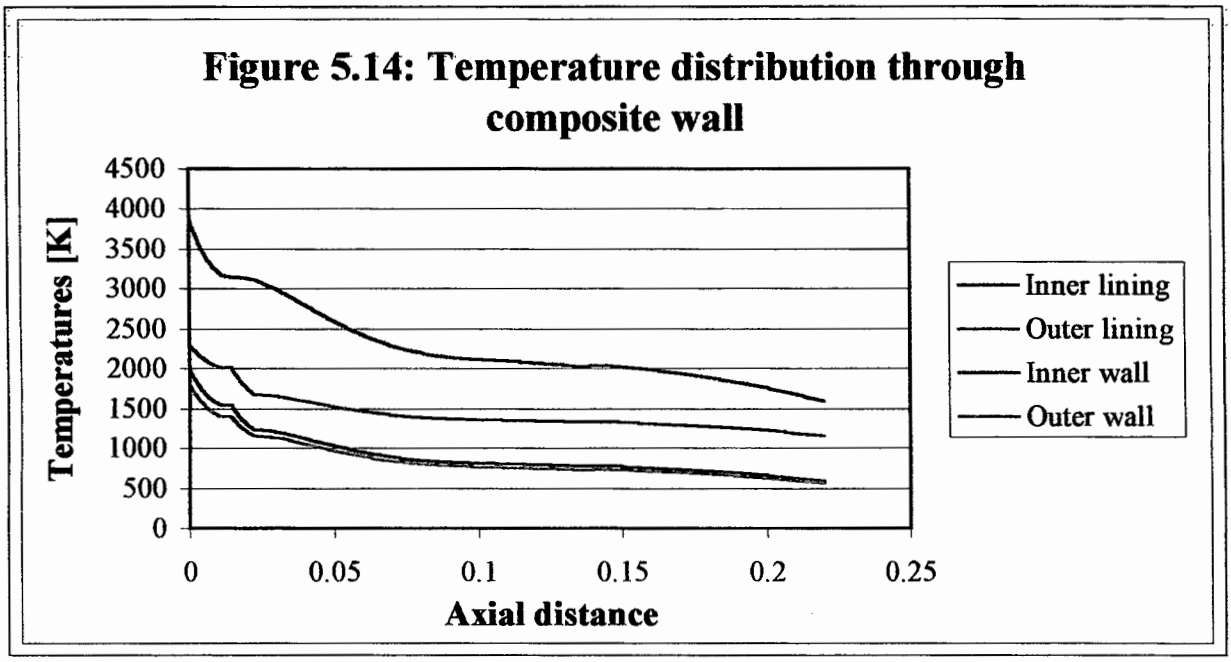

5.7 Particle Temperature

Figure 5.15 show the particle temperature with respect to the gas temperature, both as predicted by the one-dimensional model. The particles are heated up quite quickly to the gas temperature, but take longer to cool down than the gas. It therefore leaves the reactor at a slightly higher temperature than the gas.

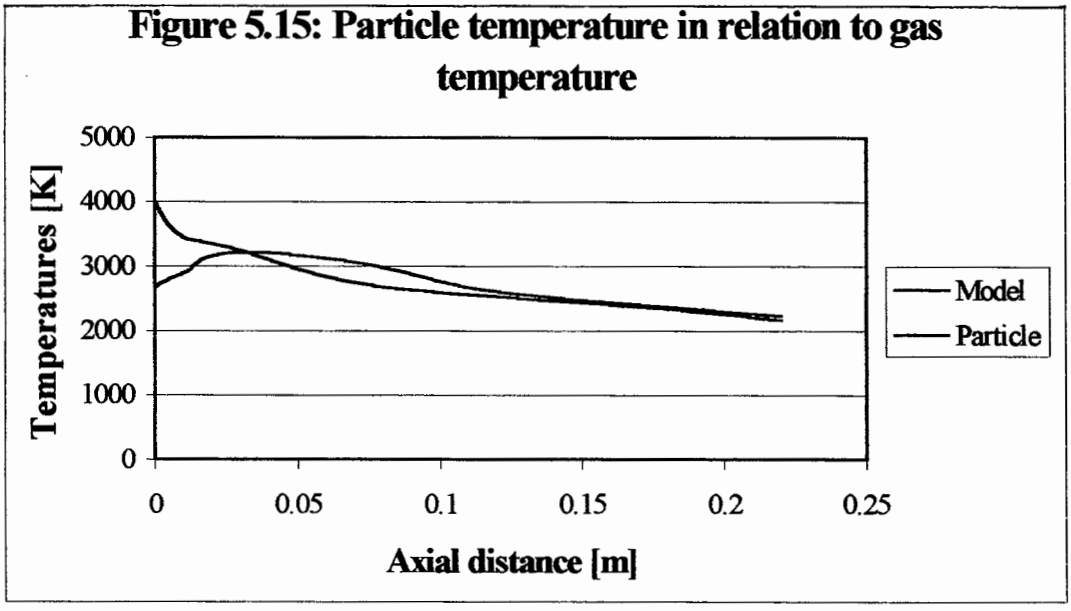

5.8 Particle velocities

Figure 5.16 show the radial and axial particle velocities as predicted by the one-dimensional model in relation to the predicted axial gas velocity. The particles are initially accelerated in the axial direction due to the higher gas velocity. It then starts to decelerate because of the deceleration of the gas, but a higher momentum keep it from decelerating as fast as the gas. In the radial direction the particles decelerate as it moves downward in the reactor, probably due to collisions with the wall and each other.

Figure 5.16: Particle velocities in relation to gas velocity

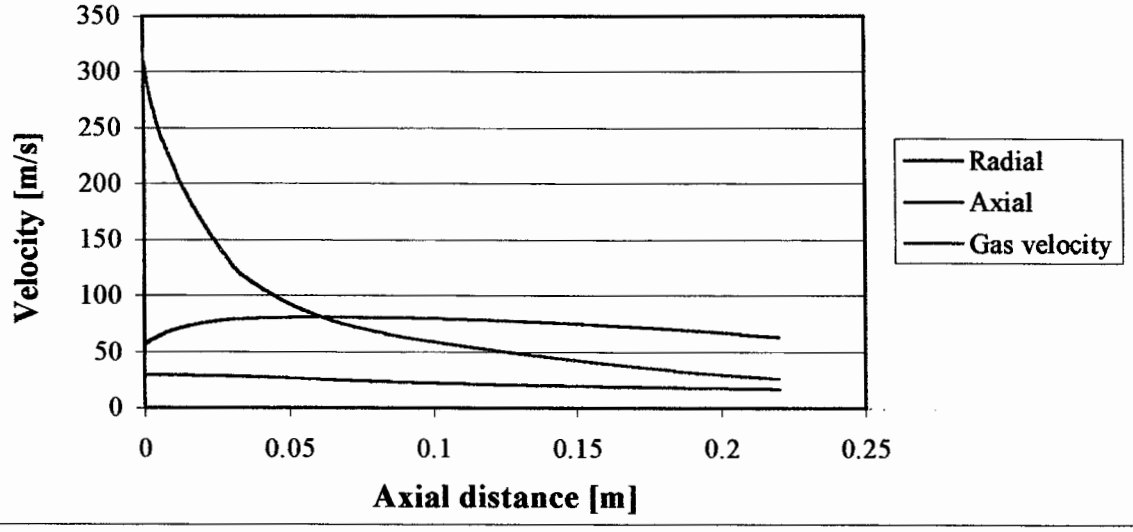

5.9 TFE yield as a function of reactor length

Gas samples were extracted through the enthalpy probe at the various measuring points to determine the TFE yield at different heights in the reactor. The results are illustrated in Figure 5.17. The TFE yield determined through the quench probe at a reactor length of 220 mm varied between 30 and 35 % for all the data points in the plot. It is clear that the TFE yield increases with an increase in reactor length. It seems to level off between 150 and 200 mm. This is in correspondence with the optimum reactor length of 220 mm as determined by Moore of the AEC.

The reaction kinetics for the formation of the necessary precursors to optimise the TFE yield is mass transfer controlled. The residence time of the reactants in the reactor therefore have to be sufficient to allow for the formation of these precursors. The gas mass flow rate has a big influence on the plasma enthalpy which is also very important for the production of the correct precursors. The residence time of the reactants is therefore best set by determining the correct reactor length.

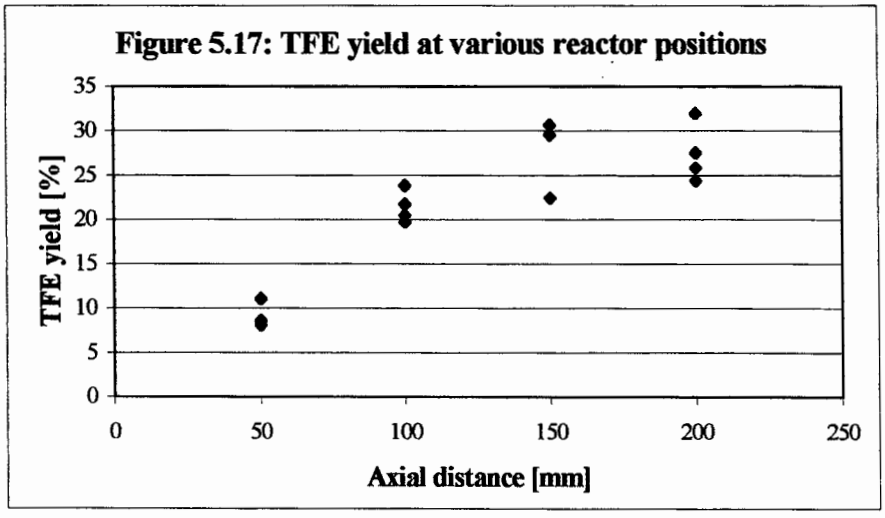

Figure 5.17: TFE yield at various reactor positions

5.10 Effect of increment size on model results

The increment size, dz, used in the one-dimensional model was varied to determine its effect on the results obtained with the model. The maximum increment size before calculation problems, e.g. gas temperatures of zero, are encountered, was determined by trial and error as 0.12 mm. The increment size employed for all the model calculations shown in this chapter, was 0.1 mm. It was found that the increment size has very little effect on the results, even when the increment size is halved from 0.1 to 0.05 mm.

5.11 Propagation of heat through particle

As mentioned in Section 2.5.2 the Biot number has to be smaller than 0.03 for uniform particle temperature to be assumed. The Biot number calculated with the aid of the one-dimensional model, varies between 0.1 and 0.6. Internal conduction in the particle should therefore to be taken into account. As the particles are extremely small, however, the internal heat propagation was neglected in these first iterations of the model.

6. CONCLUSIONS AND SUGGESTIONS

In its present form the one-dimensional model developed is adequate for predicting trends in the reactor used for this work and has been fitted quite accurately to experimental data. It has already fulfilled a useful purpose during the scale-up of the reactor system. For the model to be more credible, however, it is essential that the reaction kinetics be incorporated. This will enable better estimation of the gas properties, which are currently being determined at local thermodynamic equilibrium. To accommodate the use of larger particles, the model will have to be expanded to track the internal conduction in the particles if the calculated Biot number is larger than 0.03. The emissivity of the plasma gas also has to be determined more accurately.

The enthalpy probe was very useful in composing an experimental image of the reactor. However, as the failure of the enthalpy as pitot tube to measure gas velocities illustrated, the use of the enthalpy probe in a rather small reactor has a serious influence on its environment. Flow patterns in the reactor will be disturbed and there is a big possibility that the enthalpy probe can have a cooling effect on the plasma gas. Further use of the enthalpy probe to verify the results of the one-dimensional model, should therefore rather be undertaken in a larger reactor.

Table A1.1: Anode geometry 24/24

Gas flow rate = 3.8-3.9 kg/h

Current	Voltage [V]				Torch efficiency				Plasma enthalpy [kWh/kg]				Accuracy of energy balance			
[A]	10 kPa	20 kPa	40 kPa	75 kPa	10 kPa	20 kPa	40 kPa	75 kPa	10 kPa	20 kPa	40 kPa	75 kPa	10 kPa	20 kPa	40 kPa	75 kPa
150	137	136	140.5	145	0.74	0.69	0.83	0.67	3.92	3.64	4.51	3.80	111.47	111.52	107.26	117.74
170	136		138	142	0.77		0.82	0.71	4.57		4.98	4.45	99.99		103.44	109.81
190	135	132	135	138	0.78	0.73	0.83	0.73	5.06	4.22	5.50	4.98	101.08	106.46	98.84	101.72
200	134				0.78				5.39				99.60			
220	134	132	134	135	0.79	0.78	0.85	0.75	6.00	5.84	6.46	5.79	96.20	98.82	93.92	99.13
240	134				0.80				6.60				92.52			
250	134	132	133	133	0.80	0.79	0.84	0.76	6.89	6.76	7.25	6.63	93.28	95.06	93.14	97.33

Gas flow rate = 3.4 kg/h

Current	Voltage [V]				Torch efficiency				Plasma enthalpy [kWh/kg]				Accuracy of energy balance			
[A]	10 kPa	20 kPa	40 kPa	75 kPa	10 kPa	20 kPa	40 kPa	75 kPa	10 kPa	20 kPa	40 kPa	75 kPa	10 kPa	20 kPa	40 kPa	75 kPa
150	132	131	135.5	140	0.68	0.66	0.76	0.64	3.93	3.85	4.55	3.96	121.08	124.75	114.92	123.98
170	130	129	133	137	0.73	0.70	0.78	0.67	4.69	4.55	5.16	4.65	109.18	108.90	108.58	113.03
190	130	128	131.5	136	0.75	0.75	0.79	0.71	5.42	5.37	5.80	5.47	100.64	100.74	103.24	103.31
200	130				0.77				5.78				99.22			
220	130	128	130	133	0.78	0.76	0.82	0.74	6.48	6.35	6.87	6.44	96.77	100.77	97.47	99.59
240	130				0.78				7.09				99.08			
250	130	128	130	131	0.78	0.78	0.83	0.76	7.37	7.38	7.92	7.36	96.75	97.71	93.71	93.90

Gas flow rate = 2.9 kg/h

Current	Voltage [V]				Torch efficiency				Plasma enthalpy [kWh/kg]				Accuracy of energy balance			
[A]	10 kPa	20 kPa	40 kPa	75 kPa	10 kPa	20 kPa	40 kPa	75 kPa	10 kPa	20 kPa	40 kPa	75 kPa	10 kPa	20 kPa	40 kPa	75 kPa
150	126	126	131	134.5	0.66	0.66	0.72	0.75	4.26	4.29	4.88	5.19	123.29	121.87	118.36	111.51
170	126	124	130.5	133.5	0.71	0.70	0.76	0.78	5.20	5.06	5.77	6.06	106.56	110.27	107.69	103.83
190	125	124	129	133	0.74	0.74	0.78	0.79	6.02	5.96	6.54	6.89	98.76	104.06	105.28	98.81
200	124.5				0.75				6.40				98.39			
220	124	123	127.5	130	0.77	0.75	0.81	0.81	7.13	7.04	7.75	7.96	98.72	100.31	99.67	93.48
240	124				0.78				7.91				97.05			
250	124	124	126.5	129	0.78	0.78	0.81	0.81	8.20	8.31	8.82	9.04	97.46	96.26	95.38	91.35

Gas flow rate = 2.4 kg/h

Current	Voltage [V]				Torch efficiency				Plasma enthalpy [kWh/kg]				Accuracy of energy balance			
[A]	10 kPa	20 kPa	40 kPa	75 kPa	10 kPa	20 kPa	40 kPa	75 kPa	10 kPa	20 kPa	40 kPa	75 kPa	10 kPa	20 kPa	40 kPa	75 kPa
150	121	120	124	127	0.64	0.62	0.71	0.66	4.80	4.65	5.40	5.21	124.98	125.92	119.18	126.00
170	120	120	123	126.5	0.69	0.68	0.74	0.72	5.76	5.72	6.32	6.34	109.25	111.79	112.53	108.19
190	120	118.5	123	126	0.73	0.71	0.77	0.75	6.83	6.64	7.35	7.38	102.54	104.74	102.58	103.49
200	120				0.74				7.29				101.86			
220	119	119	123	126	0.75	0.75	0.79	0.78	8.11	8.08	8.76	8.87	100.28	101.30	100.18	98.74
240	119				0.76				8.95				96.70			
250	119	118.5	122	125	0.76	0.76	0.80	0.77	9.32	9.29	10.05	9.88	97.95	98.77	94.07	98.58

Table A1.2: Anode geometry 33/15

Gas flow rate = 3.8 kg/h

Current	Voltage [V]				Torch efficiency				Plasma enthalpy [kWh/kg]				Accuracy of energy balance			
[A]	10 kPa	20 kPa	40 kPa	75 kPa	10 kPa	20 kPa	40 kPa	75 kPa	10 kPa	20 kPa	40 kPa	75 kPa	10 kPa	20 kPa	40 kPa	75 kPa
150	139	139	134	136	0.54	0.52	0.50	0.54	2.9	2.9	2.6	2.9	117.9	110.2	111.2	102.3
170	136	137	133	135	0.59	0.58	0.56	0.60	3.6	3.5	3.3	3.6	107.7	98.1	98.2	102.1
190	135	135	132	133	0.63	0.62	0.60	0.63	4.2	4.2	4.0	4.1	100.6	101.4	101.3	99.7
200	135	133	131	132	0.64	0.64	0.62	0.64	4.6	4.4	4.3	4.4	99.1	102.2	102.4	98.1
220	134	132	131	131	0.65	0.66	0.65	0.66	5.1	5.0	4.9	4.9	99.4	99.1	99.2	101.5
240	133	131	130	129	0.68	0.68	0.66	0.67	5.7	5.6	5.5	5.4	95.1	97.4	96.6	99.8
250	132	130	128	128	0.67	0.68	0.66	0.67	5.8	5.8	5.6	5.5	96.2	98.2	97.9	99.8

Gas flow rate = 3.34 kg/h

Current	Voltage [V]				Torch efficiency				Plasma enthalpy [kWh/kg]				Accuracy of energy balance			
[A]	10 kPa	20 kPa	40 kPa	75 kPa	10 kPa	20 kPa	40 kPa	75 kPa	10 kPa	20 kPa	40 kPa	75 kPa	10 kPa	20 kPa	40 kPa	75 kPa
150	133	131	128	131	0.48	0.50	0.46	0.50	2.9	2.9	2.7	2.9	128.8	116.3	117.9	109.9
170	130	129	127	130	0.55	0.56	0.52	0.56	3.6	3.7	3.4	3.6	112.4	115.1	101.3	97.1
190	128	127	126	128.5	0.59	0.62	0.58	0.61	4.3	4.5	4.2	4.4	103.3	107.2	105.0	106.5
200	128	127	125	127	0.62	0.63	0.60	0.62	4.7	4.8	4.5	4.7	100.9	102.9	100.3	99.7
220	128	126	125	126	0.63	0.65	0.66	0.67	5.3	5.4	5.4	5.5	97.7	102.6	98.0	99.4
240	128	126	124	125	0.67	0.67	0.68	0.68	6.2	6.1	6.1	6.1	101.6	97.9	94.2	96.0
250	128	125	124	124	0.67	0.67	0.68	0.67	6.4	6.2	6.3	6.2	103.9	99.0	95.8	99.3

Gas flow rate = 2.87 kg/h

Current	Voltage [V]				Torch efficiency				Plasma enthalpy [kWh/kg]				Accuracy of energy balance			
[A]	10 kPa	20 kPa	40 kPa	75 kPa	10 kPa	20 kPa	40 kPa	75 kPa	10 kPa	20 kPa	40 kPa	75 kPa	10 kPa	20 kPa	40 kPa	75 kPa
150	127	126	123	130	0.49	0.49	0.48	0.52	3.3	3.2	3.1	3.5	113.2	115.2	121.1	107.1
170	124	122	121	126	0.55	0.55	0.54	0.58	4.1	4.0	3.9	4.3	103.2	100.9	100.1	105.8
190	123	121	120	122	0.60	0.60	0.59	0.61	4.9	4.8	4.7	4.9	105.3	106.2	101.0	104.4
200	123	120	119	121	0.62	0.61	0.60	0.62	5.3	5.1	5.0	5.2	104.7	105.3	101.3	103.3
220	122	119	119	120	0.64	0.64	0.64	0.65	6.0	5.8	5.8	5.9	100.4	100.3	101.8	98.8
240	121	119	119	119	0.66	0.65	0.66	0.66	6.6	6.5	6.6	6.5	98.8	99.2	99.0	97.5
250	121	120	119	119	0.66	0.66	0.67	0.66	7.0	6.8	6.9	6.8	98.8	100.1	98.9	97.8

Gas flow rate = 2.4 kg/h

Current	Voltage [V]				Torch efficiency				Plasma enthalpy [kWh/kg]				Accuracy of energy balance			
[A]	10 kPa	20 kPa	40 kPa	75 kPa	10 kPa	20 kPa	40 kPa	75 kPa	10 kPa	20 kPa	40 kPa	75 kPa	10 kPa	20 kPa	40 kPa	75 kPa
150	120	121	117	130	0.45	0.46	0.45	0.52	3.4	3.5	3.3	4.2	125.0	115.8	117.7	102.6
170	119	118	114.5	124	0.53	0.52	0.52	0.57	4.4	4.4	4.2	4.9	108.1	102.4	100.4	95.1
190	118	117	113	120	0.58	0.58	0.56	0.61	5.4	5.4	5.0	5.7	98.4	104.8	105.3	105.1
200	117	116	112	119	0.58	0.59	0.58	0.62	5.7	5.8	5.5	6.1	99.9	104.8	102.1	102.2
220	116	115	114	117	0.61	0.63	0.61	0.63	6.5	6.6	6.4	6.7	97.7	100.9	99.1	100.1
240	116	114		116	0.63	0.64		0.64	7.3	7.3		7.4	93.9	100.5		99.0
250	105	114	114	116	0.60	0.65	0.65	0.65	6.6	7.7	7.8	7.7	97.4	100.0	96.2	98.0

Table A2.1: Conductivity of lining

Relative time	Average water temperatures					Heat losses between segments [kW]				Average		Reactor lining temp.		S type thermocouple		Conductivity [W/m.K]	
[min]	W3	W4	W5	W6	W7	Q34	Q45	Q56	Q67	Q4	Q6	Seg 4	Seg 6	Seg 4	Seg 6	Seg 4	Seg 6
00:00	11.46	11.23	10.89	10.55	10.21	0.127	0.184	0.184	0.190	0.155	0.187	275	141	291	221	14.65	2.88
00:22	12.13	12.00	11.89	11.70	10.40	0.073	0.056	0.105	0.713	0.065	0.409	348	172	390	282	2.26	4.58
00:44	12.04	11.89	11.76	11.45	10.58	0.084	0.072	0.169	0.478	0.078	0.323	417	223	491	356	1.55	2.98
01:06	13.93	12.79	12.68	12.08	10.63	0.620	0.063	0.326	0.796	0.342	0.561	481	275	616	430	3.70	4.46
02:12	15.00	13.71	13.65	13.14	11.65	0.701	0.037	0.276	0.814	0.369	0.545	608	421	846	610	2.27	3.55
02:34	15.72	14.36	13.58	13.33	11.55	0.742	0.427	0.139	0.974	0.585	0.556	636	467	885	669	3.45	3.39
02:56	16.71	15.52	14.49	13.54	11.63	0.649	0.563	0.519	1.040	0.606	0.779	657	501	926	714	3.31	4.51
03:18	17.46	16.53	14.72	13.67	11.85	0.505	0.991	0.572	0.994	0.748	0.783	675	553	961	748	3.83	4.94
03:40	18.28	17.15	14.72	13.84	11.79	0.615	1.330	0.481	1.122	0.973	0.801	680	607	986	782	4.66	5.63
04:02	19.65	18.18	15.12	13.98	11.73	0.807	1.668	0.623	1.230	1.237	0.927	693	644	1006	804	5.80	7.11
04:24	20.55	18.92	15.27	13.99	11.92	0.886	1.996	0.701	1.131	1.441	0.916	708	667	1023	823	6.71	7.22
04:46	20.84	18.93	15.49	14.15	12.45	1.042	1.880	0.730	0.928	1.461	0.829	716	680	1040	839	6.61	6.43
05:30	21.17	19.42	15.44	14.68	12.63	0.961	2.173	0.415	1.122	1.567	0.768	741	697	1074	853	6.90	6.05
05:53	21.86	19.54	15.57	14.90	12.31	1.268	2.166	0.369	1.415	1.717	0.892	757	700	1089	870	7.59	6.47
06:37	21.81	19.27	15.77	15.16	12.45	1.389	1.909	0.337	1.481	1.649	0.909	765	718	1117	888	6.88	6.58
08:27	22.38	20.72	16.39	15.15	12.40	0.911	2.363	0.678	1.502	1.637	1.090	771	732	1156	914	6.23	7.36
08:49	23.09	20.89	16.66	15.35	12.66	1.201	2.308	0.720	1.466	1.754	1.093	784	742	1163	919	6.79	7.58
11:45	23.10	21.95	16.91	15.84	12.69	0.627	2.755	0.584	1.723	1.691	1.154	791	749	1177	942	6.42	7.34
13:35	23.91	21.66	16.49	15.91	12.10	1.230	2.823	0.317	2.080	2.027	1.198	793	750	1181	951	7.66	7.34
13:57	23.72	22.79	16.68	15.93	12.59	0.511	3.339	0.410	1.822	1.925	1.116	797	753	1183	953	7.31	6.87
18:44	23.68	22.71	16.89	16.08	12.66	0.527	3.177	0.444	1.870	1.852	1.157	798	761	1181	964	7.10	7.00

A.3 Pyrometric measurements of graphite lining wall temperatures

Table A3.1: Lining Temperatures

	Graphite lining inner wall				Graphite lining outer wall			
Axial position:	50 mm	100 mm	150 mm	200 mm	50 mm	100 mm	150 mm	200 mm
Temperature	2202	2151	1779	1455	1598	1538	1343	1194
Values [K]:	2206	2132	1784	1455	1578	1531	1368	1212
	2287	2159	1814	1455	1688	1634	1446	1240
	2298	2184	1817	1460	1716	1630	1459	1253
	2307	2178	1823	1470	1695	1594	1454	1252
	2299	2171		1469				
	2310							
	2301							
Minimum:	2202	2132	1779	1455	1578	1531	1343	1194
Maximum:	2310	2184	1823	1470	1716	1634	1459	1253
Average:	2276	2163	1803	1461	1655	1585	1414	1230
Std. Deviation:	45.1	19.2	20.3	7.1	62.4	49.1	54.3	26.1

A.4 Carbon injectors

Table A4.1: Results obtained with different carbon injectors

Groove depth = 2.5 mm

						Max	Min	Avg
C2F6	7.92	6.4	5.17	5.45	5.23	7.92	5.17	6.03
C2F4	38.46	31.58	27.68	29	24.94	38.46	24.94	30.33
C3F6	2.17	1.42	1.15	1.27	0.9	2.17	0.90	1.38

Groove depth = 2.2 mm

				Max	Min	Avg
C2F6	8.57	5.13	5.15	8.57	5.13	6.28
C2F4	40.05	30.34	30.19	40.05	30.19	33.53
C3F6	1.35	0.59	1.05	1.35	0.59	1.00

Groove depth = 1.9 mm

								Max	Min	Avg
C2F6	6.32	7.09	6.05	6.82	5.85	6.11	5.63	7.09	5.63	6.27
C2F4	25.53	29.97	24.54	28.57	30.71	33.53	31.21	33.53	24.54	29.15
C3F6	0.986	1.22	0.91	0.584	1.24	0.675	1.13	1.24	0.58	0.96

Groove depth = 1.77 mm

								Max	Min	Avg
C2F6	7.63	5.15	6.57	8.04	6.11	7.71	7.76	8.04	5.15	7.00
C2F4	34.07	24.53	31.28	38.01	26.48	33.62	35.86	38.01	24.53	31.98
C3F6	1.43	1.01	1.39	1.66	1.16	1.69	1.46	1.69	1.01	1.40

Groove depth = 1.5 mm

			Max	Min	Avg
C2F6	6.26	7.11	7.11	6.26	6.69
C2F4	24.71	29.6	29.60	24.71	27.16
C3F6	0.85	1.11	1.11	0.85	0.98

Groove depth = 1.25 mm

			Max	Min	Avg
C2F6	7	8.13	8.13	7.00	7.57
C2F4	31.59	32.81	32.81	31.59	32.20
C3F6	1.2	1.25	1.25	1.20	1.23

A.5 Enthalpy probe results

Table A5.1: Temperatures obtained with no carbon feed

Experiment name	Axial position [mm]	Radial position	Temperature [K]	Error Percentage	Reactor pressure [kPa]	Plasma enthalpy [kWh/kg CF4]	Torch efficiency
H1016b	50	Ro	2682	18.44	10.4	7.1	0.75
H0505a	50	Ro	2684	12.81	14.5	7.53	0.8
H1023d	50	0.5 Ro	2704	23.91	10.1	7.23	0.78
H0505b	50	0.5 Ro	2703	14.01	15.1	7.46	0.76
H1006c	50	0	2685	7.18	12	7.5	0.77
H0530c	50	0	2714	15.09	12.2	7.47	0.78
H1002a	100	Ro	2626	15.18	12.7	7.3	0.78
H0504a	100	Ro	2615	15.07	11	7.32	0.8
H0423b	100	Ro	2601	11.82	11	7.58	0.78
H1002b	100	0.5 Ro	2631	11.4	10.7	7.3	0.78
H0423c	100	0.5 Ro	2626	10.01	11.1	7.6	0.78
H1020d	100	0	2640	20.53	9.8	7.21	0.79
H1020c	100	0	2645	24.18	10.2	7.66	0.78
H0504d	100	0	2645	7.84	13.2	7.39	0.8
H1001a	150	Ro	2545	15.04	10.4	7.2	0.77
H0429c	150	Ro	2518	9.34	12.8	7.68	0.81
H0421d	150	Ro	2506	20.41	11.1	7.63	0.78
H0429d	150	0.5 Ro	2562	16.25	13.5	7.62	0.8
H0421e	150	0.5 Ro	2570	18.91	10.9	7.55	0.78
H1001c	150	0	2553	24.57	10.4	7.2	0.77
H0429e	150	0	2559	25.39	14.7	7.88	0.81
H0421f	150	0	2558	16.95	10.9	7.65	0.79
H0429a	200	Ro	2426	9.26	10.5	-	-
H0930a	200	Ro	2467	13.2	11	7.2	0.77
H0424a	200	Ro	2438	20.28	11.2	7.76	0.78
H0930c	200	0.5 Ro	2479	23.35	11.2	7.1	0.77
H0424b	200	0.5 Ro	2439	23.43	11.3	7.98	0.81
H0424c	200	0	2461	15.19	11.6	7.81	0.8
H0423a	200	0	2473	25.5	11.1	7.66	0.78

Table 5.2: Temperature results with carbon feed

Experiment name	Axial position [mm]	Radial position	Error percentage	Reactor pressure [kPa]	Plasma enthalpy [kWh/kg CF4]	Torch efficiency	C(s)/CF4 (Hprobe)	C(s)/CF4 (reactor)	% TFE (Hprobe)	% TFE (Quench)	Measured enthalpy [kWh/kg]	Reaction heat [kWh/kg]	Total enthalpy [kWh/kg]	Temperature [K]
H1023a	50	Ro	17.01	10.4	7.31	0.78	0.148	0.313	13.59	24.32	2.8	0.1273	2.93	2737
H1016e	50	Ro	23.08	11.9	7.52	0.78	0.0798	0.291	8.59	15.31	2.85	0.0829	2.93	2711
H1026a	50	0.5 Ro	19.21	11.2	7.16	0.77	0.147	0.333	11.07	31.4	2.82	0.1035	2.92	2743
H1023c	50	0.5 Ro	17.95	10.2	7.32	0.78	0.19	0.313	10.09	24.32	2.78	0.0975	2.88	2742
H1026b	50	0	16.74	12.2	7.13	0.77	0.372	0.333	8.65	31.4	2.59	0.0360	2.63	2735
H0330c	50	0	11.96	11.7	7.79	0.8	0.111	0.334	8.13	30.43	2.86	0.0772	2.94	2732
H0327c	100	Ro	14.83	12.2	7.85	0.8	0.251	0.357	21.77	32.58	2.24	0.1978	2.44	2644
H1020a	100	Ro	17.38	10.1	7.87	0.8	0.157	0.343	23.81	35.27	2.41	0.2325	2.64	2649
H1020b	100	0.5 Ro	14.66	10.2	7.78	0.79	0.437	0.343	20.52	35.27	2.31	0.2696	2.58	2708
H0327b	100	0.5 Ro	16.67	11.4	7.87	0.79	0.162	0.283	19.74	28.65	2.45	0.1805	2.63	2665
H0327a	100	0	18.49	11.3	7.75	0.79	0.342	0.316	23.89	32.92	2.28	0.2144	2.49	2677
H0327d	100	0	15.56	13.9	7.78	0.79	0.185	0.318	19.75	33.07	2.37	0.1790	2.55	2679
H1022a	150	Ro	14.78	10.2	7.29	0.79	0.199	0.382	30.62	34.97	1.97	0.2765	2.25	2558
H1022b	150	Ro	15.11	10.2	7.39	0.81	0.678	0.382	29.57	34.97	1.66	0.2650	1.93	2556
H0417b	150	0.5 Ro	9.47	12.4	7.61	0.78	0.176	0.354	-	28.5	2.11	0.1577	2.27	2586
H0326a	150	0.5 Ro	16.82	15.3	7.63	0.77	0.0905	0.303	13.01	28.05	2.03	0.1185	2.15	2605
H1022c	150	0	17.61	9.8	7.56	0.79	0.749	0.335	16.81	26.82	1.89	0.1550	2.05	2603
H0325a	150	0	12.59	13.2	7.71	0.77	0.266	0.294	22.42	31.77	1.94	0.2029	2.14	2578
H1013a	200	Ro	14.4	10.5	7.4	0.79	0.211	0.34	28.54	28.48	1.51	0.2524	1.76	2459
H0414a	200	Ro	12.89	10.2	7.74	0.8	0.328	0.322	38.05	39.07	1.44	0.3364	1.78	2474
H0930b	200	Ro	21.83	13.1	7.2	0.77	0.159	0.357	36.82	37.23	1.42	0.3207	1.74	2475
H0324a	200	Ro	16.76	10.4	7.93	0.78	0.0528	0.328	31.96	33.2	1.58	0.2844	1.86	2508
H0320b	200	Ro	13.99	13.1	7.78	0.78	0.116	0.277	14.57	22.7	1.55	0.1364	1.69	2473
H1013b	200	0.5 Ro	14.56	10.5	7.4	0.78	0.264	0.34	27.56	28.48	1.62	0.2445	1.86	2486
H0416a	200	0.5 Ro	10.6	10.1	7.53	0.77	0.23	0.276	25.87	33.57	1.51	0.2318	1.74	2453
H0324b	200	0.5 Ro	23.19	11.4	7.96	0.78	0.358	0.336	-	33.2	1.54	0.2440	1.78	2483
H1015a	200	0	23.1	10.3	8.1	0.8	0.0886	0.427	27.57	30.37	1.59	0.2519	1.84	2489
H1015b	200	0	17.92	10.5	8.1	0.8	0.164	0.427	24.38	30.37	1.78	0.2166	2.00	2501

Table A5.3: Velocity results

Experiment name	Axial position [mm]	Radial position	Velocity [m/s]	Error Percentage	Reactor pressure [kPa]	Plasma enthalpy [kWh/kg CF_4]	Torch efficiency
H1006a	50	Ro	79.2	4.97	12	7.5	0.77
H0505a	50	Ro	88.08	9.29	14.5	7.53	0.8
H0430a	50	Ro	444.27	14.07	10.9	7.2	0.78
H0430d	50	Ro	106.82	12.72	13.7	7.74	0.8
H0505b	50	0.5 Ro	216.11	12.41	15.1	7.46	0.76
H0430b	50	0.5 Ro	482.06	10.53	10.2	7.63	0.79
H0505c	50	0	245.48	23.58	20.1	7.55	0.77
H0430c	50	0	559.84	7.56	12.2	7.47	0.78
H0504a	100	Ro	222.04	8.23	11	7.32	0.8
H1002a	100	Ro	270.15	7.6	10.7	7.3	0.78
H0504c	100	Ro	102.56	13.02	12.2	7.28	0.81
H0423b	100	Ro	255.89	6.16	11	7.58	0.78
H1002b	100	0.5 Ro	246.27	10.01	10.7	7.3	0.78
H1002e	100	0.5 Ro	126.88	10.01	10.7	7.3	0.78
H0504b	100	0.5 Ro	150.18	12.86	10.2	7.45	0.8
H0423c	100	0.5 Ro	233.32	5.01	11.1	7.6	0.78
H1002c	100	0	157.13	2.2	10.7	7.3	0.77
H1002d	100	0	160.44	2.24	10.7	7.3	0.78
H0504d	100	0	226.1	3.93	13.2	7.39	0.8
H0423d	100	0	170.48	8.73	11	7.62	0.78
H1001a	150	Ro	212.68	7.61	10.4	7.2	0.77
H0429c	150	Ro	150.03	5.48	12.5	7.68	0.81
H0421d	150	Ro	188.66	10.21	11.1	7.63	0.78
H1001b	150	0.5 Ro	155.8	12.66	10.4	7.2	0.77
H0429d	150	0.5 Ro	139.15	8.13	13.5	7.62	0.8
H0421e	150	0.5 Ro	189.28	9.5	10.9	7.55	0.78
H1001c	150	0	171.85	12.29	10.4	7.2	0.77
H1001d	150	0	146.78	9.04	12.4	7.2	0.77
H0429e	150	0	146.73	12.7	14.7	7.88	0.81
H0421f	150	0	194.17	8.48	10.9	7.65	0.79
H0429a	200	Ro	155.92	10.82	10.5	-	-
H0930a	200	Ro	158.31	6.88	11	7.2	0.77
H0429b	200	Ro	129.86	8.88	12.5	-	-
H0424a	200	Ro	136.85	10.39	11.2	7.76	0.78
H0421c	200	Ro	106.36	11.1	10.9	7.57	0.78
H0930c	200	0.5 Ro	117.58	11.68	11.2	7.1	0.77
H0424b	200	0.5 Ro	148.2	11.72	11.3	7.98	0.81
H0421b	200	0.5 Ro	126.31	8.23	11	7.45	0.78
H0424c	200	0	156.242	7.61	11.6	7.81	0.8
H0423a	200	0	183.31	12.78	11.1	7.66	0.78
H0421a	200	0	130.2	15.86	10.9	7.54	0.78

A.6 Pitot tube experiments

Table A6.1: Pitot tube results

D = 12.4 mm

Setting [%]	Q [m3/h]	v(avg) [m/s]	Re	Delta P [Pa]	v(calc) [m/s]	v(calc) / v(avg)
8	3.42	7.88	5293	189	19.47	2.47
10	4.28	9.85	6616	298	24.45	2.48
12	5.14	11.82	7939	407	28.57	2.42
15	6.42	14.77	9924	621	35.30	2.39
18	7.71	17.72	11909	846	41.20	2.32
20	8.56	19.69	13232			
25	10.70	24.62	16540			

D = 21.5 mm

Setting [%]	Q [m3/h]	v(avg) [m/s]	Re	Delta P [Pa]		v(calc) [m/s]		v(calc)/v(avg)	
				Middle	Wall	Middle	Wall	Middle	Wall
10	4.28	3.28	3816	13	10	5.11	4.48	1.56	1.37
15	6.42	4.91	5724	29	24	7.63	6.94	1.55	1.41
20	8.56	6.55	7632	53	45	10.31	9.50	1.57	1.45
25	10.70	8.19	9540	89	76	13.36	12.35	1.63	1.51
30	12.84	9.83	11448	126	100	15.90	14.16	1.62	1.44
35	14.98	11.46	13355	181	144	19.05	17.00	1.66	1.48
40	17.12	13.10	15263	238	192	21.85	19.63	1.67	1.50

D = 43 mm

Setting [%]	Q [m3/h]	v(avg) [m/s]	Re	Delta P [Pa]		v(calc) [m/s]		v(calc)/v(avg)	
				Middle	Wall	Middle	Wall	Middle	Wall
30	12.84	2.46	5724	3	1	2.45	1.42	1.00	0.58
35	14.98	2.87	6678	5	1	3.17	1.42	1.11	0.49
40	17.12	3.28	7632	8	4	4.01	2.83	1.22	0.86
45	19.26	3.68	8586	11	6	4.70	3.47	1.27	0.94
50	21.41	4.09	9540	14	9	5.30	4.25	1.29	1.04
55	23.55	4.50	10494	19	11	6.17	4.70	1.37	1.04
58	24.83	4.75	11066	24	16	6.94	5.67	1.46	1.19

Table A6.2: Capillary results

D = 12.4 mm

Setting [%]	Q [m3/h]	v(avg) [m/s]	Re	Delta P [Pa]	v(calc) [m/s]	v(calc) v(avg)
8	3.42	7.88	5293	42	9.18	1.17
10	4.28	9.85	6616	84	12.98	1.32
12	5.14	11.82	7939	118	15.39	1.30
15	6.42	14.77	9924	184	19.21	1.30
18	7.71	17.72	11909	267	23.14	1.31
20	8.56	19.69	13232	334	25.88	1.31
25	10.70	24.62	16540	570	33.81	1.37

D = 21.5 mm

Setting [%]	Q [m3/h]	v(avg) [m/s]	Re	Delta P [Pa]		v(calc) [m/s]		v(calc)/v(avg)	
				Middle	Wall	Middle	Wall	Middle	Wall
10	4.28	3.28	3816	7	6	3.75	3.47	1.14	1.06
15	6.42	4.91	5724	17	14	5.84	5.30	1.19	1.08
20	8.56	6.55	7632	40	25	8.96	7.08	1.37	1.08
25	10.70	8.19	9540	58	55	10.79	10.50	1.32	1.28
30	12.84	9.83	11448	96	74	13.88	12.18	1.41	1.24
35	14.98	11.46	13355	132	97	16.27	13.95	1.42	1.22
40	17.12	13.10	15263	178	110	18.90	14.85	1.44	1.13

D = 43 mm

Setting [%]	Q [m3/h]	v(avg) [m/s]	Re	Delta P [Pa]		v(calc) [m/s]		v(calc)/v(avg)	
				Middle	Wall	Middle	Wall	Middle	Wall
30	12.84	2.46	5724	3	0	2.45	0.00	1.00	0.00
35	14.98	2.87	6678	4.5	0.5	3.00	1.00	1.05	0.35
40	17.12	3.28	7632	6	2	3.47	2.00	1.06	0.61
45	19.26	3.68	8586	8	3.5	4.01	2.65	1.09	0.72
50	21.41	4.09	9540	11	4.5	4.70	3.00	1.15	0.73
55	23.55	4.50	10494	16	7.5	5.67	3.88	1.26	0.86
58	24.83	4.75	11066	17	9.5	5.84	4.37	1.23	0.92

Table A6.3: Enthalpy probe results

D = 12.4 mm

Setting	Q	v(avg)	Re	Delta P [Pa] at radial position [mm]							v(calc) [m/s] at radial position [mm]							v(calc)/v(avg) at radial position [mm]						
[%]	[m3/h]	[m/s]		0	1	2	3	4	5	6	0	1	2	3	4	5	6	0	1	2	3	4	5	6
8	3.42	7.88	5293	132	110	90	81	76	63	58	16.27	14.85	13.44	12.75	12.35	11.24	10.79	2.07	1.89	1.71	1.62	1.57	1.43	1.37
10	4.28	9.85	6616	212	188	154	139	128	107	95	20.62	19.42	17.58	16.70	16.02	14.65	13.80	2.09	1.97	1.78	1.70	1.63	1.49	1.40
12	5.14	11.82	7939	298	265	220	202	187	152	136	24.45	23.06	21.01	20.13	19.37	17.46	16.52	2.07	1.95	1.78	1.70	1.64	1.48	1.40
15	6.42	14.77	9924	475	411	335	319	288	241	212	30.87	28.71	25.92	25.30	24.04	21.99	20.62	2.09	1.94	1.76	1.71	1.63	1.49	1.40
18	7.71	17.72	11909	673	593	486	449	423	342	301	36.74	34.49	31.22	30.01	29.13	26.19	24.57	2.07	1.95	1.76	1.69	1.64	1.48	1.39
20	8.56	19.69	13232	810	741	603	543	514	418	364	40.31	38.55	34.78	33.00	32.11	28.96	27.02	2.05	1.96	1.77	1.68	1.63	1.47	1.37
25	10.70	24.62	16540	1320	1169	947	885	815	669	583	51.46	48.43	43.59	42.13	40.43	36.63	34.20	2.09	1.97	1.77	1.71	1.64	1.49	1.39

D = 21.5 mm

Setting	Q	v(avg)	Re	Delta P [Pa] at radial position [mm]							v(calc) [m/s] at radial position [mm]							v(calc)/v(avg) at radial position [mm]						
[%]	[m3/h]	[m/s]		0	2	4	5	7	9	10.5	0	2	4	5	7	9	10.5	0	2	4	5	7	9	10.5
10	4.28	3.28	3816	12	11	11	11	9	8	5	4.91	4.70	4.70	4.70	4.25	4.01	3.17	1.50	1.43	1.43	1.43	1.30	1.22	0.97
15	6.42	4.91	5724	30	25	24	24	21	19	14	7.76	7.08	6.94	6.94	6.49	6.17	5.30	1.58	1.44	1.41	1.41	1.32	1.26	1.08
20	8.56	6.55	7632	53	47	45	44	39	34	28	10.31	9.71	9.50	9.39	8.85	8.26	7.49	1.57	1.48	1.45	1.43	1.35	1.26	1.14
25	10.70	8.19	9540	85	79	76	72	62	56	46	13.06	12.59	12.35	12.02	11.15	10.60	9.61	1.59	1.54	1.51	1.47	1.36	1.29	1.17
30	12.84	9.83	11448	128	118	111	107	92	82	68	16.02	15.39	14.92	14.65	13.59	12.83	11.68	1.63	1.57	1.52	1.49	1.38	1.31	1.19
35	14.98	11.46	13355	180	167	157	152	131	115	94	19.00	18.30	17.75	17.46	16.21	15.19	13.73	1.66	1.60	1.55	1.52	1.41	1.32	1.20
40	17.12	13.10	15263	241	218	210	204	171	154	124	21.99	20.91	20.52	20.23	18.52	17.58	15.77	1.68	1.60	1.57	1.54	1.41	1.34	1.20

D = 43 mm

Setting	Q	v(avg)	Re	Delta P [Pa] at radial position [mm]							v(calc) [m/s] at radial position [mm]							v(calc)/v(avg) at radial position [mm]						
[%]	[m3/h]	[m/s]		0	3	6	10	14	18	21	0	3	6	10	14	18	21	0	3	6	10	14	18	21
30	12.84	2.46	5724	4	3	2	2	1	1	1	2.83	2.45	2.00	2.00	1.42	1.42	1.42	1.15	1.00	0.82	0.82	0.58	0.58	0.58
35	14.98	2.87	6678	6	4	3	3	3	3	1	3.47	2.83	2.45	2.45	2.45	2.45	1.42	1.21	0.99	0.86	0.86	0.86	0.86	0.49
40	17.12	3.28	7632	8	7	6	6	5	5	3.5	4.01	3.75	3.47	3.47	3.17	3.17	2.65	1.22	1.14	1.06	1.06	0.97	0.97	0.81
45	19.26	3.68	8586	11	11	10	9	8	8	4	4.70	4.70	4.48	4.25	4.01	4.01	2.83	1.27	1.27	1.22	1.15	1.09	1.09	0.77
50	21.41	4.09	9540	16	15	14	13	11	10	6	5.67	5.49	5.30	5.11	4.70	4.48	3.47	1.38	1.34	1.29	1.25	1.15	1.09	0.85
55	23.55	4.50	10494	20	19	18	18	16	16	8	6.33	6.17	6.01	6.01	5.67	5.67	4.01	1.41	1.37	1.33	1.33	1.26	1.26	0.89
58	24.83	4.75	11066	24	22	21	21	19	17	11	6.94	6.64	6.49	6.49	6.17	5.84	4.70	1.46	1.40	1.37	1.37	1.30	1.23	0.99

Appendix B: Typical Mass and Energy Balance

Experimental Data

Voltage = 127 V

Current = 230 A

Water flow rates (calculated with the use of calibration data) through:

(a) Anode - 406.2 kg/h

(b) Cathode - 393 kg/h

(c) Carbon feeder - 609.2 kg/h

(d) Top part of reactor - 592.7 kg/h

(e) Bottom part of reactor - 222.3 kg/h

(f) Inner part of quench probe - 543.9 kg/h

(g) Outer part of quench probe - 719.2 kg/h

Gas flow rates (according to calibration data):

(a) CF_4 plasma gas: $\dot{m}_{CF_4(plasma)} = 2.86$ kg/h

(b) CF_4 carrier gas: $\dot{m}_{CF_4(carrier)} = 0.393$ kg/h

Composition of product gas:

(a) CF_4 - 57.16 vol %

(b) C_2F_6 - 8.41 vol %

(c) C_2F_4 - 33.2 vol %

(d) C_3F_6 - 1.26 vol %

Temperature rise in cooling water for the different reactor components:

(a) Anode - 12.3 °C

(b) Cathode - 1.68 °C

(c) Carbon feeder - 3.75 °C

(d) Top part of reactor - 12.9 °C

(e) Bottom part of reactor - 3.39 °C

(f) Inner part of quench probe - 8.84 °C

(g) Outer part of quench probe - 5.66 °C

Mass flow rate of carbon: $\dot{m}_c = 17.8$ g/min ≡ 1.068 kg/h

Temperature of product gas = 51.2 °C

Ambient temperature = 25 °

Mass balance

Fluorine balance

Total CF_4 feed rate = $\frac{2.86}{88} + \frac{0.393}{88} = 0.037$ kmol/h

Feed rate of F molecules = 4 x CF_4 feed rate = 0.148 kmol/h

= rate at which F molecules leave reactor

Suppose 1 kmol/h of product gas stream leaves the reactor, then the rate at which the different product gases leave the reactor would be:

(a) CF_4 - 0.5716 kmol/h

(b) C_2F_6 - 0.0841 kmol/h

(c) C_2F_4 - 0.332 kmol/h

(d) C_3F_6 - 0.0126 kmol/h

The total rate at which F molecules leave the reactor would then amount to:

4(0.5716) + 6(0.0841) + 4(0.332) + 6(0.0126) = 4.19 kmol/h

However, the rate at which F molecules leave the reactor is equal to the rate at which F molecules is fed to the reactor. The flow rate of the product gas stream is therefore: 0.148/4.19 = .0353 kmol/h

The flow rate of the individual product gas components:

(a) CF_4 - 0.5716(0.0353) = 0.0202 kmol/h

(b) C_2F_6 - 0.0841(0.0353) = 0.00297 kmol/h

(c) C_2F_4 - 0.332(0.0353) = 0.0117 kmol/h

(d) C_3F_6 - 0.0126(0.0353) = 0.00044 kmol/h

Carbon balance

Feed rate of C molecules in gas phase = total CF_4 feed rate = 0.037 kmol/h

Feed rate of C molecules in solid phase = 1.068/12 = 0.089 kmol/h

Flow rate of gaseous C molecules leaving the reactor = 0.0202 + 2(0.00297) + 2(0.0117) + 3(4.4E-4)

= 0.0509 kmol/h

Flow rate of solid carbon leaving the reactor = 0.089 – (0.0509 – 0.037) = 0.075 kmol/h

Energy balance

Energy in

$\dot{Q}_{in}$ = Currant x Voltage = 230(127) = 29 210 W ≡ **29.21** kW

Energy out

Energy out in cooling water:

(a) Anode: $\dot{Q}_a = \dot{m}\, c_p \Delta T = 406.2(4.187)(12.3) = 20\,919$ kJ/h ≡ 5.81 kW

(b) Cathode: $\dot{Q}_c = 393(4.187)(1.68) = 2\,764.4$ kJ/h ≡ 0.768 kW

(c) Carbon feeder : $\dot{Q}_f = 2.66$ kW

(d) Top part of reactor: $\dot{Q}_{R1} = 8.89$ kW

(e) Bottom part of reactor: $\dot{Q}_{R2} = 0.876$ kW

(f) Inner part of quench probe: $\dot{Q}_{Qi} = 5.59$ kW

(g) Outer part of quench probe: $\dot{Q}_{Qo} = 4.73$ kW

Total energy out in cooling water = 29.32 kW

Energy out with solid carbon leaving the reactor:

Assume that the temperature of the solid carbon leaving the reactor is the same as the temperature of the product gas stream, i.e. 51.2 °C. The ambient temperature of 25 °C is used as reference temperature.

$$\dot{Q}_{Carb} = \dot{m}\ c_p(T - T_{ref}) = 0.075(8.5)(51.2 - 25) = 16.7\ kJ/h \equiv \underline{0.00464\ kW}$$

Energy out with product gas stream:

Reference temperature taken as the ambient temperature of 25 °C.

$$\text{Specific heat: } c_p = A + B\left[\frac{C/T}{\sinh(C/T)}\right]^2 + D\left[\frac{E/T}{\cosh(E/T)}\right]^2 \text{ J/kmol.K}$$

Enthalpy:

$$h = \int_{T_{ref}}^{T} c_p dT = A(T - T_{ref}) + BC\left[\coth\left(\frac{C}{T}\right) - \coth\left(\frac{C}{T_{ref}}\right)\right] - DE\left[\tanh\left(\frac{E}{T}\right) - \tanh\left(\frac{E}{T_{ref}}\right)\right] \text{ J/kmol}$$

Component	A	B	C	D	E
CF4	33670	74300	807	40500	385
C2F4	51239	81635	978.9	59315	-443.23
C2F6	47255	131850	683.78	71315	-305.92
C3F6	121520	123760	873.44	-2.26 e 7	8.2899

$$\dot{Q}_{CF_4} = \dot{m}_{CF_4} h_{CF_4} = 0.0202(1644561) = 33\ 220\ J/h \equiv 0.00923\ kW$$

$$\dot{Q}_{C_2F_6} = \dot{m}_{C_2F_6} h_{C_2F_6} = 0.00297(2861884) = 8\ 499.8\ J/h \equiv 0.00236\ kW$$

$$\dot{Q}_{C_2F_4} = \dot{m}_{C_2F_4} h_{C_2F_4} = 0.0117(2153708) = 25\ 198\ J/h \equiv 0.007\ kW$$

$$\dot{Q}_{C_3F_6} = \dot{m}_{C_3F_6} h_{C_3F_6} = 0.00044(17627874) = 7\ 756.3\ J/h \equiv 0.00215\ kW$$

Total energy in product gas stream = <u>0.0207 kW</u>

$\dot{Q}_{out}$ = Energy out in cooling water + Energy out with solid C + Energy out with product gas

= **<u>29.35 kW</u>**

Accuracy of Energy Balance

$$\text{Accuracy} = \frac{\dot{Q}_{out}}{\dot{Q}_{in}} \times 100\ \% = \frac{29.35}{29.21} \times 100 = 100.48\ \%$$

Appendix C: Plasma-enthalpies and Torch Efficiency

Torch Efficiency

$$\eta_t = \frac{\dot{Q}_{in} - \dot{Q}_a - \dot{Q}_c}{\dot{Q}_{in}} = \frac{29.21 - 5.81 - 0.768}{29.21} = 0.775$$

Plasma Enthalpy

$$\text{Plasma enthalpy} = \frac{\dot{Q}_{in} - \dot{Q}_a - \dot{Q}_c}{CF_4 \text{ plasma gas}} = \frac{29.21 \times 0.775}{2.86} = 7.91 \text{ kWh/kg } CF_4$$

Mixing Enthalpy

$$\text{Mixing enthalpy} = \frac{\dot{Q}_{in} - \dot{Q}_a - \dot{Q}_c - \dot{Q}_f}{\dot{m}_{CF_4(\text{plasma})} + \dot{m}_{CF_4(\text{carrier})} + \dot{m}_C} = \frac{29.21 - 5.81 - 0.768 - 2.66}{2.86 + 0.393 + 1.068}$$

$$= 4.62 \text{ kWh/ kg } CF_4 + C(s)$$

Quenching Enthalpy

$$\text{Quenching enthalpy} = \frac{\dot{Q}_{in} - \dot{Q}_a - \dot{Q}_c - \dot{Q}_f - \dot{Q}_{R1} - \dot{Q}_{R2}}{\dot{m}_{CF_4(\text{plasma})} + \dot{m}_{CF_4(\text{carrier})} + \dot{m}_C} =$$

$$\frac{29.21 - 5.81 - 0.768 - 2.66 - 8.89 - 0.876}{2.86 + 0.393 + 1.068}$$

$$= 2.36 \text{ kWh/kg } CF_4 + C(s)$$

Appendix D: Processing of Enthalpy Probe Results

Experimental Data

Variable	Calculated Mean Value	Calculated Standard Deviation
dP radial	411.09	21.88
dP axial	810.5	1.83
T_{in} tare	10.93	0.04
T_{out} tare	18.55	0.15
T_{in} sampling	10.94	0
T_{out} sampling	19.49	0.06
T_{out} gas sample	19.14	0
Mass flow controller reading [mV]	136.13	0.61

Reading on water flow meter = 110

Ambient temperature = 19 °C

Mass flow rate of carbon = 0 kg/min

Processing of results

CF_4 mass flow rate = m*reading + c

$$\dot{m}_g = (6.586E\text{-}6)*(136.13) + 3.474E\text{-}4$$

$$= 1.244E\text{-}3 \text{ kg/min}$$

Water flow rate = m*reading + c

$$\dot{m}_w = 0.013475(110) - 0.11973$$

$$= 1.36 \text{ kg/min}$$

Gas enthalpy at exit of probe:

$$h_e = c_{p,s}(T_{exit} - T_{ref})$$

$$= 0.7(19.14\text{-}19)$$

$$= 0.098 \text{ kJ/kg}$$

Gas enthalpy at inlet of probe:

$$\dot{m}_g (h_i - h_e) = \dot{m}_w c_{p,w}[(\Delta T_w)_{sampling} - (\Delta T_w)_{tare}]$$

$$\Rightarrow h_i = h_e + \frac{\dot{m}_w}{\dot{m}_g} c_{p,w}\left[(\Delta T_w)_{sampling} - (\Delta T_w)_{tare}\right]$$

$$= 0.098 + (1.36/1.244E\text{-}3)(4.187)[(19.49\text{-}10.94)\text{-}(18.55\text{-}10.93)]$$

$$= 4\,257.1 \text{ kJ/kg}$$

$$\equiv 1.18 \text{ kWh/kg}$$

Input to CFP program:

Reactor pressure = 10 kPa

$C(s)/CF_4 = 0$

Gas enthalpy = 1.18 kWh/kg

Output of CFP program:

Gas temperature = 2397 K

Gas density = 0.02 kg/m^3

Calculated free stream gas velocity:

$$U = \sqrt{\frac{2(dP_{axial} - dP_{radial})}{\rho_{CF_4}}}$$

$$= [2(810.5 - 411.09)/0.02]^{0.5}$$

$$= 199.8 \text{ m/s}$$

Probe inlet velocity:

$$U_{probe} = \frac{\dot{V}_{inlet}}{A_{probe}}$$

$$= \frac{\dot{m}_g / \rho_{CF_4}}{\pi d_i^2 / 4}$$

$$= \frac{(1.244E-3)/0.02}{\pi(0.003)^2/4}$$

$$= 8799 \text{ m/min} \equiv 147 \text{ m/s}$$

$$\text{Quench Rate} > \frac{\Delta T_{probe} \times \dot{V}_{probe}}{\text{Volume}_{probe}}$$

$\Delta T_{probe} = T_{gas}(inlet) - T_{gas}(outlet)$

$= 2397 - (19.14+273.15)$

$= 2104.7\ K$

$$\dot{V}_{inlet} = \frac{\dot{m}_g}{\rho_{CF_4}} = \frac{1.244E-3}{0.02 \times 60} = 1.04E\text{-}3\ m^3/s$$

$$\dot{V}_{outlet} = \frac{\dot{m}_g R\ T_{gas}(outlet)}{P\ M} = \frac{(1.244E-3)(8.314)(19.14+273.15)}{10(88) \times 60}$$

$$= 5.73E\text{-}5\ m^3/s$$

$$\dot{V}_{probe} = \frac{\dot{V}_{inlet} + \dot{V}_{outlet}}{2} = 5.5E\text{-}4\ m^3/s$$

$$Volume_{probe} = \frac{\pi}{4} d_i^2 \ell = \frac{\pi}{4}(0.003)^2(0.4)$$

$$= 2.83E\text{-}6\ m^3$$

$\Rightarrow$ Quench rate > 4.1×10^5 K/s

Calculation of total error margin

CF_4 mass flow rate:

$\dot{m}_g = m*x + c$ (x = reading)

$\sigma(m) = 9.42E\text{-}8$

$\sigma(c) = 5.94E\text{-}5$

$$\frac{\sigma(mx)}{mx} = \sqrt{\left(\frac{\sigma(m)}{m}\right)^2 + \left(\frac{\sigma(x)}{x}\right)^2} = \sqrt{\left(\frac{9.42E-8}{6.59E-6}\right)^2 + \left(\frac{0.61}{136.13}\right)^2}$$

$\sigma(mx) = (6.586E\text{-}6)(136.13) \times 0.015 = 1.34E\text{-}5$

$$\sigma(\dot{m}_g) = \sqrt{\sigma^2(mx) + \sigma^2(c)} = \sqrt{(1.34E-5)^2 + (5.94E-5)^2}$$

$$= 6.1E\text{-}5\ kg/min$$

Water flow rate:

$\dot{m}_w = m*x + c$ (x = reading)

$\sigma(m) = 2.17E\text{-}4$

$\sigma(c) = 2.657E\text{-}2$

$\sigma(\dot{m}_w) = 3.817E\text{-}2$ kg/min (calculation method same as for CF_4 flow rate)

Gas enthalpy at exit of probe:

$$h_e = c_{p,s}(T_{exit} - T_{ref})$$

$\sigma(c_{p,s}) = 0.01$

$$\sigma(T_{exit} - T_{ref}) = \sqrt{\sigma^2(T_{exit}) + \sigma^2(T_{ref})} = 0.0$$

$$\sigma(h_e) = h_e \times \sqrt{\left(\frac{\sigma(c_{p,s})}{c_{p,s}}\right)^2 + \left(\frac{\sigma(\Delta T)}{\Delta T}\right)^2} = \sqrt{\left(\frac{0.01}{0.7}\right)^2 + 0}$$

$= 0.098 \times 0.0143 = 0.0014$ kJ/kg

Gas temperature at inlet of probe:

$$h_i = h_e + \frac{\dot{m}_w}{\dot{m}_g} c_{p,w}\left[(\Delta T_w)_{sampling} - (\Delta T_w)_{tare}\right]$$

$$\sigma[\Delta(\Delta T)] = \sqrt{\sigma^2(\Delta T_w)_{sampling} + \sigma^2(\Delta T_w)_{tare}}$$

$$= \sqrt{(0.04^2 + 0.15^2) + (0 + 0.06^2)} = 0.17 \text{ K}$$

$$\sigma\left\{\frac{\dot{m}_w}{\dot{m}_g} c_{p,w}[\Delta(\Delta T)]\right\} = \frac{\dot{m}_w}{\dot{m}_g} c_{p,w}[\Delta(\Delta T)]$$

$$\times \sqrt{\left(\frac{\sigma(\dot{m}_w)}{\dot{m}_w}\right)^2 + \left(\frac{\sigma(\dot{m}_g)}{\dot{m}_g}\right)^2 + \left(\frac{\sigma(c_{p,w})}{c_{p,w}}\right)^2 + \left(\frac{\sigma[\Delta(\Delta T)]}{[\Delta(\Delta T)]}\right)^2}$$

$$= 4257 \times \sqrt{\left(\frac{3.817E-2}{1.36}\right)^2 + \left(\frac{6.1E-5}{1.244E-3}\right)^2 + \left(\frac{0.0001}{4.187}\right)^2 + \left(\frac{0.17}{0.93}\right)^2}$$

$$= 814.48$$

$$\sigma(h_i) = \sqrt{\sigma^2(h_e) + \sigma^2\left\{\frac{\dot{m}_w}{\dot{m}_g} c_{p,w}[\Delta(\Delta T)]\right\}} = 814.48 \text{ kJ/kg}$$

Percentage Error = (814.48/4257.1)*100 = 19.13 %

$\Rightarrow \sigma(T_{gas,inlet}) = 0.1913(2397) = 458.6$ K

$\rho_{CF_4} = 0.1913(0.02) = 3.83E\text{-}3\ kg/m^3$

Probe inlet velocity:

$$U_{probe} = \frac{\dot{V}_{inlet}}{A_{probe}} = \frac{\dot{m}_g / \rho_{CF_4}}{\pi d_i^2 / 4}$$

$$\sigma(U_{probe}) = U_{probe}\, x \sqrt{\left(\frac{\sigma(\dot{m}_g)}{\dot{m}_g}\right)^2 + \left(\frac{\sigma(\rho_{CF_4})}{\rho_{CF_4}}\right)^2 + \left(\frac{\sigma(d_i)}{d_i}\right)^2 + \left(\frac{\sigma(d_i)}{d_i}\right)^2}$$

$$= 8799\ x \sqrt{\left(\frac{6.1E-5}{1.244E-3}\right)^2 + \left(\frac{3.83E-3}{0.02}\right)^2 + \left(\frac{0.0002}{0.003}\right)^2 + \left(\frac{0.0002}{0.003}\right)^2}$$

$$= 1927\ m/min \equiv 32.1\ m/s$$

Quench Rate:

$$\text{Quench Rate} = \frac{\Delta T_{probe} \times \dot{V}_{probe}}{Volume_{probe}}$$

$\Delta T_{probe} = T_{gas}(inlet) - T_{gas}(outlet)$

$\sigma(\Delta T_{probe}) = 458.6\ K$

$$\dot{V}_{inlet} = \frac{\dot{m}_g}{\rho_{CF_4}}$$

$\sigma(\dot{V}_{inlet}) = 2.06E\text{-}4\ m^3/s$

$$\dot{V}_{outlet} = \frac{\dot{m}_g R\ T_{gas}(outlet)}{P\ M}$$

$\sigma(\dot{V}_{outlet}) = 6.38E\text{-}6\ m^3/s$

$$\dot{V}_{probe} = \frac{\dot{V}_{inlet} + \dot{V}_{outlet}}{2}$$

$\sigma(\dot{V}_{probe}) = 1.03E\text{-}4\ m^3/s$

$$Volume_{probe} = \frac{\pi}{4} d_i^2 \ell$$

$\sigma(Volume_{probe}) = 8.56E\text{-}8$

$\Rightarrow \sigma(\text{Quench rate}) = 1.18E5\ K/s$

(Method for calculation of error margin on quench rate the same as used for the others.)

Appendix E: One-dimensional Model

E.1 Derivation of model

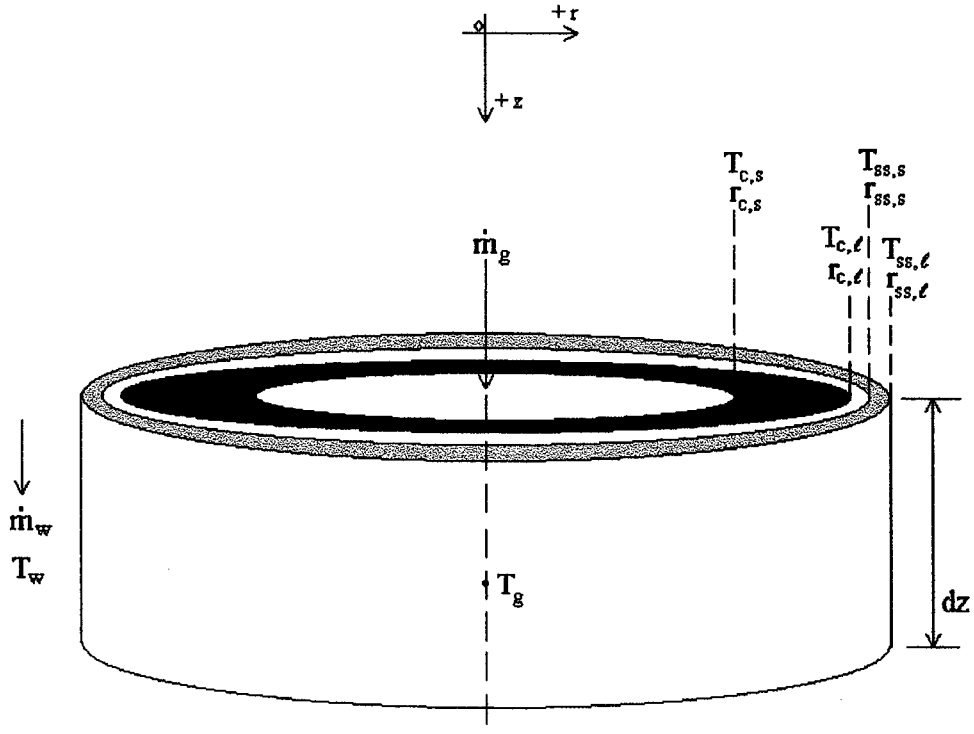

Heat Transfer

Thermal Resistances:

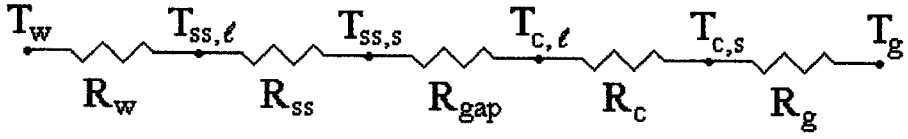

1) Thermal resistance of water :

$$R_w = \frac{1}{h_w A_w} = \frac{1}{h_w \left(2\pi\, r_{ss,\ell} dz\right)}$$

$$Nu_w = \frac{h_w d_h}{k_w} \Rightarrow \qquad h_w = \frac{Nu_w k_w}{d_h}$$

Hydraulic diameter: $d_h = d_{ss,o} - 2r_{ss,\ell}$

where $d_{ss,o}$ is the outside diameter of the annulus in which the cooling water flows.

$$\Rightarrow \qquad R_w = \frac{d_h}{2Nu_w k_w \pi\, r_{ss,\ell} dz}$$

2) Thermal resistance of reactor wall:

$$R_{ss} = \frac{1}{2\pi\, k_{ss} dz} \ell n\left(\frac{r_{ss,\ell}}{r_{ss,s}}\right)$$

3) Thermal resistance of gap between reactor wall and carbon lining:

The gas in the gas is assumed to be unmoving, thus heat transfer across the gap is due to radiation and conduction.

$$Q_{gap} = \varepsilon\, \sigma\, A\left(T_{c,\ell}^4 - T_{ss,s}^4\right) + \frac{2\pi\, \bar{k}_{gas} dz}{\ell n\left(r_{ss,s}/r_{c,\ell}\right)}\left(T_{c,\ell} - T_{ss,s}\right)$$

Let: $\qquad h_r = \varepsilon\, \sigma\, \left(T_{c,\ell} + T_{ss,s}\right)\left(T_{c,\ell}^2 + T_{ss,s}^2\right)$

$$\therefore\ Q_{gap} = \left(2\pi\, r_{c,\ell} h_r dz + \frac{2\pi\, \bar{k}_{gas} dz}{\ell n\left(r_{ss,s}/r_{c,\ell}\right)}\right)\left(T_{c,\ell} - T_{ss,s}\right) = \frac{T_{c,\ell} - T_{ss,s}}{R_{gap}}$$

$$\Rightarrow \qquad R_{gap} = \left(2\pi\, r_{c,\ell} h_r dz + \frac{2\pi\, \bar{k}_{gas} dz}{\ell n\left(r_{ss,s}/r_{c,\ell}\right)}\right)^{-1}$$

4) Thermal resistance of carbon lining:

$$R_c = \frac{\ell n(r_{c,\ell}/r_{c,s})}{2\pi\, k_c dz}$$

5) Thermal resistance of plasma gas:

Heat transfer between gas and lining wall:

$$Q = h_g A_g \left(T_g - T_{c,s}\right) + \varepsilon_g \sigma A_g T_g^4 = \left(T_g - T_{c,s}\right)\left[Nu_g \bar{k}_{gas} \pi dz + \frac{2\pi r_{c,s} dz \varepsilon_g \sigma T_g^4}{\left(T_g - T_{c,s}\right)}\right]$$

$$\Rightarrow \quad R_g = \left(\frac{1}{dz}\right)\left[Nu_g \bar{k}_{gas} \pi + \frac{2\pi r_{c,s} \varepsilon_g \sigma T_g^4}{\left(T_g - T_{c,s}\right)}\right]^{-1}$$

Total thermal resistance:

$$\frac{R_{tot}}{dz} = R_w + R_{ss} + R_{gap} + R_c + R_g$$

Heat Losses:

Gas heat loss after flowing distance dz:

$$Q_g = \dot{m}_g c_{p,g}\left[\left(T_g + \frac{1}{2}\frac{dT_g}{dz}dz\right) - \left(T_g - \frac{1}{2}\frac{dT_g}{dz}dz\right)\right] = \dot{m}_g c_{p,g} dT_g$$

The gas temperature is affected by the particles injected into the plasma tail flame. For 1 particle the convective heat gain is:

$$Q_{con,p} = h_p A_p (T_g - T_p) = \frac{Nu_p \bar{k}_g}{D_p}(\pi D_p^2)(T_g - T_p)$$

$$= \pi D_p Nu_p \bar{k}_g (T_g - T_p)$$

If n_p [m^{-3}] is the particle number density, then the convective heat losses from the gas to the particle, per volume element, is:

$$Q_{con} = n_p(\pi r_{c,s}^2 dz) Q_{c,p} = n_p \pi^2 r_{c,s}^2 D_p Nu_p \bar{k}_g (T_g - T_p)\, dz$$

and the radiation heat losses from the gas to the particles is:

$$Q_{rad} = n_p(\pi r_{c,s}^2 dz)\varepsilon_g \sigma(\pi D_p^2) T_g^4$$

Radiative heat transfer between the graphite lining and the particles per element volume is:

$$Q_r = n_p(\pi r_{c,s}^2 dz)[\varepsilon\ \sigma\ \pi\ D_p^2(T_{c,s}^4 - T_p^4)]$$

Total heat transfer to the particles:

$$Q_p = m_p c_{p,p} dT_p = Q_{con} + Q_{rad} + Q_r$$

$$= n_p \pi^2 r_{c,s}^2 D_p \left[Nu_p \bar{k}_g (T_g - T_p) + \varepsilon_g \sigma\ D_p T_g^4 + \varepsilon\ \sigma\ D_p (T_{c,s}^4 - T_p^4)\right] dz$$

$$\Rightarrow \quad \frac{dT_p}{dz} = \frac{n_p \pi^2 r_{c,s}^2 D_p}{\dot{m}_p c_{p,p}}\left[Nu_p \bar{k}_g (T_g - T_p) + \varepsilon_g \sigma\ D_p T_g^4 + \varepsilon\ \sigma\ D_p (T_{c,s}^4 - T_p^4)\right]$$

Total heat losses from the gas = heat loss to reactor wall + heat loss to particles:

$$Q_g = \dot{m}_g c_{p,g} dT_g = -\left[\begin{array}{l} Nu_g \bar{k}_g \pi (T_g - T_w) + 2\pi r_{c,s} \varepsilon_g \sigma T_g^4 \\ + n_p \pi^2 r_{c,s}^2 D_p \left(Nu_p \bar{k}_g (T_g - T_p) + D_p \varepsilon_g \sigma T_g^4\right) \end{array}\right] dz$$

$$\Rightarrow \quad \frac{dT_g}{dz} = -\left(\frac{1}{\dot{m}_g c_{p,g}}\right)\left[\begin{array}{l} Nu_g \bar{k}_g \pi (T_g - T_w) + 2\pi r_{c,s} \varepsilon_g \sigma T_g^4 \\ + n_p \pi^2 r_{c,s}^2 D_p \left(Nu_p \bar{k}_g (T_g - T_p) + D_p \varepsilon_g \sigma T_g^4\right) \end{array}\right]$$

Particle number density:

n_p = number of particles per volume element

$$= \frac{\left(\frac{\dot{m}_p dt_p}{\rho_p (4/3)\pi r_p^3}\right)}{\pi r_{c,s}^2 dz}$$

$$\Rightarrow \quad n_p = \frac{6\dot{m}_p}{\rho_p \pi^2 D_p^3 r_{c,s}^2 v_p}$$

<u>Temperature distribution through composite wall</u>:

1) Inner temperature of graphite lining:

$$Q_{tot} = \frac{T_g - T_w}{R_{tot}} dz = \frac{T_g - T_{c,s}}{R_g}$$

$$\Rightarrow \quad T_{c,s} = T_g - \frac{R_g}{R_{tot}}(T_g - T_w)$$

2) Outer temperature of graphite lining:

$$Q_{tot} = \frac{T_g - T_w}{R_{tot}} dz = \frac{T_{c,s} - T_{c,\ell}}{R_c}$$

$$\Rightarrow \quad T_{c,\ell} = T_{c,s} - \frac{\ell n(r_{c,\ell} / r_{c,s})}{2\pi k_c R_{tot}}(T_g - T_w)$$

3) Inner temperature of reactor wall:

$$Q_{tot} = \frac{T_g - T_w}{R_{tot}} dz = \frac{T_{c,\ell} - T_{ss,s}}{R_{gap}}$$

$$\Rightarrow \qquad T_{ss,s} = T_{c,\ell} - \frac{1}{\left[2\pi\, r_{c,\ell} h_r + \frac{2\pi\, \bar{k}_{gas}}{\ell n\left(r_{ss,s}/r_{c,\ell}\right)}\right] R_{tot}} \left(T_g - T_w\right)$$

4) Outer temperature of reactor wall:

$$Q_{tot} = \frac{T_g - T_w}{R_{tot}} dz = \frac{T_{ss,s} - T_{ss,\ell}}{R_{ss}}$$

$$\Rightarrow \qquad T_{ss,\ell} = T_{ss,s} - \frac{\ell n\left(r_{ss,\ell}/r_{ss,s}\right)}{2\pi\, k_{ss} R_{tot}} \left(T_g - T_w\right)$$

Momentum Transfer

$u_p(0)$ = given

$u_g(0) = 0 = u_g(t)$

$v_p(0) = 0$

$v_g(0)$ = given

Relative velocity:

$$U_R = \sqrt{\left(u_g - u_p\right)^2 + \left(v_g - v_p\right)^2} = \sqrt{u_p^2 + \left(v_g - v_p\right)^2}$$

Particle Reynolds number:

$$Re_p = \frac{\rho_g U_R D_p}{\mu_g}$$

Residence time of gas:

$$v_g = \frac{dz}{dt_g} = \frac{\dot{V}_g}{A_{cs}} = \frac{\dot{m}_g/\rho_g}{\pi\, r_{c,s}^2}$$

$$\Rightarrow \qquad \frac{dt_g}{dz} = \frac{\rho_g \pi\, r_{c,s}^2}{\dot{m}_g}$$

Particle residence time:

$$v_p = \frac{dz}{dt_p} \qquad \Rightarrow \qquad \frac{dt_p}{dz} = \frac{1}{v_p}$$

Forces acting on particles:

1) Inertia Force:

Radial direction: $$F_{I,r} = \frac{4}{3}\pi\, r_p^3 \rho_p \frac{du_p}{dt_p} = \frac{1}{6}\pi\, D_p^3 \rho_p \frac{du_p}{dt_p}$$

Axial direction: $$F_{I,z} = \frac{1}{6}\pi\, D_p^3 \rho_p \frac{dv_p}{dt_p}$$

2) Drag Force:

Radial direction: $$F_{D,r} = \frac{1}{2}\rho_g \left(\pi\, \frac{D_p^2}{4}\right) C_D (u_g - u_p)\left|u_g - u_p\right| = -\frac{1}{8}\pi\, D_p^2 C_D \rho_g u_p^2$$

Axial direction: $$F_{D,z} = \frac{1}{8}\pi\, D_p^2 C_D \rho_g (v_g - v_p)\left|v_g - v_p\right|$$

3) Gravitation:

Axial direction: $$F_{G,z} = m\, g = \frac{1}{6}\pi\, D_p^3 \rho_p g$$

Force balance:

$$F_I = F_D + F_G$$

Radial direction: $$\frac{1}{6}\pi\, D_p^3 \rho_p \frac{du_p}{dt_p} = -\frac{1}{8}\pi\, D_p^2 C_D \rho_g u_p^2$$

$$\Rightarrow \quad \frac{du_p}{dt_p} = \frac{du_p}{dz}\frac{dz}{dt_p} = -\frac{3}{4}\left(\frac{\rho_g}{\rho_p D_p}\right) C_D u_p^2$$

$$\Rightarrow \quad \frac{du_p}{dz} = -\frac{3}{4}\left(\frac{\rho_g}{\rho_p D_p}\right) C_D \frac{u_p^2}{v_p}$$

Axial direction: $$\frac{1}{6}\pi\, D_p^3 \rho_p \frac{dv_p}{dt_p} = \frac{1}{8}\pi\, D_p^2 C_D \rho_g (v_g - v_p)\left|v_g - v_p\right| + \frac{1}{6}\pi\, D_p^3 \rho_p g$$

$$\Rightarrow \quad \frac{dv_p}{dt_p} = \frac{dv_p}{dz}\frac{dz}{dt_p} = -\frac{3}{4}\left(\frac{\rho_g}{\rho_p D_p}\right) C_D (v_p - v_g)\left|v_p - v_g\right| + g$$

$$\Rightarrow \qquad \frac{dv_p}{dz} = -\frac{3}{4}\left(\frac{\rho_g}{\rho_p D_p}\right) C_D \frac{\left(v_p - v_g\right)}{v_p}\left|v_p - v_g\right| + \frac{g}{v_p}$$

Assumptions

- Water temperature stays constant
- Graphite lining treated as one
- No contact resistances taken into account

List of symbols

A	- surface area
A_{cs}	- cross-sectional area
c_p	- specific heat capacity
D, d	- diameter
F	- force
g	- gravitational acceleration
h	- convection coefficient
k	- thermal conductivity
$\bar{k}$	- mean thermal conductivity
$\dot{m}$	- mass flow rate
n_p	- particle number density
Nu	- Nusselt number
Q	- heat loss
r	- radius measured from centre of reactor
R	- thermal resistance
Re	- Reynolds number
t	- residence time
T	- temperature
u	- radial velocity
U_R	- relative velocity
v	- axial velocity
$\dot{V}$	- volumetric flow rate

z	- axial distance
ε	- emissivity
ρ	- density
σ	- Stefan-Boltzmann Constant

Subscripts:

c	- pertaining to graphite lining
con	- pertaining to convection
D	- pertaining to drag force
g	- pertaining to gas
G	- pertaining to gravitation
gap	- pertaining to gap between graphite lining and reactor wall
I	- pertaining to inertia
ℓ	- pertaining to outer radius
p	- pertaining to carbon particles
r	- pertaining to radiation
s	- pertaining to inner radius
ss	- pertaining to reactor wall
tot	- total
w	- pertaining to cooling water

E.2 Program Code

//1DRK4.cpp

```
/*This program calculates the 1D-model parameters in the axial direction
using a Runge-Kutta routine and given the initial values.*/

#include "pcutil.h"
#include "1DFunctions.h"

void Derivs(REAL, REAL[], REAL[]);
void Rk4(REAL[], REAL[], int, REAL, REAL, REAL[],
             void (*Derivs)(REAL, REAL[], REAL[]));

//initializing global variables for 1D functions
      REAL  cpGas,
            cpFilmGas,
            cpIntGas,
            cpParticle,
            densityFilmGas,
            densityGas,
            densityParticle,
            diameterHydraulic,
            diameterParticle,
            diameterParticleInit,
            dragCoefficient,
            emissivityGas,
            emissivityParticle,
            enthalpyGas,
            filmTemp,
            loadingRatio,
            mdotGas,
            mdotParticle,
            numbDensParticles,
            nusseltGas,
            nusseltParticle,
            nusselt2Phase,
            nusseltWater,
            positionRadialParticle,
            positionRadialParticlePrev,
            **ppCF4,     // matrix of physical properties of CF4
            **ppC,       // matrix of physical properties of carbon particles
            prandtlGas,
            prandtlParticle,
            prandtlFilm,
            radiationCoef,
            radiusGraphiteLong,
            radiusGraphiteShort,
            radiusSSLong,
            radiusSSShort,
            reynoldsGas,
            reynoldsParticle,
            reynoldsFilmPart,
            temperatureWater,
            tempGraphiteLong,
            tempGraphiteShort,
            tempSSLong,
            tempSSShort,
            thermalCondGas,
            thermalCondGraphite,
            thermalCondFilmGas,
```

```
            thermalCondIntGas,
            thermalCondIntGas2,
            thermalCondIntGas3,
            thermalCondParticle,
            thermalCondSS,
            thermalCondWater,
            thermalResistance2Phase,
            thermalResistanceWalls,
            velocityAxialGas,
            velocityRelative,
            viscosityGas,
            viscosityFilmGas,
            viscosityIntGas;

void main()
{
      REAL biot, tempGSPrev, h=0.0001, *dydx, *yout, *y, x=0.0;
      int i,j;
      char fName[12], fCF4Name[12];
      FILE *out,    // pointer to the new text file
           *inCF4,  // pointer to file with physical properties of CF4
           *inC;    // pointer to file with physical properties of C

      //Open file for output
      puts("\nFilename for output : ");
      gets(fName);
      if(  (out=fopen(fName,"w")) ==NULL)
      {
            fprintf(stderr,"Cannot open output file \n");
            exit (1);
      }

      //Open file for input of CF4 properties
      puts("\nFilename for input of CF4 physical properties : ");
      gets(fCF4Name);
      if( (inCF4=fopen(fCF4Name,"r"))==NULL)
      {
            fprintf(stderr,"Cannot open input file for CF4 properties\n");
            exit (1);
      }

      //Open file for input of carbon Cp values
      if( (inC=fopen("JanafCref.txt","r"))==NULL)
      {
            fprintf(stderr,"Cannot open input file for graphite Cp
                           values\n");
            exit (1);
      }

      //dynamic memory allocation
      y=Vector(1,N);
      dydx=Vector(1,N);
      yout=Vector(1,N);
      ppCF4=Matrix(1,601,1,6);
      ppC=Matrix(1,65,1,2);

      //read physical properties into ppCF4
      i=1;
      while(fscanf(inCF4,"%f,%f,%f,%f,%f,%f,",&ppCF4[i][1],&ppCF4[i][2],
              &ppCF4[i][3],&ppCF4[i][4],&ppCF4[i][5],&ppCF4[i][6])!= EOF)
```

```
{
      printf("%14.6f %14.6f %14.6f %14.6f %14.6f %14.6f\n",ppCF4[i][1],
ppCF4[i][2],ppCF4[i][3],ppCF4[i][4],ppCF4[i][5],ppCF4[i][6]);

      i++;
}
fclose(inCF4);
printf("Finished reading CF4 props...\n");

//read physical properties into ppC
i=1;
while(fscanf(inC,"%f %f",&ppC[i][1],&ppC[i][2]) != EOF)
{
      printf("%10.3f %10.3f\n",ppC[i][1],ppC[i][2]);
      i++;
}
fclose(inC);

//Initial values: user supplied
y[1]=4050.0;            //Tg Gas temperature  \K
y[2]=0.000;             //tg Gas dwell time  \s
y[3]=30.0;              //up Particle radial velocity  \m.s-1
y[4]=0.1;               //vp Particle axial velocity  \m.s-1
y[5]=0.000;             //tp Particle dwell time  \s
y[6]=293.0;             //Tp Particle temperature  \K

//Initial temperature for inner graphite lining
tempGraphiteShort=3800.0;

//Initial temperature for outer graphite lining
tempGraphiteLong=2300;

//Initial temperature for inner reactor wall
tempSSShort=2000;

//Initial temperature for outer reactor wall
tempSSLong=1800.0;

//Initial particle number density
numbDensParticles=8.682e9;

//radial position of particle inlet
positionRadialParticle=RadiusGraphiteShort(x);
positionRadialParticlePrev=positionRadialParticle+h;

//user supplied constants for 1D Model
densityParticle=1950.0;       // kg.m3
diameterParticleInit=0.00005; // m
emissivityParticle=0.87;      // unity
mdotGas=0.000917;             // kg.s-1
mdotParticle=0.0003;          // kg.s-1
loadingRatio=mdotParticle/mdotGas;

nusseltWater=36.9;
      thermalCondWater=0.598;       // W.m-1.K-1
temperatureWater=290;         // K
diameterHydraulic=0.004;      // m

//Headings for output file
fprintf(out,"%15s %15s %15s %15s %15s %15s %15s %15s %15s %15s %15s
             %15s %15s %15s %15s %15s %15s %15s %15s %15s %15s %15s
             %15s %15s %15s %15s %15s %15s %15s %15s %15s %15s %15s
```

```
            %15s %15s %15s %15s %15s %15s %20s
            %15s\n","z","TempGas","tauGas","VelRadPart","VelAxPart",
            "tauPart","TempPart","T_Gs","T_Gl","T_SSs","T_SSl",
            "EpsGas","posRadPart","CpGas","ViscGas","CondGas",
            "CondIntGas","DensityGas","VeloAxGas","ReGas","PrGas",
            "NuGas","VeloR","ReParticle","ReFilmPart","Nu2Ph","CD",
            "PrParticle","PrFilmPart","NuParticle","CpIntGas",
            "CondIntGas","ViscIntGas","RadGS","RadGL","RadSSS",
            "R2Ph","RWalls","BiotNumber","NumbDensParticles",
            "CpParticle");

//solve ordinary differential equations
for (i=0;i<=2200;i++)          //reactor length = 220 mm
{
      if(y[1]==0.0) break;
      if(y[6]==0.0) break;

      //Function Calls

      //Gas properties at gas temperature
      thermalCondGas=ThermalCondGas(y[1]);
      emissivityGas=EmissivityGas(y[1]);
      enthalpyGas=EnthalpyGas(y[1]);
      cpGas=CpGas(y[1]);
      densityGas=DensityGas(y[1]);
      viscosityGas=ViscosityGas(y[1]);
      prandtlGas=PrandtlGas();
      reynoldsGas=ReynoldsGas();
      nusseltGas=NusseltGas(y[6]);

      //Film temperature
      filmTemp=(y[1]+y[6])/2;

      //Gas properties at film temperature
      thermalCondFilmGas=ThermalCondGas(filmTemp);
      cpFilmGas=CpGas(filmTemp);
      prandtlFilm=PrandtlFilm();
      densityFilmGas=DensityGas(filmTemp);
      viscosityFilmGas=ViscosityGas(filmTemp);

      //Integrated mean of gas properties
      thermalCondIntGas=ThermalCondIntGas(y[1],y[6]);
      cpIntGas=CpIntGas(y[1],y[6]);
      viscosityIntGas=ViscosityIntGas(y[1],y[6]);

      //Particle properties
      thermalCondParticle=ThermalCondParticle(y[6]);
      cpParticle=CpParticle(y[6]);
      prandtlParticle=PrandtlParticle();
      reynoldsParticle=ReynoldsParticle();
      nusseltParticle=NusseltParticle(y[6]);

      //2-phase Nusselt number
      nusselt2Phase=Nusselt2Phase();

      //Biot number
      biot=thermalCondIntGas/thermalCondParticle;

      //thermal conductivity of gas at average temperature of gas and
        lining
      thermalCondIntGas2=ThermalCondIntGas(y[1],tempGraphiteShort);
```

```
//thermal conductivity of gas in gap between reactor wall and
  graphite lining

thermalCondIntGas3=ThermalCondIntGas(tempGraphiteLong,
                                     tempSSShort);

//Radiation coefficient for gap
radiationCoef=RadiationCoef();

//Radiuses
radiusGraphiteShort=RadiusGraphiteShort(x);
radiusGraphiteLong=RadiusGraphiteLong(x);
radiusSSShort=RadiusSSShort(x);
radiusSSLong=radiusSSShort+0.005;

//Axial velocity of the gas
velocityAxialGas=VelocityAxialGas();

//Relative Velocity
velocityRelative=VelocityRelative(y[3],y[4]);

//ParticleDiameter
diameterParticle=DiameterParticle(diameterParticleInit);
//Particle Reynolds number at film temperature
reynoldsFilmPart=ReynoldsFParticle();

//Drag Coefficient
dragCoefficient=DragCoefficient();

//Thermal conductivity of the graphite wall
thermalCondGraphite=ThermalCondGraphite();

//Thermal conductivity of reactor wall
thermalCondSS=ThermalCondSS();

//Thermal resistance 2 phase
thermalResistance2Phase=ThermalResistance2Phase();

//Total thermal resistance of the walls
thermalResistanceWalls=ThermalResistanceWalls(y[1],
                                              tempGraphiteShort);

//end of function calls

printf("\ni = %d",i);

//print results to output file out
fprintf(out,"%15.8f %15.8f %15.8f %15.8f %15.8f %15.8f %15.8f
             %15.8f %15.8f %15.8f %15.8f %15.8f %15.8f %15.8f
             %15.8f %15.8f %15.8f %15.8f %15.8f %15.8f %15.8f
             %15.8f %15.8f %15.8f %15.8f %15.8f %15.8f %15.8f
             %15.8f %15.8f %15.8f %15.8f %15.8f %15.8f %15.8f
             %15.8f %15.8f %15.8f %15.8f %20.2f %15.8f\n",
             x,y[1],y[2],y[3],y[4],y[5],y[6],tempGraphiteShort,
             tempGraphiteLong,tempSSShort,tempSSLong,
             emissivityGas,positionRadialParticle,cpGas,
             viscosityGas,thermalCondGas,thermalCondIntGas,
             densityGas,velocityAxialGas,reynoldsGas,
             prandtlGas,nusseltGas,velocityRelative,
             reynoldsParticle,reynoldsFilmPart,nusselt2Phase,
             dragCoefficient,prandtlParticle,prandtlFilm,
             nusseltParticle,cpIntGas,thermalCondIntGas,
             viscosityIntGas,radiusGraphiteShort,
```

```
                        radiusGraphiteLong,radiusSSShort,
                        thermalResistance2Phase,thermalResistanceWalls,biot,
                        numbDensParticles,cpParticle);

            //Runge-Kutta starts
            Derivs(x,y,dydx);
            Rk4(y,dydx,N,x,h,yout,Derivs);
            x+=h;
            for (j=1;j<=N;j++)
            {
                y[j]=yout[j];
            }

            //Update values

            //Temperatures
            tempGSPrev=tempGraphiteShort;
            tempGraphiteShort=TempGraphiteShort(y[1],temperatureWater,
            tempGSPrev,y[6]);
            tempGraphiteLong=TempGraphiteLong(y[1],temperatureWater);
            tempSSShort=TempSSShort(y[1],temperatureWater);
            tempSSLong=TempSSLong(y[1],temperatureWater);

            //Number density of the Particles
            numbDensParticles=NumbDensParticles(y[4]);

            //particle radial position
            positionRadialParticle=PositionRadialParticle(y[3],h,y[4]);
        }

        printf("\n\nFinito.....\n\n");

        FreeVector(yout,1,N);
        FreeVector(dydx,1,N);
        FreeVector(y,1,N);
        fclose(out);

}       // end main

void Derivs(REAL x, REAL *y, REAL *dydx)
{
        //dTg/dz
        dydx[1]=-(nusselt2Phase*thermalCondIntGas*PI*(y[1]-tempGraphiteShort)
                  +2*PI*emissivityGas*SIGMA*radiusGraphiteShort*pow(y[1],4))/
                  (mdotGas*cpGas)
                  -(numbDensParticles*pow(PI,2)*pow(radiusGraphiteShort,2)
                  *diameterParticle)*(nusseltParticle*thermalCondIntGas*
                  (y[1]-y[6])+diameterParticle*emissivityGas*SIGMA*
                  pow(y[1],4))/(mdotGas*cpGas);

        //dtg/dz
        dydx[2]=(densityGas*PI*pow(radiusGraphiteShort,2))/mdotGas;

        //dup/dz
        dydx[3] = -(3.0/4.0)*densityGas*dragCoefficient*pow(y[3],2)/
                            (densityParticle*diameterParticle*y[4]);

        //dvp/dz
        dydx[4]=-(3.0/4.0)*dragCoefficient
                          *(densityGas/(densityParticle*diameterParticle))
                          *((y[4]-velocityAxialGas)/y[4])
                          *fabs(velocityAxialGas-y[4]) + G/y[4];
```

```
	//dtp/dz
	dydx[5]=1.0/y[4];

	//dTp/dz
	dydx[6]=((numbDensParticles*pow(PI,2)*pow(radiusGraphiteShort,2)
		*diameterParticle)/(mdotParticle*cpParticle))
		*(nusseltParticle*thermalCondIntGas*(y[1]-y[6])
		+diameterParticle*emissivityParticle*SIGMA
		*(pow(tempGraphiteShort,4)-pow(y[6],4))
		+diameterParticle*emissivityGas*SIGMA*pow(y[1],4);
	x=x;

}	//end Derivs

void Rk4(REAL y[], REAL dydx[], int n, REAL x, REAL h, REAL yout[],
	void (*Derivs)(REAL, REAL [], REAL []))
{
	int i;
	REAL xh,hh,h6,*dym,*dyt,*yt;

	dym=Vector(1,n);
	dyt=Vector(1,n);
	yt=Vector(1,n);
	hh=h*0.5;
	h6=h/6.0;
	xh=x+hh;
	for (i=1;i<=n;i++) yt[i]=y[i]+hh*dydx[i];
	(*Derivs)(xh,yt,dyt);
	for (i=1;i<=n;i++) yt[i]=y[i]+hh*dyt[i];
	(*Derivs)(xh,yt,dym);


	for (i=1;i<=n;i++)
	{
		yt[i]=y[i]+h*dym[i];
		dym[i] += dyt[i];
	}
	(*Derivs)(x+h,yt,dyt);
	for (i=1;i<=n;i++)
	{
		yout[i]=y[i]+h6*(dydx[i]+dyt[i]+2.0*dym[i]);
		if (yout[i]<0.0) yout[i]=0.0;
	}
	FreeVector(yt,1,n);
	FreeVector(dyt,1,n);
	FreeVector(dym,1,n);

}	//end Rk4
```

//1DFunctions.h

```
//Header File with 1D Model functions prototypes

#define N 6
#define G 9.8                   //gravitational acceleration 9.8 m/s
#define PI 3.141593
#define SIGMA 5.670E-08         //Stefan-Boltzmann constant W.m-2.K-1

REAL CpGas(REAL);
REAL CpIntGas(REAL, REAL);
REAL CpParticle(REAL);
```

```
REAL DensityGas(REAL);
REAL DiameterParticle(REAL);
REAL DragCoefficient();

REAL EmissivityGas(REAL);
REAL EnthalpyGas(REAL);

REAL NumbDensParticles(REAL);
REAL NusseltGas(REAL);
REAL NusseltParticle(REAL);
REAL Nusselt2Phase();

REAL PositionRadialParticle(REAL, REAL, REAL);
REAL PrandtlGas();
REAL PrandtlParticle();
REAL PrandtlFilm();

REAL RadiationCoef();
REAL RadiusGraphiteLong(REAL);
REAL RadiusGraphiteShort(REAL);
REAL RadiusSSShort(REAL);
REAL ReynoldsGas();
REAL ReynoldsParticle();
REAL ReynoldsFParticle();

REAL TempGraphiteLong(REAL, REAL);
REAL TempGraphiteShort(REAL, REAL, REAL, REAL);
REAL TempSSShort(REAL,REAL);
REAL TempSSLong(REAL, REAL);
REAL ThermalCondGas(REAL);
REAL ThermalCondGraphite();
REAL ThermalCondIntGas(REAL, REAL);
REAL ThermalCondParticle(REAL);
REAL ThermalCondSS();
REAL ThermalResistance2Phase();
REAL ThermalResistanceWalls(REAL,REAL);
REAL VelocityAxialGas();
REAL VelocityRelative(REAL, REAL);
REAL ViscosityGas(REAL);
REAL ViscosityIntGas(REAL, REAL);
```

//1DFunctions.cpp

```
//Functions for 1D Model

#include "pcutil.h"
#include "1DFunctions.h"

//declaring external variables defined in 1DRK4.cpp
      extern REAL cpGas,
                  cpFilmGas,
                  cpIntGas,
                  cpParticle,
                  densityFilmGas,
                  densityGas,
                  densityParticle,
                  diameterHydraulic,
                  diameterParticle,
                  diameterParticleInit,
                  dragCoefficient,
                  emissivityGas,
                  emissivityParticle,
```

```
                    enthalpyGas,
                    filmTemp,
                    loadingRatio,
                    mdotGas,
                    mdotParticle,
                    numbDensParticles,
                    nusseltGas,
                    nusseltParticle,
                    nusselt2Phase,
                    nusseltWater,
                    positionRadialParticle,
                    positionRadialParticlePrev,
                    prandtlGas,
                    prandtlParticle,
                    prandtlFilm,
                    radiationCoef,
                    radiusGraphiteLong,
                    radiusGraphiteShort,
                    radiusSSLong,
                    radiusSSShort,
                    reynoldsGas,
                    reynoldsParticle,
                    reynoldsFilmPart,
                    temperatureWater,
                    tempGraphiteLong,
                    tempGraphiteShort,
                    tempSSLong,
                    tempSSShort,
                    thermalCondGas,
                    thermalCondGraphite,
                    thermalCondFilmGas,
                    thermalCondIntGas,
                    thermalCondIntGas3,
                    thermalCondParticle,
                    thermalCondSS,
                    thermalCondWater,
                    thermalResistance2Phase,
                    thermalResistanceWalls,
                    velocityAxialGas,
                    velocityRelative,
                    viscosityGas,
                    viscosityFilmGas,
                    viscosityIntGas,
                    **ppCF4,
                    **ppC;

//Functions

REAL CpGas(REAL tempG)
{
      int i;
      REAL loT, hiT, loCp, hiCp;

      if (tempG<340.0) tempG=340.0;
      loT=ppCF4[1][1];
      i=1;

      while(loT>tempG)
      {
            i++;
            loT=ppCF4[i][1];
      }
```

```
        if(loT==tempG)
                return 1000.0*ppCF4[i][3];
        else
        {
                loCp=ppCF4[i][3];
                hiT=ppCF4[i-1][1];
                hiCp=ppCF4[i-1][3];
                return 1000.0*(loCp + (hiCp-loCp)*(tempG-loT)/(hiT-loT));
        }
}       //end CpGas

REAL CpIntGas(REAL tempG, REAL tempP)
{
        REAL  temp,deltaT,cp1,cp2,intMean;

        cp1=0.0;
        cp2=0.0;
        deltaT=10;
        if ((tempP<tempG)&&((tempG-tempP)>deltaT))
        {
                temp=tempP;
                while (temp<(tempG-deltaT))
                {
                        cp1 +=deltaT*CpGas(temp);
                        temp+=deltaT;
                }
                cp1 +=(tempG-temp)*CpGas(temp);

                temp=tempG;
                while (temp>(tempP+deltaT))
                {
                        cp2 +=deltaT*CpGas(temp);
                        temp=temp-deltaT;
                }
                cp2 +=(temp-tempP)*CpGas(temp);

                intMean=(cp1+cp2)/(2*(tempG-tempP));
        }
        else if ((tempP>tempG)&&((tempP-tempG)>deltaT))
        {
                temp=tempG;


                while(temp<(tempP-deltaT))
                {
                        cp1+=deltaT*CpGas(temp);
                        temp+=deltaT;
                }
                cp1+=(tempP-temp)*CpGas(temp);

                temp=tempP;
                while (temp>(tempG+deltaT))
                {
                        cp2+=deltaT*CpGas(temp);
                        temp=temp-deltaT;
                }
                cp2 += (temp-tempG)*CpGas(temp);

                intMean=(cp1+cp2)/(2*(tempP-tempG));
        }
        else
                intMean=(CpGas(tempG)+CpGas(tempP))/2;
```

```
        return intMean;

}       //end CpIntGas

REAL CpParticle(REAL tempP)
{
        int i=1;
        REAL loT, hiT, loCp, hiCp;

        hiT=ppC[1][1];

        while(hiT<tempP)
        {
                i++;
                hiT=ppC[i][1];
        }
        if(hiT==tempP)
                return 1000*ppC[i][2]/12.011;
        else
        {
                hiCp=ppC[i][2];
                loT=ppC[i-1][1];
                loCp=ppC[i-1][2];
                return 1000*(loCp + (hiCp-loCp)*(tempP-loT)/(hiT-loT))/12.011;
        }

}       //end CpParticle

REAL DensityGas(REAL tempG)
{
        int i;
        REAL loT, hiT, loRho, hiRho;

        if (tempG<340.0) tempG=340.0;
        loT=ppCF4[1][1];
        i=1;

        while(loT>tempG)
        {
                i++;
                loT=ppCF4[i][1];
        }
        if(loT==tempG)
                return 1/ppCF4[i][2];
        else
        {
                loRho=1/ppCF4[i][2];
                hiT=ppCF4[i-1][1];
                hiRho=1/ppCF4[i-1][2];
                return loRho + (hiRho-loRho)*(tempG-loT)/(hiT-loT);
        }
}       //end DensityGas

REAL DiameterParticle(REAL diamPinit)
{
        return diamPinit;
}       //end DiameterParticle

REAL DragCoefficient()
{
        REAL dragC;

        if(reynoldsParticle<0.2)
```

```
            dragC=24/reynoldsParticle;
      if((reynoldsParticle>=0.2) && (reynoldsParticle<2.0))
            dragC=24/reynoldsParticle*(1+0.187*reynoldsParticle);
      if((reynoldsParticle>=2.0) && (reynoldsParticle<20.0))
            dragC=24/reynoldsParticle*(1+0.110*pow(reynoldsParticle,0.81));
      if((reynoldsParticle>=20.0) && (reynoldsParticle<200.0))
            dragC=24/reynoldsParticle*(1+0.189*pow(reynoldsParticle,0.62));
      if(reynoldsParticle>=200.0)
            dragC=24/reynoldsParticle + 6/(1+pow(reynoldsParticle,0.5)) +0.4;

      return dragC;
}     //end DragCoefficient


REAL EmissivityGas(REAL tempGas)
{
      return 0.0136*exp(0.00106*tempGas);
}     //end EmissivityGas

REAL EnthalpyGas(REAL tempGas)
{
      int i;
      REAL loT, hiT, loH, hiH;

      if (tempGas<340.0) tempGas=340.0;
      loT=ppCF4[1][1];
      i=1;

      while(loT>tempGas)
      {
            i++;
            loT=ppCF4[i][1];
      }
      if(loT==tempGas)
            return ppCF4[i][6];
      else
      {
            loH=ppCF4[i][6];
            hiT=ppCF4[i-1][1];
            hiH=ppCF4[i-1][6];
            return loH + (hiH-loH)*(tempGas-loT)/(hiT-loT);
      }
}     //end EnthalpyGas

REAL NumbDensParticles(REAL veloAxiaP)
{
      return
(6*mdotParticle)/(densityParticle*pow(PI,2)*pow(diameterParticle,3)
            *pow(radiusGraphiteShort,2)*veloAxiaP);
}     //end NumbDensParticles

REAL NusseltGas(REAL tempPart)
{
      //Dittus-Boelter equation
      return 0.023*pow(reynoldsGas,0.8)*pow(prandtlGas,0.3);
}     //end NusseltGas

REAL NusseltParticle(REAL tempPart)
{
      REAL kinViscFilm,kinViscGas,viscPartGas,densPartGas,cpPartGas;
      REAL C, enthalpyPartGas,thermalCondPartGas,prandtlPartGas,nusselt;

      kinViscFilm=viscosityFilmGas/densityFilmGas;
```

```
      kinViscGas=viscosityGas/densityGas;
      viscPartGas=ViscosityGas(tempPart);
      densPartGas=DensityGas(tempPart);
      cpPartGas=CpGas(tempPart);
      enthalpyPartGas=EnthalpyGas(tempPart);
      thermalCondPartGas=ThermalCondGas(tempPart);
      prandtlPartGas=cpPartGas*viscPartGas/thermalCondPartGas;

      //basic equation
      return 2.0 + 0.6*pow(reynoldsParticle,0.5)*pow(prandtlParticle,0.3333);


      //Lewis & Gauvin
      return (2.0+0.515*pow(reynoldsFilmPart,0.5))
                  *pow((kinViscFilm/kinViscGas),0.15);

      //Fizsdon
      return (2.0+0.6*pow(reynoldsFilmPart,0.5)*pow(prandtlFilm,0.333))
*pow(((densityGas*viscosityGas)/(densPartGas*viscPartGas)),0.6);

      //Lee
      return (2.0+0.6*pow(reynoldsFilmPart,0.5)*pow(prandtlFilm,0.333))
             *pow(((densityGas*viscosityGas)/(densPartGas*viscPartGas)),0.6)
             *(cpGas/cpPartGas);

      //Chen
      C=(1-pow((enthalpyPartGas/enthalpyGas),1.1))
        /(1-pow((enthalpyPartGas/enthalpyGas),2));

      nusselt= 2*(1 + 0.63*reynoldsGas*pow(prandtlGas,0.8)
                *pow((prandtlPartGas/prandtlGas),0.42)
*pow((densityGas*viscosityGas/(densPartGas*viscPartGas)),0.52)
*pow(C,2));
      return nusselt;

}     //end NusseltParticle

REAL Nusselt2Phase()
{
      REAL nu2Ph, diameter;

      diameter=2*radiusGraphiteShort;
      nu2Ph=nusseltGas*(1+0.37*pow(reynoldsGas,-
0.7)*pow(reynoldsParticle,0.7)

      *pow(diameter/diameterParticle,0.6)*loadingRatio*cpParticle/cpGas);
      return nu2Ph;
}     //end Nusselt2Phase

REAL PositionRadialParticle(REAL velocityRadialPart, REAL dz, REAL
                            velocityParticle)
{
      REAL pos,timeParticle;

      timeParticle=dz/velocityParticle;

      if(positionRadialParticle<positionRadialParticlePrev&&
         fabs(positionRadialParticle-velocityRadialPart*timeParticle)
        <fabs(radiusGraphiteShort))
```

```
      {
            pos=positionRadialParticle-velocityRadialPart*timeParticle;
      }
      if(positionRadialParticle<positionRadialParticlePrev&&
         fabs(positionRadialParticle-velocityRadialPart*timeParticle)
        >fabs(radiusGraphiteShort))

      {
            pos=positionRadialParticle+velocityRadialPart*timeParticle;
      }
      if(positionRadialParticle>positionRadialParticlePrev&&
         positionRadialParticle+velocityRadialPart*timeParticle
         <radiusGraphiteShort)
      {
            pos=positionRadialParticle+velocityRadialPart*timeParticle;
      }
      if(positionRadialParticle>positionRadialParticlePrev&&
         positionRadialParticle+velocityRadialPart*timeParticle
         >radiusGraphiteShort)


      {
            pos=positionRadialParticle-velocityRadialPart*timeParticle;
      }

      positionRadialParticlePrev=positionRadialParticle;
      positionRadialParticle=pos;

      return pos;
}     //end PositionRadialParticle

REAL PrandtlGas()
{
      return cpGas*viscosityGas/thermalCondGas;
}     //end PrandtlGas

REAL PrandtlParticle()
{
      return cpIntGas*viscosityIntGas/thermalCondIntGas;
}     //end PrandtlParticle

REAL PrandtlFilm()      //Prandtl number at film temperature
{
      return cpFilmGas*viscosityFilmGas/thermalCondFilmGas;
}     //end PrandtlFilm

REAL RadiationCoef()
{
      return emissivityParticle*SIGMA*(tempGraphiteLong+tempSSShort)
            *(pow(tempGraphiteLong,2)+pow(tempSSShort,2));
}     //end RadiationCoef

REAL RadiusGraphiteShort(REAL xPos)
{
      if (xPos <= 0.01)
            return 0.011;
      else if ((xPos >0.01) && (xPos < 0.0325))
            return 0.011+(1.5/22.5)*(xPos-0.01);
      else
            return 0.025/2;
}     //end RadiusGraphiteShort
```

```
REAL RadiusGraphiteLong(REAL x)            //with gas gap
{
      REAL rad;

      if (x < 0.0145)
            rad = 0.0215;
      else if ((x>0.0145)&&(x<=(0.0145+137.5/17.5/1000)))
            rad = 0.0215 + (218.75/137.5)*(x-0.0145);
      else
            rad = 0.068/2;
      return rad;
}     //end RadiusGraphiteLong

REAL RadiusSSShort(REAL x)           //with gas gap
{
      return (radiusGraphiteLong+0.005);
}     //end RadiusSSShort

REAL ReynoldsGas()
{
      return (2*mdotGas)/(PI*radiusGraphiteShort*viscosityGas);
}     //end ReynoldsGas

REAL ReynoldsParticle()
{
      return (densityGas*velocityRelative*diameterParticle)/viscosityGas;
}     end ReynoldsParticle

REAL ReynoldsFParticle()          //Particle Reynolds number at film
temperature
{
      return
densityFilmGas*velocityRelative*diameterParticle)/viscosityFilmGas;
}     //end ReynoldsFParticle

REAL TempGraphiteLong(REAL tempG, REAL tempW)
{
      return tempGraphiteShort - ((log(radiusGraphiteLong/
            radiusGraphiteShort)/(2*PI*thermalCondGraphite))/
            thermalResistanceWalls)*(tempG-tempW);
}     //end TempGraphiteLong

REAL TempGraphiteShort(REAL tempG, REAL tempW, REAL tempGraph, REAL tempP)
{
      REAL resistGas;

      resistGas = 1.0/(PI*nusselt2Phase*thermalCondIntGas + (2*PI*SIGMA
                  *emissivityGas*radiusGraphiteShort*pow(tempG,4))
                  /(tempG-tempGraph));

      return tempG - (resistGas/thermalResistanceWalls)*(tempG-tempW);
}     //end TempGraphiteShort

REAL TempSSShort(REAL tempG, REAL tempW)
{
      return tempGraphiteLong - (tempG-tempW)/thermalResistanceWalls/
            (2*PI*radiusGraphiteLong*radiationCoef+2*PI*thermalCondIntGas3
            /log(radiusSSShort/radiusGraphiteLong));
}     //end TempSSShort

REAL TempSSLong(REAL tempG, REAL tempW)
{
      return tempSSShort - ((log(radiusSSLong/radiusSSShort)/
```

```
            (2*PI*thermalCondSS))/thermalResistanceWalls)*(tempG-tempW);
}     //end TempSSLong

REAL ThermalCondGas(REAL tempG)
{
      int i;
      REAL loT, hiT, loLT, hiLT;

      loT=ppCF4[1][1];
      i=1;

      while(loT>tempG)
      {
            i++;
            loT=ppCF4[i][1];
      }
      if(loT==tempG)
            return ppCF4[i][5];
      else
      {
            loLT=ppCF4[i][5];
            hiT=ppCF4[i-1][1];
            hiLT=ppCF4[i-1][5];
            return loLT + (hiLT-loLT)*(tempG-loT)/(hiT-loT);
      }
}     //end ThermalCondGas
REAL ThermalCondGraphite()
{
      return 7.0;
}     //end ThermalCondGraphite

REAL ThermalCondIntGas(REAL tempG, REAL tempP)
{
      REAL temp,deltaT,k1,k2,intMean;

      k1=0.0;
      k2=0.0;
      deltaT=10;
      if ((tempP<tempG)&&((tempG-tempP)>deltaT))
      {
            temp=tempP;
            while (temp<(tempG-deltaT))
            {
                  k1 +=deltaT*ThermalCondGas(temp);
                  temp+=deltaT;
            }
            k1 +=(tempG-temp)*ThermalCondGas(temp);

            temp=tempG;
            while (temp>(tempP+deltaT))
            {
                  k2 +=deltaT*ThermalCondGas(temp);
                  temp=temp-deltaT;
            }
            k2 +=(temp-tempP)*ThermalCondGas(temp);

            intMean=(k1+k2)/(2*(tempG-tempP));
      }
      else if ((tempP>tempG)&&((tempP-tempG)>deltaT))
      {
            temp=tempG;
            while(temp<(tempP-deltaT))
            {
```

```
                k1+=deltaT*ThermalCondGas(temp);
                temp+=deltaT;
            }
            k1+=(tempP-temp)*ThermalCondGas(temp);
            temp=tempP;
            while (temp>(tempG+deltaT))
            {
                k2+=deltaT*ThermalCondGas(temp);
                temp=temp-deltaT;
            }
            k2 += (temp-tempG)*ThermalCondGas(temp);

            intMean=(k1+k2)/(2*(tempP-tempG));
        }
        else
            intMean=(ThermalCondGas(tempG)+ThermalCondGas(tempP))/2;

        return intMean;
}       //end ThermalCondIntGas

REAL ThermalCondParticle(REAL tempP)
{
        tempP=tempP;
        return 8.0;
}       //end ThermalCondParticle

REAL ThermalCondSS()
{
        //thermal conductivity of Inconel, from Perry, 15 W.K-1.m-1
        return 15.0;
}       //end ThermalCondSS

REAL ThermalResistance2Phase()
{
        return 1.0/(PI*nusselt2Phase*thermalCondIntGas);
}       //end ThermalResistance2Phase

REAL ThermalResistanceWalls(REAL tempGas,REAL tempGraph)
//total thermal resistance

{
        REAL rWater,rSS,rGraphite,rGap,rGas;

        rWater=diameterHydraulic/(2*PI*nusseltWater*thermalCondWater*
                                  radiusSSLong);
        rSS=(1.0/(2*PI*thermalCondSS))*log(radiusSSLong/radiusSSShort);
        rGraphite=(1.0/(2*PI*thermalCondGraphite))*log(radiusGraphiteLong/
                          radiusGraphiteShort);
        rGap=1.0/(2*PI*radiusGraphiteLong*radiationCoef+
              2*PI*thermalCondIntGas3/log(radiusSSShort/radiusGraphiteLong));
        rGas=1.0/(PI*nusselt2Phase*thermalCondIntGas +
                  (2*PI*SIGMA*emissivityGas*radiusGraphiteShort*pow(tempGas,4))
                  /(tempGas-tempGraph));

        return rSS+rGraphite+rWater+rGas+rGap;
}       //end ThermalResistanceWalls

REAL VelocityAxialGas()
{
        return mdotGas/(densityGas*PI*radiusGraphiteShort*radiusGraphiteShort);
}       //end VelocityAxialGas
```

```
REAL VelocityRelative(REAL veloRadiP, REAL veloAxiaP)
{
      return sqrt(pow(veloRadiP,2) + pow((velocityAxialGas-veloAxiaP),2));
}     //end VelocityRelative

REAL ViscosityGas(REAL tempG)
{
      int i;
      REAL loT, hiT, loMU, hiMU;
      if (tempG<340.0) tempG=340.0;
      loT=ppCF4[1][1];
      i=1;

      while(loT>tempG)
      {
            i++;
            loT=ppCF4[i][1];
      }
      if(loT==tempG)
            return ppCF4[i][4];
      else
      {
            loMU=ppCF4[i][4];
            hiT=ppCF4[i-1][1];
            hiMU=ppCF4[i-1][4];
            return loMU + (hiMU-loMU)*(tempG-loT)/(hiT-loT);
      }
}     //end ViscosityGas

REAL ViscosityIntGas(REAL tempG, REAL tempP)
{
      REAL temp,mu1,mu2,deltaT,intMean;

      mu1=0.0;
      mu2=0.0;
      deltaT=10;
      if ((tempP<tempG)&&((tempG-tempP)>deltaT))
      {
            temp=tempP;
            while (temp<(tempG-deltaT))
            {
                  mu1 +=deltaT*ViscosityGas(temp);
                  temp+=deltaT;
            }
            mu1 +=(tempG-temp)*ViscosityGas(temp);

            temp=tempG;
            while (temp>(tempP+deltaT))
            {
                  mu2 +=deltaT*ViscosityGas(temp);
                  temp=temp-deltaT;
            }
            mu2 +=(temp-tempP)*ViscosityGas(temp);

            intMean=(mu1+mu2)/(2*(tempG-tempP));
      }
      else if ((tempP>tempG)&&((tempP-tempG)>deltaT))
      {
            temp=tempG;

            while(temp<(tempP-deltaT))
            {
                  mu1+=deltaT*ViscosityGas(temp);
```

```
                temp+=deltaT;
            }
            mu1+=(tempP-temp)*ViscosityGas(temp);

            temp=tempP;
            while (temp>(tempG+deltaT))
            {
                mu2+=deltaT*ViscosityGas(temp);
                temp=temp-deltaT;
            }
            mu2 += (temp-tempG)*ViscosityGas(temp);

            intMean=(mu1+mu2)/(2*(tempP-tempG));
        }
        else
            intMean=(ViscosityGas(tempG)+ViscosityGas(tempP))/2;

        return intMean;
}       //end ViscosityIntGas
```

E3. Nusselt number for convective heat transfer to cooling water

Cooling water flow through an annulus on the outside of the reactor.

Annulus inner diameter: $D_i = 88$ mm

Annulus outer diameter: $D_o = 92$ mm

Equivalent diameter of annulus: $D_h = D_o - D_i = 0.004$ m

Water mass flow rate: $\dot{m} = 700$ kg/h $\equiv 0.194$ kg/s

Volumetric flow rate: $Q = \frac{\dot{m}}{\rho} = \frac{0.194}{999} = 1.95E-4\ m^3/s$

Water velocity: $v = \frac{Q}{A} = \frac{4Q}{\pi\left(D_o^2 - D_i^2\right)} = 0.344\ m/s$

Reynolds number: $Re = \frac{\rho v D_h}{\mu} = \frac{999(0.344)(0.004)}{1080E-6} = 1273.5$

Assumption: Water temperature is uniform.

Nusselt number for cooling water:

$$Nu = 1.02 Re^{0.45} Pr^{0.5} \left(\frac{D_h}{L}\right)^{0.4} \left(\frac{D_o}{D_i}\right)^{0.8} \left(\frac{\mu_b}{\mu_i}\right)^{0.14} Gr^{0.05}$$

Prandtl number: $Pr = 7.56$

Length of annulus: $L = 0.21$ m

Viscosity of water at bulk temperature: $\mu_b = 1080E\text{-}6$ N.s.m^{-2}

Viscosity of water at inner surface temperature: $\mu_i = 76E\text{-}6$ N.s.m^{-2}

Grashof number: $Gr = \frac{D_h^3 \rho^2 g \beta \Delta T}{\mu_b^2}$

Gravitational acceleration: $g = 9.81$ m.s^{-2}

Thermal expansion coefficient for Inconel: $\beta = 0.207E\text{-}3\ K^{-1}$

Temperature difference between metal surface and water: $\Delta T = 400$ K

$\Rightarrow$ $Gr = 4.45E4$

$\Rightarrow$ $Nu = 36.9$